Space-Frequency Equalization in Broadband Single Carrier Systems

Gayathri Kongara

A Thesis Submitted in Partial Fulfillment

of the Requirements for the Degree of

Doctor of Philosophy

in

Electrical and Computer Engineering

University of Canterbury

Christchurch, New Zealand

October 19, 2009

Abstract

Broadband wireless access systems can be used to deliver a variety of high data rate applications and services. Many of the channels being considered for such applications exhibit multipath propagation coupled with large delay spreads. Currently, orthogonal frequency division multiplexing is employed in these channels to compensate the effect of dispersion. Single carrier (SC) modulation in conjunction with frequency-domain equalization (FDE) at the receiver has been shown to be a practical alternate solution as it has lower peak to average power ratio and is less sensitive to frequency offsets and phase noise compared to OFDM. The effect of multipath propagation increases with increasing data rate for SC systems. This leads to larger inter-symbol-interference (ISI) spans. In addition the achievable capacity of SC-broadband systems depends on their ability to accommodate multiple signal transmissions in the same frequency band, which results in co-channel interference (CCI) when detecting the desired data stream. The effects of CCI and ISI are more pronounced at high data rates. The objective of this research is to investigate and a develop low-complexity frequency domain receiver architectures capable of suppressing both CCI and ISI and employing practical channel estimation.

In this thesis, a linear and a non-linear receiver architecture are developed in the frequency domain for use in highly dispersive channels employing multiple input multiple output (MIMO) antennas. The linear receiver consists of parallel branches each corresponding to a transmit data stream and implements linear equalization and demodulation. Frequency domain joint CCI mitigation and ISI equalization is implemented based on estimated channel parameters and is called space-frequency

equalization. The non-linear receiver implements hybrid decision feedback equalization by extending the parallel branch linear MMSE receiver to include a decision feedback back end and is referred to as the space-frequency decision feedback equalization (SF-DFE). As with the linear equalizer, the SF-DFE also performs frequency domain CCI mitigation and MMSE-FDE. In addition, it implements a time domain feedback filter performing post-cursor ISI cancellation based on the recently detected data symbols.

A training sequence based time domain channel estimation algorithm is developed which estimates the effective channel parameters by maximizing the signal to interference plus noise ratio. These parameters are Fourier transformed and utilized by the frequency domain receiver. The effective channel parameters are estimated in parallel using a parameter estimation algorithm. Further, an iterative QR-decomposition based parameter estimation algorithm is developed which yields performance improvement over the non-iterative parameter estimation algorithm.

Acknowledgments

First of all I would like to express my sincere gratitude to Professor Desmond P. Taylor (Des) for providing technical advice over the years of my Ph. D research work. The guidance and technical support I received from Des are invaluable. Also, I am grateful to Des for arranging a scholarship for my research work at the University of Canterbury.

I am thankful to Dr. Philippa A. Martin (Phil) for the motivation and inspiration at crucial times. Technical discussions with Phil helped a great deal in improving the quality of my thesis. I would like to thank many friends at the Communications research laboratory. I am thankful to Dr. Peter Green for his encouragement during the initial period of my research. Thanks also to Michael Krause for many technical discussions. Also, I would like to acknowledge my friends Nick J. Pau, Yau Hee Kho, Judy and Rui Lin for creating a friendly work environment.

My heartfelt thanks to my husband Krishna Prasad for his love, patience and always believing in me. I will always cherish the period that we spent pursuing Ph. D research together at the communications research group University of Canterbury. I am grateful to Krishna for many technical discussions that motivated new ideas in to my research work. Also, I am thankful to my five year old son Aadarsh. Finally, my sincere gratitude to my parents Smt. Padmavathy, Sri. Venkata Chalam, and Smt. Usha Devi for their love and patience. I couldn't have done this research without their support.

Contents

List of Figures

List of Tables

Acronyms

AWGN	Additive White Gaussian Noise
BER	Bit Error Rate
BWA	Broadband Wireless Access
CCI	Co-Channel Interference
CDMA	Code Division Multiple Access
CSI	Channel State Information
CP	Cyclic Prefix
DFE	Decision Feedback Equalizer
FBF	Feed Back Filter
FD	Frequency Domain
FDMA	Frequency Division Multiple Access
FDE	Frequency Domain Equalization
FFF	Feed Forward Filter
FIR	Finite Impulse Response
FFT	Fast Fourier Transform

FDM	Frequency Division Multiplexing
GSM	Global System for Mobile Communication
IFFT	Inverse Fast Fourier Transform
ISI	Inter-Symbol-Interference
JEA	Joint Estimation Algorithm
LOS	Line-Of-Sight
LSF	Layered Space Frequency Equalizer
LTE	Long Term Evolution
MIMO	Multiple-Input Multiple-Output
MISO	Multiple-Input Single-Output
ML	Maximum Likelihood
MLSE	Maximum Likelihood Sequence Estimation
MMSE	Minimum Mean Square Error
MSE	Mean Square Error
NLOS	No-Line-Of-Sight
NP	Noise Predictive
OFDM	Orthogonal Frequency Division Multiplex
PIC	Parallel Interference Cancelation
QAM	Quadrature Amplitude Modulation
QPSK	Quadrature Phase Shift Keying

QR-JEA	Orthogonal triangular decomposition based Joint Estimation Algorithm
RMS	Root Mean Square
SC	Single Carrier
SC-FDE	Single Carrier Frequency Domain Equalization
SFE	Space-Frequency Equalizer
SFP	Space-Frequency Pre-Processor
SF-DFE	Space-Frequency Decision Feedback Equalizer
SIC	Successive Interference Cancelation
SIMO	Single-Input Multiple-Output
SINR	Signal to Interference and Noise Ratio
SISO	Single-Input Single-Output
SM	Spatial Multiplexing
SNR	Signal to Noise Ratio
STBC	Space Time Block Coding
SUI	Stanford University Interim
TD	Time Domain
TDE	Time Domain Equalizer
TDM	Time Domain Multiplexing
VBLAST	Vertical Bell Labs Space-Time

WLAN Wireless Local Area Network

WPAN Wireless Personal Area Network

Chapter 1

Introduction

Wired high-speed communication systems delivering voice, data and video are often less effective than wireless systems in their ability to scale with the ever-changing telecommunication environment [2, 3]. Some of the reasons for this are higher capital costs, recurring maintenance costs and a lack of flexibility in wired systems. Broadband wireless has emerged as an exceptional last mile access alternative to wired systems such as xDSL and cable modems [2–4]. Wireless systems offer the advantage of diversity in the time and frequency domains that can be exploited using suitable transceiver algorithms [4]. However, wireless channels suffer from time varying dispersive fading that must be compensated in order that wireless systems can provide a viable alternative.

In this chapter, an overview of broadband wireless systems is first presented which points out some of the key technical challenges for broadband data transmissions. A system level description of the two main competing wireless techniques for broadband communications is then provided. Finally, we summarize the use of multiple antennas at both ends of a broadband wireless link in order to significantly improve both spectral efficiency and link reliability.

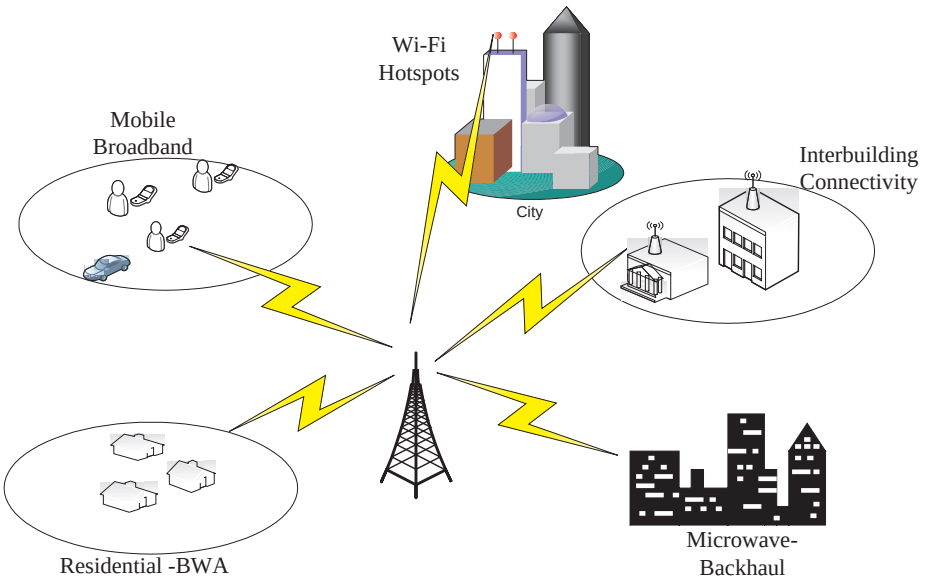

Figure 1.1: A typical BWA network.

1.1 Broadband Wireless Access - An Overview

It is an exciting time for broadband wireless access (BWA) systems with key developments and a range of new technologies being developed [4]. Apart from being quick and easy to deploy, BWA networks involve comparatively low initial investment and can be easily expanded to accommodate more users. Since their initial deployment in the 1990's, BWA services have enjoyed significant growth [4]. BWA services that attempt to provide services similar to those of traditional fixed-line systems are called fixed BWA [5]. Another type that offers the additional functionality of mobility is mobile BWA [6]. Fixed BWA applications can be either point-to-point or point-to-multi-point architectures as illustrated in Fig. 1.1. Point-to-point applications include inter-building connectivity within a campus and microwave backhaul [4]. Point-to-multi-point applications include broadband for residential, small office/home office, small-to-medium-enterprise markets, wireless fidelity (Wi-Fi) hotspots and worldwide interoperability for microwave access (WiMax) and broadcast as shown in Fig. 1.1.

The first generation of BWA systems, called local multi-point distribution services [4], evolved as an alternative to high speed wired solutions such as ADSL and cable modems. These used millimeter wave carrier frequencies, such as 24GHz and 39GHz and delivered data rates of 32 megabits-per-second (Mbps) and higher [4,7]. Later, multi-channel-multi-point services were used for delivering very high data rates. These first generation services using highly directional antennas required a clear line of sight (LOS) communication path between the transmitter and the receiver. Hence, high power transmitters were installed on tall buildings which provided fixed BWA with a range of up to 35 miles [4].

Second generation BWA systems used carrier frequencies in the 2-11GHz range and dealt with the LOS problem existing with the first generation systems. Further, they provided improved quality of service and system capacity over the first generation systems [4, 8]. First generation BWA used single carrier (SC) transmission, whereas multi-carrier based orthogonal frequency division multiplexing (OFDM) was exploited in the second generation systems. Both generations aimed at delivering broadband services to fixed users.

The third generation high-rate wireless services emerged in 2003 with the standard, institute of electrical and electronics engineers (IEEE), IEEE 802.16a, offering broadband data and multimedia services to mobile users in the 2-11GHz radio spectrum [6]. These systems support internet protocol (IP) based voice, and high speed data in the form of both multicast and broadcast services. Such systems use both SC and OFDM transmission schemes to deliver fixed and mobile BWA services in the 2-11GHz and 2-6GHz frequency bands respectively. These are described as scalable orthogonal frequency division multiple access (OFDMA) systems [4]. These second and third generation services are capable of delivering peak data rates of 75Mbps [9].

Further developments in BWA communications include employing multiple input multiple output (MIMO) antenna configurations in order to meet the demand for higher data rates. The available MIMO techniques include precoding, space-time

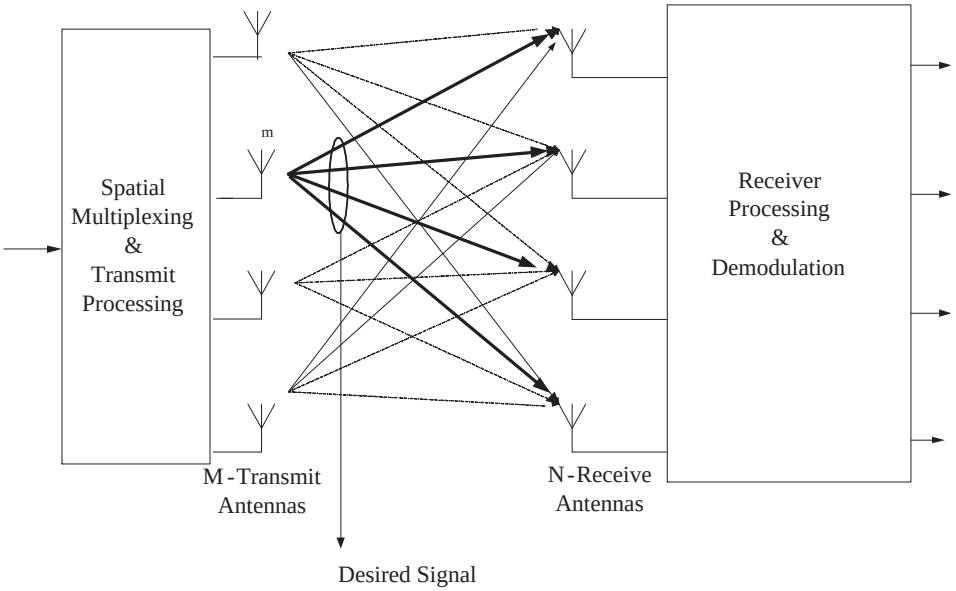

Figure 1.2: A SC MIMO system using joint transmit-receive processing for CCI and ISI mitigation.

coding and spatial multiplexing (SM) [10–12]. All these MIMO techniques have been exploited for BWA communication systems [1, 13, 14].

The second and third generation BWA systems support services in non-line-of-sight (NLOS) channels, which are subject to strong multipath propagation leading to large channel dispersions. This results in temporal interference between successive data symbols, known as inter-symbol-interference (ISI). In addition, in both multi-user systems and MIMO systems cochannel interference (CCI) arises due to frequency re-use. The effects of CCI and ISI in broadband systems are discussed in more detail in chapter 2. The combined effects of CCI and ISI need to be compensated either at the transmitter, or the receiver [1] or by some form of joint transmit-receive processing [13]. In the following, we discuss some of the transmitter based techniques used to mitigate CCI and ISI.

Ideally a SC-MIMO system as shown in Fig. 1.2, uses joint transmit-receiver

processing to mitigate the CCI and ISI. In order to implement transmitter processing, channel state information (CSI) is required at the transmitter and this requires a feedback link back to the transmitter. Pre-processing techniques can then be used to decrease the error-rate, improve the throughput and to control the CCI [10, 13, 14]. Some of the pre-processing techniques that have been studied in conjunction with SC systems use spatial beamforming, eigenmode optimization and Tomlinson-Harashima pre-coding (THP) [15, 16].

Transmitter techniques which require full CSI to be fed back are generally less attractive because of the associated complexity and the associated feedback delay. The use of simple power control mechanisms at the transmitter only requires information about the total received power levels. However, more sophisticated schemes such as spatial beamforming and eigenmode optimization techniques (or eigenbeamforming) require full CSI for optimal performance [10].

A particular form of pre-coding known as THP [15–17] can be used at the transmitter to subtract or cancel the interference prior to transmission. This has been utilized in [17] in conjunction with SC-FDE for SISO systems, and in [13] in conjunction with non-linear receiver techniques for MIMO systems. In contrast, in this thesis we consider broadband communication systems without any CSI available at the transmitter. We focus on entirely multi antenna receiver processing techniques for high-rate SC MIMO systems. In the following, an overview of prominent receiver techniques used in conjunction with FD systems is given.

1.1.1 Receiver Processing Techniques

In spatial multiplexing (SM) systems, a high rate data signal is split into multiple lower rate streams which are transmitted simultaneously from distinct transmit antennas using the same carrier frequency [10]. Use of SM increases the effective data rate as different transmitters are transmitting the different signals. In the absence of transmit processing, a superposed sum of channel distorted signals arrive at the

receiver antenna array. Some form of receiver processing is then required to decouple these signals before detection at the receiver. This usually involves interference suppression or cancellation [1]. The most common type is successive cancellation, which is employed in the so-called V-BLAST system [1, 13]. Parallel interference mitigation techniques have also been employed in a number of instances [18].

Another approach is the use of space-time coding (STC), which seeks to provide transmit diversity in addition to the more common receive diversity [10, 12]. STC techniques can be used either with or without transmit CSI . However, space-time codes do not require more than one receiver [10, 12, 19]. STC exploits the diversity in the multiple antenna links. The orthogonal STCs exploit orthogonality to separate the transmitted signals at the receiver [12, 20].

In SM systems that do not employ precoding techniques, the receiver must cope with CCI from the other transmitters. This CCI is a major limiting factor on the spectral efficiency and performance of BWA systems [21]. In order to demodulate the signals in the presence of CCI, the receiver must be able to separate them by employing multiple receivers. Therefore, BWA systems using SM are required to mitigate interference due to CCI and ISI while maintaining practical complexity. Example architectures which handle SM with receiver processing only are given in [1, 22].

In summary, SC-MIMO receivers operating in a SM framework are required to deal with both CCI and ISI. In the absence of CSI at the transmitter, the complexity of these receivers must be carefully controlled. Broadband MIMO systems are usually characterized by heavy CCI and ISI. MIMO receivers that perform frequency domain processing to compensate these dispersive channels typically have lower complexity than the equivalent time domain receiver architectures [23, 24]. In contrast, channel estimation is often preferably performed in the time domain (TD) as it results in lower estimation complexity [9, 12]. Despite these known complexity issues, most existing architectures perform both equalization and channel estimation in the frequency domain (FD). Hence, in this thesis we focus on 2 main

areas. Firstly, a hybrid domain (TD and FD) linear receiver architecture for broadband MIMO is developed and shown to have several advantages over existing FD receiver architectures. Secondly, a non-linear decision feedback receiver that builds on the hybrid domain linear receiver architecture is developed and compared with existing FD interference cancellation receivers [1, 25–28].

1.2 Thesis Overview

In chapter 2 we examine the impact of wireless channel characteristics on the MIMO BWA communications. Then, the importance of FD processing for broadband channels is discussed. A system level description of the two competing techniques using the single-carrier and multi-carrier transmissions is further discussed.

In chapter 3, we describe some channel estimation techniques used in conjunction with SC-FDE systems. Specifically, we compare several time and frequency domain channel estimation techniques in the MIMO context to identify the superiority of time domain based channel estimation. Secondly, we focus on a TD approach that estimates the MIMO channel based on a composite channel model. We focus on this approach as it has lower processing time than other approaches [1, 25–28]. The composite channel estimation approach computes the MIMO CSI corresponding to each of the transmitters in parallel. Based on this estimated CSI, frequency domain receivers that process and detect signals in parallel are developed in the rest of the thesis.

In chapter 4 a linear space-frequency receiver architecture is developed that uses the time-domain estimated channel parameters to perform CCI mitigation and ISI equalization in the frequency domain for a MIMO SC-BWA system. The receiver, referred to as an integrated space-frequency-equalizer (SFE), yields equal diversity gains for all data streams. A QR-decomposition based iterative joint estimation algorithm (QR-JEA) is developed to estimate the channel parameters in the TD. These are Fourier transformed and passed to the SFE to perform frequency domain

CCI mitigation and ISI equalization. The integrated SFE including the iterative QR-JEA is shown to have lower processing time and comparable complexity to other frequency domain receivers [1, 25–28]. The resulting receiver exhibits excellent error performance even on highly dispersive broadband wireless channels.

In chapter 5, the linear SFE is extended to a non-linear receiver architecture described as a space frequency decision feedback equalizer (SF-DFE). The SF-DFE uses the FD pre-processor of chapter 4 in conjunction with a hybrid-DFE receiver architecture similar to that discussed in chapter 3. The existing hybrid-DFE architecture for MIMO [1,13] is derived based on the knowledge of the complete MIMO channel matrix. In contrast, the SF-DFE of the present work is developed using the effective channel and receiver parameters estimated by the iterative QR-JEA. This provides both processing time and complexity savings. Using simulations, we show that the SF-DFE outperforms its linear counterpart presented in chapter 4.

In chapter 6 we draw conclusions and suggest some future directions for the work in this area.

1.3 Thesis Contributions

The key contributions of this thesis are the new receiver architectures described in chapters 4 and 5 in highly dispersive environments, these require the estimation of fewer channel and receiver parameters to implement frequency domain processing compared to the approaches given in [1, 13, 26–29]. The MIMO frequency domain receivers for SC systems in [1,13,27–29] require estimation of the complete MIMO channel matrix in order to derive the MIMO FDE coefficients. Moreover, all these algorithms estimate the MIMO channel frequency response matrix despite the fact that a MIMO channel impulse response is usually characterized by fewer parameters [9, 21, 30].

Key advantages of the proposed SFE receiver of chapter 4 over existing approaches are summarized below:

- Due to parallel processing, all transmitted data streams achieve equal diversity gains. The multiple stage interference cancellation based approaches of [1, 22] do not achieve this.

- Unlike SM systems such as V-BLAST [1, 13] any number of receive antennas can be used. For good performance, we still require as many receivers as the the number of transmitters. Performance degradation is seen otherwise however, it will be seen to be more graceful than that exhibited by V-BLAST systems [10].

- The performance of the integrated-SFE based on the QR-JEA approach to channel estimation with 1 and 2 iterations is better than that of the LSF equalizer of [1] with 4 stages.

- The proposed schemes require lower processing time to estimate the effective channel and receiver parameters than the channel frequency response estimation techniques in [1, 25–28].

- The complexity of iterative QR-JEA channel estimation with 1 iteration is comparable to the least squares channel estimation complexity of [1, 27, 28]. Moreover, the processing for each additional iteration is very small.

Key advantages of the proposed SF-DFE receiver developed in chapter 5 over existing non-linear FD receivers are summarized below:

- The SF-DFE architecture inherits all the advantages of a linear SFE such as parallel processing based on low complexity QR-JEA, equal diversity gains achieved by all data streams.

- Due to the parallel branch architecture, the proposed SF-DFE receivers have lower latency compared to DFE architectures given in [1, 13, 31].

- The system complexity of the SF-DFE is slightly lower than the MIMO hybrid-DFE architectures of [1, 13, 31]. In addition, when channel estimation complexity is considered, then, SF-DFE system has significantly lower complexity than DFE architectures of [1, 13, 31].

1.3.1 List of Publications

1. G. Kongara, D. P. Taylor, and P. A. Martin, *Space-frequency equalization for broadband single carrier MIMO systems*, in Proc. VTC, Calgary, Canada, Sept. 2008, pp. 58 - 66.

2. G. Kongara, D. P. Taylor, and P. Martin, *Space-Frequency Equalizer with Iterative Parameter Estimation*, Submitted to IEEE transactions on Communications.

3. G. Kongara, P. A. Martin and D. P. Taylor, *Space-Frequency Decision Feedback Equalization with Iterative Parameter Estimation*, in preparation for submission to an IEEE journal.

Chapter 2

Broadband Wireless Channel

In this chapter, we consider some of the challenges posed by the channel characteristics of MIMO-BWA systems. We also investigate channel models that are suitable for evaluating the performance of broadband MIMO systems. An understanding of such issues and models is critical in order to design efficient systems. The main goal of this chapter is to explain the fundamental factors affecting the received signal in a BWA system. Finally, two competing transceiver solutions based on FD processing are discussed.

2.1 Wireless Propagation Environment

Based on a number of practical measurements, the wireless channel is commonly described by a statistical characterization of the following phenomena:

- Path loss and shadowing based on specific terrain types.
- Multipath propagation and fading.
- Doppler-spread due to mobility of the transmitter or receiver.
- Co-channel interference.

In the following subsections, we consider all of these in more detail beginning with the characterization of path loss.

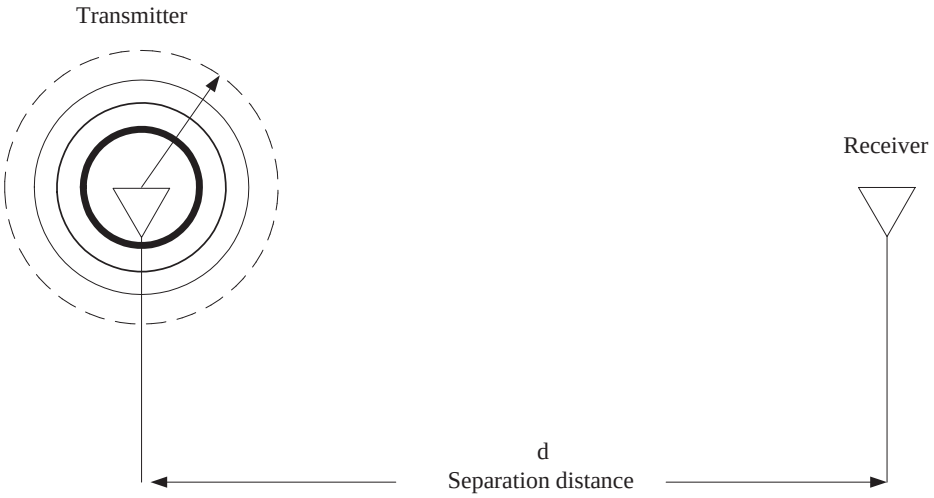

Figure 2.1: Free space propagation path loss.

2.2 Path loss and Shadowing

The loss in signal power at the receiver due to the wireless propagation medium is known as path loss [19]. Its characterization is based on environments such as free-space or rural and urban terrestrial, all of which lead to different modes of propagation. If the transmit signal power in Watts is represented by P_t and the corresponding received signal power by P_r, then, the path loss in a linear scale is defined [19] as

$$P_L = \frac{P_r}{P_t}. \tag{2.1}$$

Equivalently, in dB it is given by

$$P_{L,dB} = 10log_{10}\frac{P_r}{P_t}. \tag{2.2}$$

A free space path loss model as shown in Fig. 2.1 represents an idealized scenario based on there being one unobstructed path from transmitter to receiver, which are separated by a distance d. The propagated signal energy expands over a spherical wavefront and the *free-space* path loss formula [32] is given by

$$P_L = \frac{\lambda^2 G_t G_r}{(4\pi d)^2}, \tag{2.3}$$

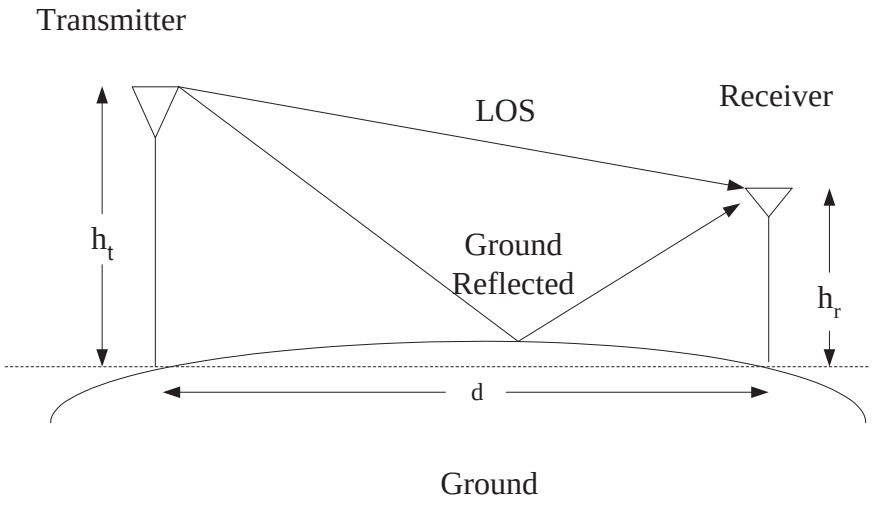

Figure 2.2: Terrestrial path loss.

where λ is the wavelength. The parameters G_t and G_r are the directional transmit and receive antenna gains, respectively. An important observation from (2.3) is that the received signal power is inversely proportional to the carrier frequency f_c^2 as $\lambda \propto \frac{1}{f_c}$. This implies that the received signal power falls quadratically with f_c. In contrast, using higher f_c improves antenna gains which can compensate for the increased pathloss. However, at higher frequencies, we can employ high gain dish antennas. For example at 5 GHz, we could in principal use a 3 metre dish and get almost 50 dB of antenna gain.

Large bandwidths are primarily available at high carrier frequencies (above 2GHz) and most broadband systems consider transmissions at these higher frequencies. Given that G_t and G_r are constants, path loss depends only on f_c and d. This implies that systems using higher f_c have access to larger bandwidths but have shorter communication range due to path loss. For example, the received signal power in (2.3) decreases by 6dB when the distance d or frequency f_c is doubled.

The path loss in a multipath environment is often different to the path loss occurring in a free-space environment. A simple example of multipath is shown in

Fig. 2.2. Here, a transmitted signal is reflected by the plane earth surface and the second component arrives at the receiver in addition to the direct LOS signal. This reflected signal may arrive with a phase shift and can destructively interfere with the LOS signal. This can cause more attenuation and transmission loss than the indicated free-space path loss. The multipath two-ray approximation for path loss is given by [33]

$$P_L = \left(\frac{h_t h_r}{d^2}\right)^2 G_t G_r, \tag{2.4}$$

where h_t and h_r are the transmit and receive antenna heights. Equation (2.4) results in an inverse-fourth power relationship between the received power and the distance, d, between the transmitter and the receiver. This two-ray approximation for path loss is also called vertical multipath [34]. This means that in a terrestrial or multipath propagation environment the signal power is attenuated more severely with distance. The additional signal power attenuation from (2.3) is 6dB, whereas from (2.4) it is 12dB when d is doubled. Note that unlike free-space path loss, the terrestrial path loss is not an explicit function of f_c. Knowledge of the path loss attenuation is essential in designing the link budget of any wireless communication system.

Wireless channels are usually non-line of sight (NLOS) channels and here the above description for path loss does not hold. For NLOS channels, empirical path loss models have been developed using experimental methods. Perhaps the simplest and most common empirical path loss formula is given by

$$P_L = P_0\left(\frac{d_0}{d}\right)^{\alpha}, \tag{2.5}$$

where the received signal power can be written as

$$P_r = P_t P_0\left(\frac{d_0}{d}\right)^{\alpha}. \tag{2.6}$$

Equation 2.6 models the various effects with two parameters, the path loss exponent α and the measured path loss P_0 at some reference distance d_0. The parameter α represents the rate of decay of signal power with distance d. For example, in free

space $\alpha = 2$. However, for environments cluttered with buildings, trees and terrain irregularities, α is determined empirically and can vary from 2 to 6. Typical values for α are between 3 and 4 [33, 35]. Widely used path loss models include the Hata Okamura model, the COST-231-Hata model, the Erceg model and the Walfisch Ikegami models each of which tends to emphasize slightly different aspects of the wave propagation [5, 32, 36].

In a multi-terminal network that is limited by interference, a large path loss is sometimes desirable in order to increase overall system capacity [4]. To illustrate the effect of path loss on system capacity, let us consider the example scenario shown in Fig. 2.3. Here, a desired base station is transmitting to a terminal (laptop computer) surrounded by several interfering base stations in the downlink of a BWA network.

For simplicity, we assume that the desired source base station and all interferers have the same common transmit power, P_t, path loss, P_0, and reference distance, $d_0 = 1$Km. Hence, the desired source and interferers only vary in their distance from the laptop. In the example, the user is at a distance of 0.5 km from the desired base station. There are three interfering base stations at a distance of 1 km, three at a distance of 2 km and six at a distance of 3 km. We temporarily neglect noise and examine the signal to interference ratio (SIR) of the desired base station for the two cases of $\alpha = 3$ and $\alpha = 5$. For $\alpha = 3$ and the desired base station's transmit power of $P_{t,D}$, the received power from (2.6) is given by

$$P_{r,D} = P_{t,D} P_0 (d_0)^{\alpha} (0.5)^{-\alpha} \tag{2.7}$$

$$= P_{t,D} P_0 (d_0)^{3} (0.5)^{-3}. \tag{2.8}$$

The total received interference power is

$$P_{r,I} = P_{t,I} P_0 (d_0)^{\alpha} [3(1)^{-\alpha} + 3(2)^{-\alpha} + 6(3)^{-\alpha}] \tag{2.9}$$

$$= P_t P_0 (d_0)^{3} [3(1)^{-3} + 3(2)^{-3} + 6(3)^{-3}]. \tag{2.10}$$

Given that all the base stations are transmitting at the same signal power level[1]

[1]Power measured in Watts

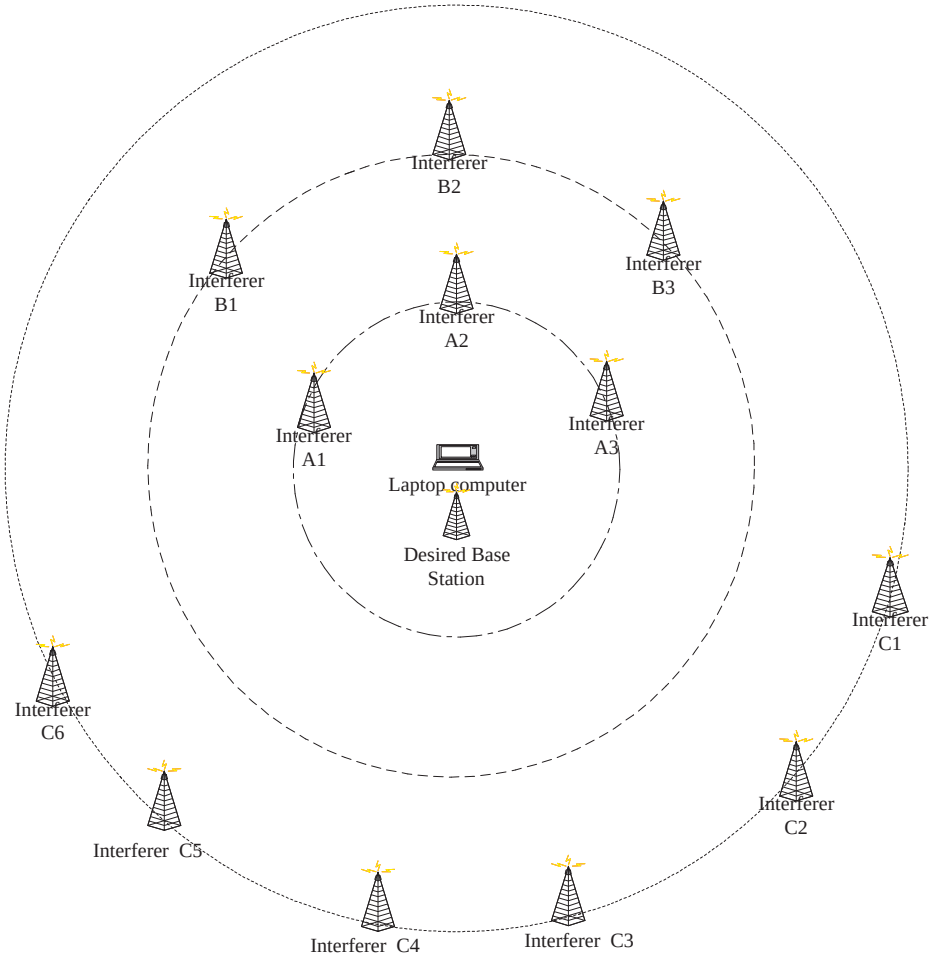

Figure 2.3: BWA communications in the downlink.

($P_{t,D} = P_{t,I}$), the SIR can be computed as

$$SIR(\alpha = 3) \quad = \quad \frac{P_{r,D}}{P_{r,I}} = 2.22. \tag{2.11}$$

Converting to dB and performing the same analysis for $\alpha = 5$ gives SIR for

$$(\alpha = 3) \quad = \quad 3.47dB \tag{2.12}$$

$$(\alpha = 5) \quad = \quad 10.11dB. \tag{2.13}$$

The received SIR thus increases as α increases. Clearly, a large path loss exponent α attenuates the signals from the more distant interferer more severely than the desired signal and leads to higher SIR. However, when the distances from the transmitters of the desired and the interfering signals to the receiver are the same, then

path loss effects both signals equally. Thus, investigating the fundamental wireless system trade-off between range and performance is essential for predicting overall system capacity [19].

In [36] and [37], a path loss model called the the Erceg model for suburban areas was proposed for fixed broadband systems operating at $f_c = 2GHz$. This model covers three major categories A, B and C, based on the most common terrain types. Category A considers hilly terrain with moderate to heavy tree densities and hence has a large path loss exponent α. Intermediate and minimum path loss conditions are captured in B and C categories respectively. Given a path loss exponent α, for a distance d_0, the Erceg path loss formula in dB is given by

$$P_{L,dB} = 20log_{10}\left(\frac{4\pi d_0}{\lambda}\right) + 10\alpha log_{10}\left(\frac{d}{d_0}\right) + s \tag{2.14}$$

where the shadowing effect is represented by the random variable s which typically follows a Gaussian distribution, which means that shadowing is modelled as a log normal random variable. Also note that even with a path loss exponent greater than 2 there is still a free space term which is wavelength dependent. Shadowing is discussed in more detail below.

Path loss, as discussed above, accounts for the distance-dependent relationship between the transmitter and the receiver. However, many other factors such as the location of trees and buildings and unknown obstructions between the transmitter and the receiver may result in long-term abnormal variation in received signal strength. This effect is called shadowing [4, 32].

2.3 Multipath Propagation

In addition to the foregoing, a broadband wireless channel is also characterized by multipath propagation. The transmitted signal propagates along many paths undergoing independent fading and arriving at the receiver at different time instants

resulting in a time spread of arrival, otherwise known as delay spread. The received signal is thus affected by multiple random attenuations and delays. The amplitude variation and phase rotation affects its contribution to the overall received signal. Two indicators of the severity of the multipath effect are the maximum delay spread, τ_{max}, and the root mean square (RMS) delay spread, τ_{rms}. The maximum delay spread represents the delay, τ_{max}, beyond which the received power is negligibly small [32]. The maximum delay spread is not necessarily the best indicator in predicting the system performance on a given channel. A more useful measure for channel dispersion is provided by the RMS delay spread given by [36]

$$\tau_{rms} = \sqrt{\sum_j P_j \tau_j^2 - (\tau_{avg})^2}, \tag{2.15}$$

where

$$\begin{aligned} \tau_{avg} &= \sum_j P_j \tau_j \\ \tau_j &\quad \text{is the delay of the } j^{th} \text{ delay component of the multipath profile} \\ P_j &= \frac{\text{Power in the } j^{th} \text{ delay component}}{\text{Total power in all components}}. \end{aligned}$$

In fading channels, the relationship between τ_{max} and the symbol period T_s can be viewed in terms of two different degradations, frequency-selective fading and frequency-non-selective or flat fading. A channel is said to exhibit frequency-selective fading if $\tau_{max} > T_s$ and frequency-flat fading occurs if $\tau_{max} < T_s$ [38]. If the channel is frequency-selective the received signal will be affected by inter-symbol interference (ISI). The distortion due to ISI can be mitigated using equalization [38]. In frequency-flat channels there is still some distortion in the system due to the destructive adding of multipath signals, but it is not easily countered using equalization. Counter measures in this latter case include power control and diversity schemes [4].

The above definition of ISI is based on spreading of the signal due to multipath propagation. In the FD, a statistical measure called the coherence bandwidth, f_B,

can be similarly defined and used to describe the fading nature of the wireless channel. The coherence bandwidth, f_B, represents the frequency range over which the channel passes all spectral components with approximately equal gain and linear phase. That is, a signal's spectral components within that bandwidth range are affected by the channel in a similar manner. Note that f_B and τ_{max} are approximately reciprocally related. An exact relationship between the two measures does not in general exist, and must be derived from an analysis of actual signal dispersions in particular channels [38].

In the FD, the relationship between coherence bandwidth, f_B, and the signal bandwidth, B, can be used to characterize the fading. If $f_B < \frac{1}{T_s} \approx B$, then frequency selective fading is said to occur. This means that spectral components of a signal are affected differently across the transmission band. Alternatively, if $f_B > \frac{1}{T_s} \approx B$ all spectral components will be affected by the channel in a similar manner resulting in flat-fading. Thus there is essentially no channel induced ISI if the channel coherence bandwidth is larger than the signal bandwidth.

On some wireless channels, the multipath delay spread spans less than 1 μs, but in other cases, it can span 10-20 μs [8]. In order to evaluate the performance of wireless systems, several channel models based on specific propagation environments have been developed [5] in order to account for large delay spreads. These include the Stanford University Interim (SUI) [36], the International Telecommunication Union (ITU) and the Wireless World Initiative New Radio (WINNER) channel models. Depending on the specific propagation environment, there are six different three-tap SUI channel models termed SUI 1-6. Similarly, there are six different six-tap ITU channel models and there are four different ten-tap WINNER channel models.

These channel models are all derived from actual measurements at radio frequencies in the frequency range of 2-11GHz in outdoor environments. In Table. 2.1, we present the mean delay spread, τ_{mean}, the rms delay spread, τ_{rms} and the maximum delay spread, τ_{max} for these channel models. From the table, the RMS

Channel Type	τ_{mean} μs	$\tau_{rms}\mu$s	τ_{max} μs
SUI-1	0.0208	0.1105	0.9
SUI-2	0.0548	0.2029	1.1
SUI-3	0.1529	0.2637	0.9
SUI-4	0.7909	1.2566	4
SUI-5	1.5993	2.8418	10
SUI-6	1.9268	5.2397	20
ITU Channel A (Indoor)	0.0245	0.0370	0.310
ITU Channel B (Indoor)	0.0675	0.0992	0.7
ITU Channel A (Outdoor-Indoor)	0.0144	0.0460	0.4
ITU Channel B (Outdoor-Indoor)	0.4091	0.6334	3.7
ITU Channel A (Vehicular)	0.2544	0.3704	2.5
ITU Channel B (Vehicular)	1.4981	4.0014	20
WINNER model B5A (LOS)	0.0104	0.0406	0.26
WINNER model C2 (NLOS)	0.2992	0.3130	14.7
WINNER model B1 LOS (LOS)	0.0141	0.0198	0.105
WINNER model B1 NLOS (NLOS)	0.1011	0.0947	0.485

Table 2.1: Comparison of multipath channel models.

delay spread is higher for the SUI channels than for the other models. The frequency responses of the SUI 1-6 channels with respect to digital frequency normalized to the signal bandwidth, fT_s is shown in Fig. 2.4. The ITU multipath channel models have higher RMS delay spread values than the WINNER channels but lower than the SUI channels. However, the ITU channels are six-tap models and exhibit deeper fades than the SUI models, therefore tending to provide a harsher propagation environment. The WINNER channels are derived based on small cell sizes and hence have smaller delay spread and reflect a more benign propagation environment. In this thesis we consider the SUI set of channel models that have highest rms τ_{rms} and maximum τ_{max} delay spreads. Using these models we investigate the complexity savings achieved by FD receiver processing in fixed broadband systems. In addition, we use ITU models and the 11 and 6 tap channel models as in [27, 28] so that direct comparisons can be made with the new receivers proposed in this thesis.

Clearly in a dispersive environment the ISI span depends on the delay spread and also the transmission data rate. For example, given a maximum delay spread of

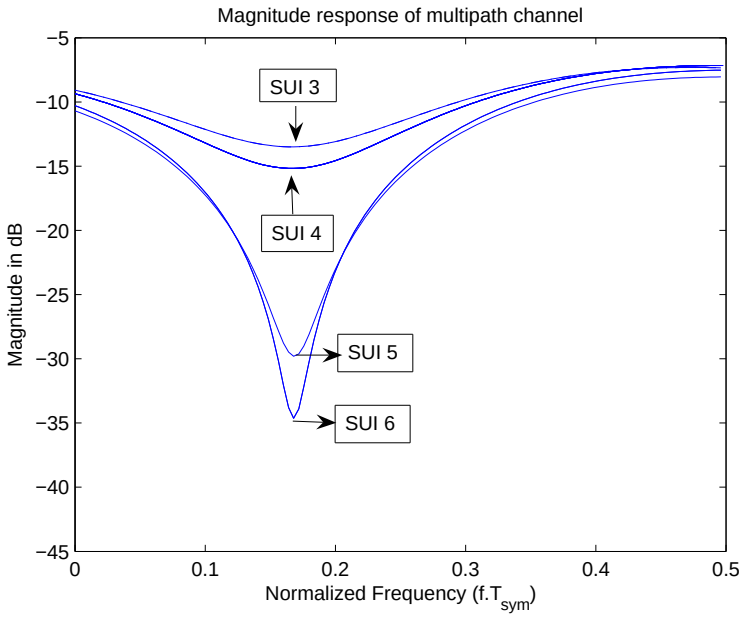

Figure 2.4: Frequency responses of SUI 3-6 channel models.

10μs with a data rate of 5-10 mega symbols per second (Msps), the ISI spans 50-100 data symbols. In order to compensate for this, channel equalization is necessary. Traditionally, equalization is implemented in the TD using a time domain equalizer (TDE). It typically consists of one or more transversal filters for which the number of tap coefficients is in the order of the number of data symbols spanned by the multipath. The complexity of implementing the TDE is very high when the channel dispersion is large. For example, in a typical outdoor propagation environment the maximum ISI span could be 100 symbols. Here the complexity of the TDE is of the order of several hundred multiplications per data symbol. Although TDE and FDE exhibit similar performance in terms of bit error rate (BER), FDE is less computationally expensive than TDE on such highly dispersive channels.

2.4 Fading

The amplitude of the received signal in fading environments is often modeled by a Rayleigh distribution when the channel is NLOS, and by a Rician distribution

when there is a LOS component in the received signal [10, 33]. In both cases the phase is uniformly distributed between 0 and 2π. In addition, the LOS signal gain or attenuation is commonly modeled by a lognormal distribution to characterize the effect of shadowing. Mathematically, these fading distributions is described in the following subsections.

2.4.1 Rayleigh Fading

In a Rayleigh fading environment the gain of each of the multipath components can be represented as a complex Gaussian random variable [39] given by

$$h = h_x + jh_y, \tag{2.16}$$

where h_x and h_y each have zero mean and variance equal to σ^2. Both h_x and h_y are Gaussian random variables with probability distribution function (pdf)

$$p(h_x) = \frac{1}{\sqrt{2\pi\sigma^2}} e^{\frac{-h_x^2}{2\sigma^2}}, \tag{2.17}$$

$$p(h_y) = \frac{1}{\sqrt{2\pi\sigma^2}} e^{\frac{-h_y^2}{2\sigma^2}}. \tag{2.18}$$

The amplitude A and the phase θ of (2.16) are given by

$$A = |h| = \sqrt{h_x^2 + h_y^2} \tag{2.19}$$

$$\theta = tan^{-1}\left(\frac{h_y}{h_x}\right). \tag{2.20}$$

The amplitude has a Rayleigh pdf, $p(A)$, given by

$$p(A) = \begin{array}{ll} \frac{A}{\sigma^2} e^{\frac{-A^2}{2\sigma^2}} & A \geq 0 \\ 0 & A < 0 \end{array}, \tag{2.21}$$

and the phase has a uniform distribution

$$p(\theta) = \frac{1}{2\pi} \quad 0 \leq \theta < 2\pi. \tag{2.22}$$

2.4.2 Rician Fading

The multipath fading when a LOS signal component exists in the received signal is commonly described by the Rician distribution. In this situation the multipath gain is a non-zero mean complex Gaussian random variable defined by

$$h = C + h_x + jh_y \tag{2.23}$$

where C is a constant and the PDFs of h_x and h_y are as defined by (2.17) and (2.18), respectively. Its quite possible for C to include the log normal effect of shadowing, which is very slow. This is usually true. The amplitude, A, of h is given by

$$A = |h| = \sqrt{(C + h_x)^2 + h_y^2}, \tag{2.24}$$

and the phase, θ given by

$$\theta = tan^{-1}\Big(\frac{h_y}{C + h_x}\Big). \tag{2.25}$$

The variable A then has a Rician PDF given by

$$p(A) = \begin{cases} \frac{A}{\sigma^2} e^{\frac{-(A^2+C^2)}{2\sigma^2}} I_0\left(\frac{AC}{\sigma^2}\right) & A \geq 0 \\ 0 & A < 0 \end{cases} \tag{2.26}$$

where I_0 is the modified Bessel function of order 0. An important quantity that measures the nature of the fading is the K-factor defined as

$$K = \frac{A^2}{2\sigma^2}. \tag{2.27}$$

A high K-factor, usually $K \gg 1$, indicates that the LOS signal is so strong that the channel is similar to an additive white Gaussian noise (AWGN) channel without fading. When $K \ll 1$ the LOS signal is weak and the channel is approximately Rayleigh as described in (2.16)- (2.22).

2.5 Doppler Spread

A major potential application of broadband wireless is in the mobile communication environment. In this context, broadband communication typically takes place

between a base station and the mobile receiver and is termed mobile BWA (MBWA) [6]. The velocity of the mobile receiver relative to the base station generates Doppler frequency shifts, and consequently spectral spreading, which is termed Doppler spread. In the case of fixed broadband applications, Doppler frequency shifts although small, still need to be accounted for on each of the multipath components. For example, a communication link between a base station and a building is fixed, but Doppler shifts of the multipath components can be caused by movement in the environment. The power spectral density (PSD) including these effects for fixed broadband applications with a maximum doppler frequency f_m is typically modeled as [36]

$$S(f) = \begin{cases} 1 - 1.72{f_0}^2 + 0.785{f_0}^4 & |f_0| \leq 1 \\ 0 & |f_0| > 1 \end{cases} \tag{2.28}$$

where $f_0 = \frac{f}{f_m}$ represents frequency normalized to f_m. In fixed broadband channels, the Doppler PSD of the scatter component is primarily distributed around 0Hz as can be seen from Fig. 2.5. Practical measurements at 2.5 GHz frequency show f_m values of about 2 Hz. This is mainly due to the wind speed combined with foliage (trees), carrier frequency, and traffic density.

In many mobile channels the Doppler spectrum when a mobile receiver is moving with velocity v and transmitting at a carrier frequency f_c is often modeled as [6, 34]

$$S(f) = \begin{cases} \frac{\sigma^2}{\pi f_m \sqrt{(1-(f/f_m)^2)}} & -f_m \leq f \leq f_m, \end{cases} \tag{2.29}$$

where σ^2 is the average power of the received signal.

The fading rapidity of the channel, usually designated either fast or slow fading, is measured in terms of the channel coherence time, T_c. The channel is described as fast fading, when the time duration in which the channel behaves in a correlated manner is short compared to the the symbol duration, *i.e.,* $T_c \ll T_s$. The channel is said to introduce slow fading when $T_c \gg T_s$. Most BWA channels being considered for fixed applications have T_c in the order of a few milliseconds and T_s typically

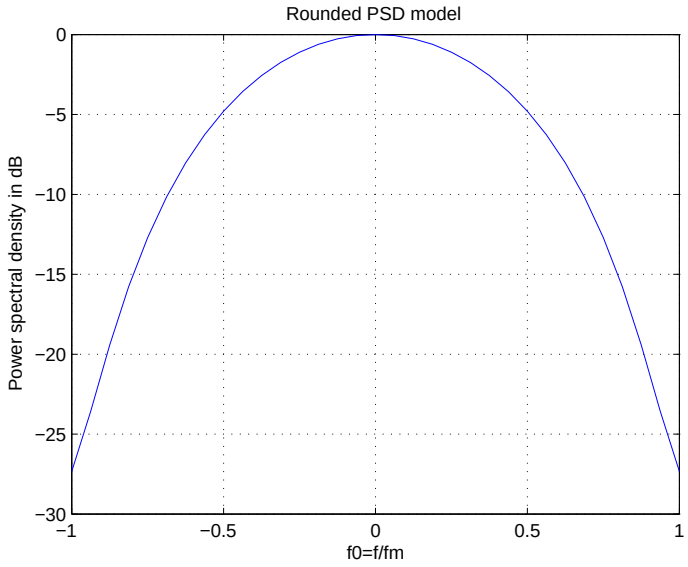

Figure 2.5: Doppler spectrum for fixed broadband channels

less than a microsecond [36]. Hence, the fading characteristics of the fixed broadband channel remain virtually unchanged for a long time compared to the symbol duration. However, in mobile applications the fading characteristics change more rapidly and the signal distortion can change from symbol to symbol. The maximum Doppler frequency f_m is inversely proportional to T_c and is is often modelled as [5]

$$f_M \approx \frac{9}{16\pi T_c} Hz. \tag{2.30}$$

2.6 Interference

As has been noted earlier, cochannel interference (CCI) and ISI are two major forms of interference that limit spectral efficiency and performance. While ISI occurs due to the temporal interference between successive data symbols particularly at very high data rates, CCI occurs due to spatial interference between signals using the same carrier frequency. CCI can result from various sources. For example, multiple signals transmitted from spatially independent antennas cause CCI due to mutual interference. In a multi-user scenario different user signals may interfere with each

other resulting in additional CCI. In high performance receivers, the effects of both types of interference must be compensated.

2.7 Diversity Techniques

In wireless systems, fading makes reliable communication extremely difficult. One way to overcome its effect is to employ transmit diversity techniques which amounts to transmitting the same information on multiple independently fading channels [10]. Diversity techniques exploit the fact that independent signal paths have low probability of simultaneously experiencing severe fades [19]. In other words the fading on different channels is essentially uncorrelated. The main aim of all diversity techniques is for the receiver to have multiple essentially independent copies of the transmitted signal. Common forms of diversity are spatial diversity (MIMO), temporal diversity and frequency diversity. Frequency selective fading leads to implicit delay diversity, which can be exploited. However, it should be noted that one can use explicit frequency diversity, where the same signal is transmitted on two or more carrier frequencies. Low levels of fading correlation between the various signal components is an important requirement for the employment of diversity.

The use of multiple antennas at the transmitter and/or the receiver is one way of realizing spatially independent fading paths. With receive spatial diversity, independent fading paths are realized without an increase in transmit signal power or bandwidth [40]. However, the spacing between receive antennas and the angle spread of the incoming rays is required to be large enough to exploit the spatial diversity [41]. Diversity combining techniques such as selection diversity combining, equal gain combining and maximal ratio combining can be used to realize the spatial diversity. Other diversity methods include polarization, angle and frequency diversity [10, 41].

Time diversity is achieved by transmitting the signal on different time slots with

a time separation of at least the channel coherence time T_c. For example, interleaving (often used with the error correction coding) is a form of time diversity [39]; however, very long interleavers are often required for this [42]. Frequency diversity is achieved by transmitting the signal on different frequencies with a frequency separation of at least the channel coherence bandwidth f_B. A FD technique that exploits frequency diversity without bandwidth expansion is OFDM. The signal bandwidth in OFDM is partitioned into multiple subbands, each exhibiting a lower symbol rate than the original signal. The basic concept of OFDM is discussed in more detail in the following.

2.8 Frequency Domain Processing

For SC transmission, ISI is traditionally compensated by the use of a TDE. Its complexity grows exponentially with the delay spread [23]. Hence, this approach is usually not considered for use in wideband wireless receivers on highly dispersive channels. When multi-carrier based OFDM transmission is employed [43], equalization complexity tends to be lower. This has lead to the finding for SC transmission that rather than TD equalization, frequency-domain equalization (FDE) is a promising solution [8]. The overall system is known as SC-FDE. FDE was first investigated by Walzman and Schwartz [44] in 1973. In [44] the authors showed that adaptive channel equalization in the FD leads to a lower computational complexity and offers better convergence properties compared to the TD approach.

Both SC-FDE and OFDM rely on FD processing through the convolution theorem which states that,

> *"circular convolution of two discrete-time signals corresponds to component-wise multiplication of their Fourier transforms"* [45, 46].

Generally, the received signal is a linear convolution of the transmitted signal with the multipath channel. Circularity is induced in the transmission by inserting a

cyclic prefix (CP) at the beginning of each frame [8]. A CP is a repetition of the last symbols at the beginning of the frame, where the length of the prefix is chosen to be at least as large as the channel delay spread. Because of the use of fast Fourier transform (FFT) techniques, the received signals have to be processed on a per-block basis. Effectively, the CP allows successive data blocks or frames to be sufficiently separated that their Fourier transform can be done in an isolated manner and there is no inter-block interference. Convolution of this CP inserted frame with the channel is calculated by circular convolution. This in the FD is equivalent to component-wise multiplication of the Fourier transform of the non-cyclically extended transmission frame with the channel frequency response. The CP acts as a guard interval that eliminates the interference between successive data blocks.

Another way to achieve pseudo periodicity is to transmit a known sequence, called the unique word in place of CP[2] , as a part of every transmission frame. This has the added benefit that the unique word can be exploited for channel estimation. In order to eliminate the interblock interference, the length of the unique word should be greater than the maximum ISI span of the channel [8, 23].

In the following subsections, we briefly describe two examples of systems employing frequency domain processing. One is a SC system and the other is an OFDM system. The objective here is to illustrate the similarity in system structure and complexity of the two.

2.8.1 SC-FDE System

The block diagram of a typical SC system employing FDE is depicted in Fig 2.6. Successive groups of $log_2 M$ information bits are mapped into complex symbols belonging to a M-ary complex constellation. Transmission is organized in blocks of N_s symbols. Each block is cyclically extended by inserting a CP or unique word as shown in Fig. 2.6. Then, pseudo-periodicity is induced over a block-length

[2]For SC-FDE systems, the overhead due to the CP can be eliminated by using the overlap-save processing at the receiver, at the expense of increased receiver complexity [23].

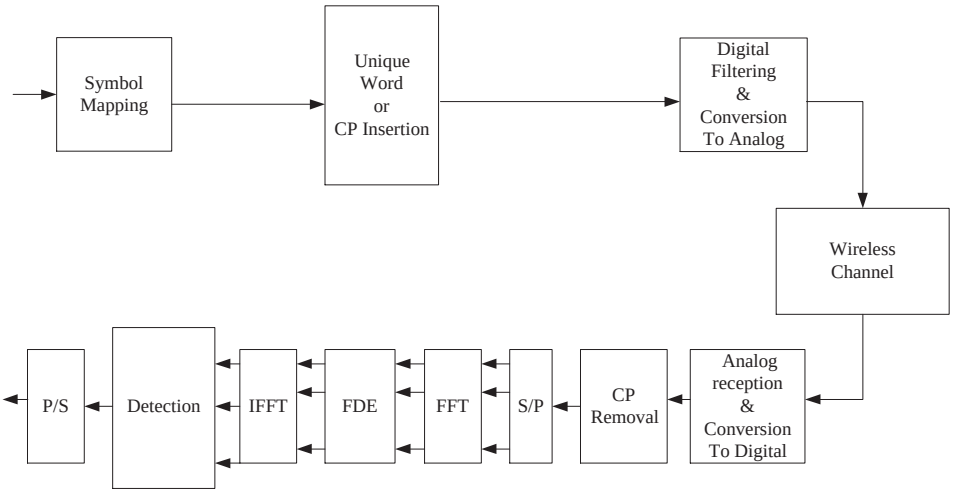

Figure 2.6: SC-FDE communication block diagram.

observation interval in the transmitted signal, at the price of a bandwidth or energy loss [47].

The transmitted symbol sequence then passes through a digital-to-analog converter, and is then up-converted to a radio frequency which is followed by filtering. The resulting radio frequency signal is transmitted over the dispersive wireless channel. At the receiver, the signal undergoes frequency down-conversion followed by sampling and analog-to-digital (A/D) conversion, producing a sequence of noisy samples. These are grouped into equal-length blocks, each associated with a transmitted data block. The samples corresponding to the CP are discarded and the resulting block is Fourier transformed using the FFT algorithm. The FDE then performs component-wise channel inversion producing a FD estimate of the signal. Note that FD channel inversion is simple component-wise inverse. An IFFT operation then transforms the resulting FD signal back into the TD. Finally, data decisions are made on the TD block of data symbols.

2.8.2 OFDM System

An OFDM system is illustrated in Fig. 2.7 [48–50]. The OFDM and SC-FDE systems have many similarities as is evident on comparing their system block diagrams

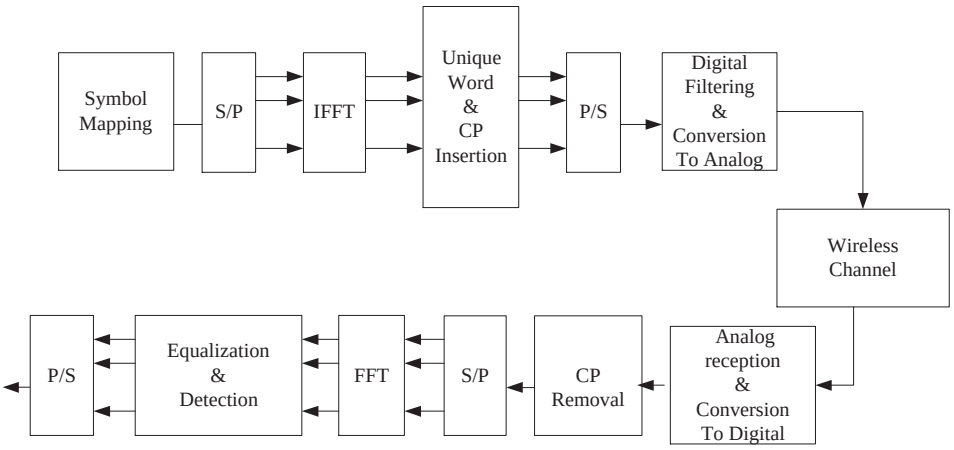

Figure 2.7: OFDM communication block diagram.

in Fig. 2.6 and Fig. 2.7, respectively. However, a difference is the implementation of IFFT processing at the transmitter for OFDM. After this, each block is cyclically extended and undergoes parallel to serial conversion followed by A/D conversion, up-conversion to radio frequency and filtering similar to the SC system. It can be shown that, in this case, the transmitted signal associated with each data block consists of a superposition of oscillations over a limited time interval, each associated with a distinct information symbol and a specific subcarrier frequency. Over that interval, the family of complex oscillations forms a set of orthogonal signals and this property plays an important role, since it simplifies the task of separating their contributions in the detection process. Note that the generation of multiple waveforms is accomplished by utilizing IFFT processing in the baseband section of the OFDM modulator.

Some of the differences and similarities between the systems of this and the preceding section are as follows:

- In both SC-FDE and OFDM, one FFT and one IFFT are employed to process each block of symbols. In the OFDM system, an IFFT is used in the transmitter and an FFT is used in the receiver for demodulation, whereas in the SC system all FD signal processing involving both an FFT and an IFFT is implemented at the receiver.

- The overall complexities of both these systems are comparable as both involve similar signal processing functions.

- A CP or unique word of duration longer than the maximum ISI span is typically used to eliminate the inter-block interference in both systems. This enables independent block processing and the linear convolution associated with channel filtering is turned to a circular convolution. This fundamental principle greatly simplifies equalization in both systems.

- Unlike SC systems, OFDM systems suffer from impairments related to the large dynamic range of the transmitted signal, frequency nulls in the channel frequency response and also from sensitivity to carrier frequency offset in demodulation.

- The complexity of SC systems is located only at the receivers and so it is very useful for deployment in the uplink.

Since the OFDM signal is the sum of multiple sinusoids modulated by independent information symbols, its envelope has a large dynamic range which is characterized by the high peak-to-average power ratio (PAPR). Due to this, the linearity requirements of the analog front-end for OFDM increases dramatically especially when the FFT size is large. However, it is worth noting that as the SC signal constellation size increases the advantage for SC systems in terms of PAPR over OFDM systems reduces [48, 50, 51].

Frequency synchronization represents a critical task for the OFDM receiver because residual frequency offset in the demodulation process produces interference between adjacent sub-carriers, known as inter-carrier-interference, which causes a loss of orthogonality between sub-carriers. Since data decisions are made in the FD, a null close to the frequency of a sub-carrier can result in loss of associated information unless powerful channel coding is employed. An un-coded CP-based OFDM system is then unable to exploit multipath diversity and its error rate performance

is dominated by its sub-carriers having lowest signal-to-noise ratio (SNR). In practical applications, this loss can be circumvented by incorporating channel coding in conjunction with frequency-interleaving among sub-carriers. In contrast, in SC systems, decisions on the received data are taken in the TD and the averaging effect of the IFFT operation mitigates the dominating effect of low-SNR sub-carriers on the overall performance [47]. A mixed-mode modem using SC-FDE for up-link transmission and OFDM for downlink transmission is a promising transceiver solution and is being considered for use in future BWA systems such as long term evolution (LTE) [4, 52]. The benefits achieved are summarized as follows:

- The signal processing complexity is concentrated at the base station performing two inverse FFT operations and one FFT, while the subsciber performs just one FFT for receiving the downlink OFDM signal.
- As noted in the above discussion, the SC transmitter is inherently more efficient than an OFDM system transmitter in terms of power consumption, due to the reduced power back-off requirement. This significantly reduces the cost of the power amplifier. On the other hand, the use of OFDM in the downlink minimizes the FFT processing in the subscriber unit.
- Moreover, in the uplink, SC transmission lengths can be adjusted to maximize the efficiency unlike OFDM transmission which requires transmission lengths as multiples of the FFT block lengths and hence is not as efficient as SC uplink.

2.9 Summary

Fundamental factors affecting broadband channels are examined in this chapter. To evaluate the performance of the broadband systems, three different multipath channel models, namely SUI, ITU and WINNER, have been considered. The SUI-5 and 6 channels exhibit large RMS and maximum delay spreads leading to long ISI

spans. This results in deeper spectral nulls in the channel frequency response. Both OFDM and SC-FDE practical equalization solutions that result in lower complexity compared to traditional SC-TDE. Some of the inherent problems with OFDM systems such as high PAPR, carrier synchronization and frequency offset issues can be overcome by SC-FDE. Hence, in this thesis, we focus on the use of broadband SC-FDE systems in the MIMO context.

Chapter 3

Channel Estimation and Equalization

In this chapter, we first discuss state-of-the art channel estimation techniques used in conjunction with SC-FDE systems. Specifically, we compare the existing time and frequency domain channel estimation techniques in a MIMO context. Secondly, we focus on a TD approach that estimates the MIMO channel based on a composite channel model [21, 30, 53]. This approach performs parallel processing and computes the MIMO CSI corresponding to each transmitter in parallel. Due to parallel processing, the channel estimation approaches of [21,30,53] have lower processing time than most previous time or frequency domain channel estimation approaches. Finally, we review existing linear and non-linear FD receiver architectures used with MIMO SC systems.

3.1 MIMO Channel Estimation

Broadband MIMO channel estimation is in general computationally expensive due to the large number of channel parameters to be estimated. A focus of the research in this thesis is the development of a novel low-complexity algorithm for estimating the CSI of broadband MIMO channels for use in implementing FD receiver processing. The MIMO channel frequency response is required to implement a

FD receiver [12]. This can be obtained using either time or frequency domain approaches. The TD approach estimates the MIMO channel impulse response which is then Fourier transformed to obtain the channel frequency response. In contrast, the FD approach directly estimates the channel frequency response.

The FD approach transforms signals through FFT's and performs channel frequency response estimation as described in [12]. Given the FFT size, N_s, this approach requires the estimation of N_s complex parameters to identify the channel frequency response. Channel estimation in the TD of a multipath component is characterized by a single amplitude and phase, whereas in the FD it is embedded in N_s amplitudes and phases. These amplitudes and phases are all inter-related, but correctly building this relationship into a FD estimator amounts to operating in the TD [9].

In the following, we compare the maximum likelihood based time and frequency domain approaches. The comparison is based on channel estimation mean square errors and shows the computational superiority of the TD channel estimation approach.

Notation: Upper case bold italic font is used to represent FD vectors (e.g., $\boldsymbol{\mathcal{H}}$) and lower case bold font is used for TD vectors (e.g., $\mathbf{h}$). A matrix is represented with a bar on top of the corresponding variables (e.g.,$\overline{\boldsymbol{\mathcal{H}}}$ and $\overline{\mathbf{h}}$). $E[.]$ is used to denote the expected value of a random process, and $||.||^2$ denotes the squared Euclidean norm. The operators $(.)^T$,$(.)^*$,$(.)^H$ and $(.)^{-1}$ are used to represent the transpose, complex conjugate, complex conjugate transpose and inverse operations, respectively. Finally, $\otimes$ represents the Kronecker product.

3.1.1 Time Domain Estimation

Channel estimation in the TD is often preferable to FD approaches as usually the estimation of fewer unknowns can characterize the multipath channel [9]. For example, using TD estimation an M-transmit and N-receive antenna system communicating over a multipath channel with an ISI span of v symbol periods requires the estimation of $M \cdot N \cdot v$ complex parameters. In the FD, channel estimation complexity is in part determined by the FFT size, N_s, and $M \cdot N \cdot N_s$ complex parameters must be estimated. Usually, FD receivers use a value of N_s much greater than v in order to exploit the advantages of FD receiver processing and to minimize the signalling overhead [8, 9, 23].

MIMO channel estimation is often based on the transmission of independent training sequences from each of the transmit antennas [28, 54, 55]. The receiver then performs some form of least-squares channel estimation upon receiving the channel distorted training sequences. This approach is fairly straight-forward for single input single output (SISO) systems. However, for MIMO using SM, it is a non-trivial problem as the training sequences interfere with each other. In order to overcome this, the training sequences are usually designed to be orthogonal either in the time or the frequency domains [28, 54, 55]. Then, MIMO channel estimation is reduced to the estimation of a set of M SIMO channel vectors.

Orthogonality in the TD may be achieved by time division multiplexing (TDM) of training symbols as shown in Fig. 3.1 [26]. Channel estimation can then be performed sequentially at the receiver. Due to this, the received signal in the TD is free from CCI. In the following, the mean squared error (MSE) of the least-squares based TD channel estimation employing TDM training is analyzed.

We start by defining the m^{th} training sequence consisting of a p[1] symbol vector

$$\mathbf{s}_m = [\ s_m(0) \quad s_m(2) \quad \ldots \quad s_m(p-1)\ ], \tag{3.1}$$

with $E[s_m(j)s_m^*(j)] = \sigma_a^2$. A $v \times p$ matrix $\bar{\mathbf{s}}_m$ formed from (3.1) with the current

[1] length p is chosen to be longer than the channel maximum delay spread in symbol periods

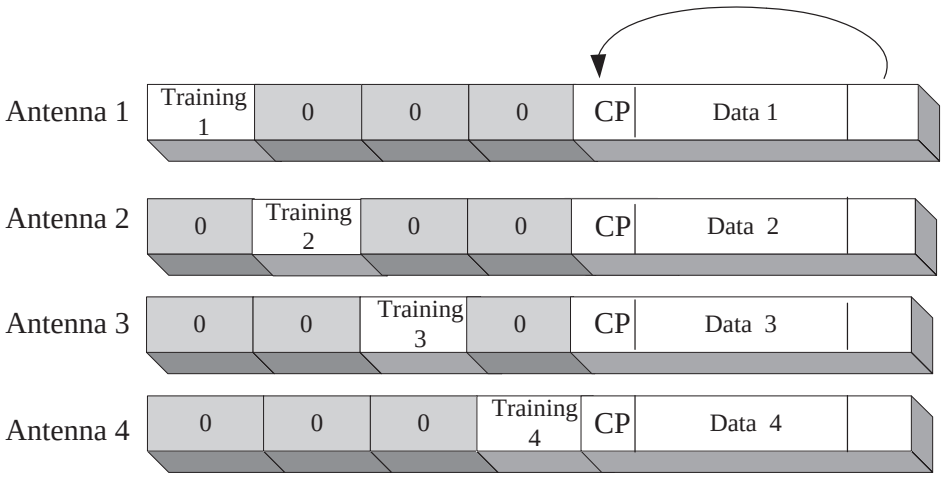

Figure 3.1: TDM-Training.

and $v-1$ previously transmitted training symbols[2] is given by

$$\overline{\mathbf{s}}_m = \begin{pmatrix} s_m(0) & s_m(1) & \dots & s_m(p-1) \\ s_m(-1) & s_m(0) & \dots & s_m(p-2) \\ \vdots & \ddots & \ddots & \vdots \\ s_m(-v+1) & \dots & & s_m(p-v) \end{pmatrix}. \tag{3.2}$$

A multipath channel, with a maximum delay spread of v symbols between the m^{th} transmitter and the n^{th} receiver may be represented by the vector

$$\mathbf{h}_{m,n} = [\ h_{m,n}(0) \quad h_{m,n}(1) \quad \dots \quad h_{m,n}(v-1)\ ], \tag{3.3}$$

as described in chapter 2. The channel matrix representing the paths between the m^{th} transmitter and the N receivers may then be written as

$$\overline{\mathbf{h}}_m = \begin{pmatrix} \mathbf{h}_{m,1} \\ \mathbf{h}_{m,2} \\ \vdots \\ \mathbf{h}_{m,N} \end{pmatrix}. \tag{3.4}$$

[2]Since the channel has memory v, the first $v-1$ training symbols of each block are used for clearing the channel memory.

A $N \times p$ matrix $\overline{\mathbf{y}}$ represents the received signal for the m^{th} training signal at the receiver array and is expressed as[3]

$$\overline{\mathbf{y}} = \overline{\mathbf{h}}_m \overline{\mathbf{s}}_m + \overline{\mathbf{n}}, \tag{3.5}$$

where the $N \times p$ matrix $\overline{\mathbf{n}}$ is the additive white Gaussian noise (AWGN) with $E[n(j)n^*(j)^2] = \sigma_n^2$. In the following, we drop the subscript m for brevity.

It is useful to rewrite (3.5) in vector form. For this we need some notation for the vectorization of the relevant matrices. Hence we define

$$\text{VEC}(\overline{\mathbf{y}}) = \overline{\mathbf{y}}_{\text{VEC}} \tag{3.6}$$

$$\text{VEC}(\hat{\overline{\mathbf{h}}}) = \hat{\overline{\mathbf{h}}}_{\text{VEC}} \tag{3.7}$$

$$\text{VEC}(\overline{\mathbf{h}}) = \overline{\mathbf{h}}_{\text{VEC}} \tag{3.8}$$

$$\text{VEC}(\overline{\mathbf{n}}) = \overline{\mathbf{n}}_{\text{VEC}} \tag{3.9}$$

where $(\hat{\overline{\mathbf{h}}})_{\text{VEC}}$ is the channel estimate defined in (3.13) below. Using the above definitions we can represent (3.5) in vector form as

$$\overline{\mathbf{y}}_{\text{VEC}} = (\overline{\mathbf{s}}^T \otimes \overline{\mathbf{I}}_N)\overline{\mathbf{h}}_{\text{VEC}} + \overline{\mathbf{n}}_{\text{VEC}}. \tag{3.10}$$

The maximum likelihood estimation of the channel $\overline{\mathbf{h}}_{\text{VEC}}$ from the received training signal is equivalent to minimizing the following metric [12]

$$||\overline{\mathbf{y}}_{\text{VEC}} - (\overline{\mathbf{s}}^T \otimes \overline{\mathbf{I}}_N)\overline{\mathbf{h}}_{\text{VEC}}||^2. \tag{3.11}$$

Minimization of (3.11) yields the maximum likelihood estimate[4]

$$\hat{\overline{\mathbf{h}}}_{\text{VEC}} = ((\overline{\mathbf{s}}^*\overline{\mathbf{s}}^T)^{-1}\overline{\mathbf{s}}^* \otimes \overline{\mathbf{I}}_N)\overline{\mathbf{y}}_{\text{VEC}}. \tag{3.12}$$

On substituting (3.10) in (3.12) we have

$$\hat{\overline{\mathbf{h}}}_{\text{VEC}} = ((\overline{\mathbf{s}}^*\overline{\mathbf{s}}^T)^{-1}\overline{\mathbf{s}}^* \otimes \overline{\mathbf{I}}_N)[(\overline{\mathbf{s}}^T \otimes \overline{\mathbf{I}}_N)\overline{\mathbf{h}}_{\text{VEC}} + \overline{\mathbf{n}}_{\text{VEC}}]. \tag{3.13}$$

[3]Due to the transmission of time orthogonal training sequences, there is no interference from other transmitters during the channel estimation period.

[4]This is a linear estimate and is optimum only when the quantities being estimated and the underlying statistics are Gaussian.

The channel estimation error vector from (3.13) is then given by

$$\hat{\overline{\mathbf{h}}}_{\text{VEC}} - \overline{\mathbf{h}}_{\text{VEC}} = ((\overline{\mathbf{s}}^*\overline{\mathbf{s}}^T)^{-1}\overline{\mathbf{s}}^* \otimes \overline{\mathbf{I}}_N)\overline{\mathbf{n}}_{\text{VEC}}, \tag{3.14}$$

and the error covariance matrix by

$$\begin{aligned}
\overline{\Gamma}_{TD} &= E[(\hat{\overline{\mathbf{h}}}_{\text{VEC}} - \overline{\mathbf{h}}_{\text{VEC}})(\hat{\overline{\mathbf{h}}}_{\text{VEC}} - \overline{\mathbf{h}}_{\text{VEC}})^H] && (3.15)\\
&= E[\Big(((\overline{\mathbf{s}}^*\overline{\mathbf{s}}^T)^{-1}\overline{\mathbf{s}}^* \otimes \overline{\mathbf{I}}_N)\overline{\mathbf{n}}_{\text{VEC}}\Big)\Big(((\overline{\mathbf{s}}^*\overline{\mathbf{s}}^T)^{-1}\overline{\mathbf{s}}^* \otimes \overline{\mathbf{I}}_N)\overline{\mathbf{n}}_{\text{VEC}}\Big)^H] && (3.16)\\
&= E[\Big(((\overline{\mathbf{s}}^*\overline{\mathbf{s}}^T)^{-1}\overline{\mathbf{s}}^* \otimes \overline{\mathbf{I}}_N)\Big)\overline{\mathbf{n}}_{\text{VEC}}\overline{\mathbf{n}}_{\text{VEC}}^H\Big(((\overline{\mathbf{s}}^*\overline{\mathbf{s}}^T)^{-1}\overline{\mathbf{s}}^* \otimes \overline{\mathbf{I}}_N)\Big)^H] && (3.17)
\end{aligned}$$

As $E[\overline{\mathbf{n}}_{\text{VEC}}\overline{\mathbf{n}}_{\text{VEC}}^H] = \sigma_n^2\overline{\mathbf{I}}_N p$, $\overline{\Gamma}_{TD}$ reduces to

$$\begin{aligned}
\overline{\Gamma}_{TD} &= \sigma_n^2\left(((\overline{\mathbf{s}}^*\overline{\mathbf{s}}^T)^{-1}\overline{\mathbf{s}}^* \otimes \overline{\mathbf{I}}_N)\right)\left(((\overline{\mathbf{s}}^*\overline{\mathbf{s}}^T)^{-1}\overline{\mathbf{s}}^* \otimes \overline{\mathbf{I}}_N)^H\right) && (3.18)\\
&= \sigma_n^2\left((\overline{\mathbf{s}}^*\overline{\mathbf{s}}^T)^{-1} \otimes \overline{\mathbf{I}}_N\right). && (3.19)
\end{aligned}$$

The TD-MSE is obtained by taking the trace of (3.19) and is given by

$$\begin{aligned}
MSE_{TD} &= Tr(\Gamma_{TD}) && (3.20)\\
&= NTr(\overline{\mathbf{s}}^*\overline{\mathbf{s}}^T)^{-1}\sigma_n^2 && (3.21)
\end{aligned}$$

For optimal training, it is necessary to satisfy the following

$$\overline{\mathbf{s}}^*\overline{\mathbf{s}}^T \propto \overline{\mathbf{I}}_v. \tag{3.22}$$

Considering optimal training and assuming that the v rows of $\overline{\mathbf{s}}$ of (3.1) are linearly independent, we can apply the result on optimal training given in [12]. This result states that if

$$Tr(\overline{\mathbf{s}}^*\overline{\mathbf{s}}^T) \leq v, \tag{3.23}$$

where v is the maximum delay spread or ISI span in symbols then,

$$Tr\big((\overline{\mathbf{s}}^*\overline{\mathbf{s}}^T)^{-1}\big) \geq v, \text{ with equality if and only if } \overline{\mathbf{s}}^*\overline{\mathbf{s}}^T = \overline{\mathbf{I}}_v. \tag{3.24}$$

Using (3.24), we can write (3.20) as

$$MSE_{TD} \geq N\sigma_n^2 v. \tag{3.25}$$

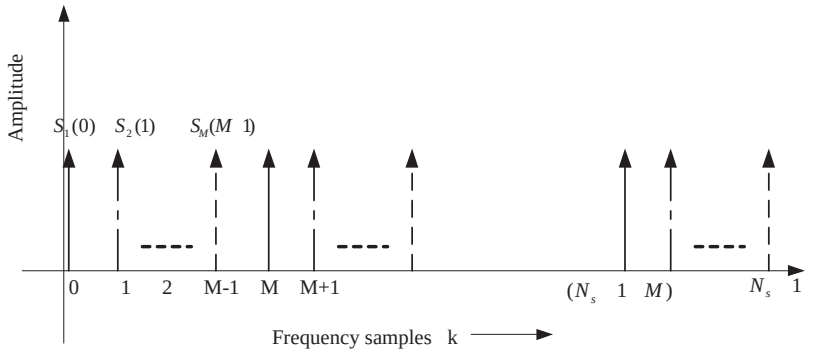

Figure 3.2: FDM-Training.

3.1.2 Frequency Domain Estimation

In this section, we discuss frequency domain channel estimation based on [26, 28]. of the estimators In [26,28], the training sequences corresponding to different transmitters are orthogonal in the FD as illustrated in Fig. 3.2. A simple method to generate a set of FD orthogonal training sequences based on [28] is summarized here.

Firstly, a base TD sequence $\mathbf{s}$ of length $p << N_s$ is zero-padded to form a length N_s vector. This is then Fourier transformed to form a length N_s FD training vector. From this, M sub-vectors that consist of non-overlapping frequency components are formed and used as training signals for the M transmitters. The k^{th} component of the FD training signal for a transmitter is given by

$$\mathcal{S}(k) = \sum_{j=0}^{N_s-1} s(j) e^{-i2\frac{\pi}{N_s}kj} \qquad k = 0, 1, \ldots, N_s - 1, \tag{3.26}$$

and the resulting FD signal by

$$\boldsymbol{\mathcal{S}} = [\ \mathcal{S}(0) \quad \mathcal{S}(1) \quad \ldots \quad \mathcal{S}(k) \quad \ldots \quad \mathcal{S}(N_s - 1)\ ]. \tag{3.27}$$

From (3.27), M sub-vectors are obtained by allocating N_s/M mutually exclusive frequency tones to each of the transmitters. The training signal from the m^{th} transmitter is then a length N_s/M FD vector $\boldsymbol{\mathcal{S}}_m$. This is a sub-vector of $\boldsymbol{\mathcal{S}}$ with certain frequency tones nulled in order to achieve training orthogonality across the multiple antennas. An iterative process at the receiver involving the use of complex interpolation filters calculates all other frequency components [1, 25, 27]. Using these orthogonal FD training vectors, in the following, the MSE of the maximum likelihood FD channel estimation is derived and compared to the TD-MSE derived in section 3.1.1.

The channel frequency response between the m^{th} transmitter and the n^{th} receiver is given by

$$\boldsymbol{\mathcal{H}}_{m,n} = [\ \mathcal{H}_{m,n}(0) \quad \mathcal{H}_{m,n}(1) \quad ... \quad \mathcal{H}_{m,n}(N_s-1)\ ]. \tag{3.28}$$

Equations (3.28) in the FD and (3.3) in the TD are related through Fourier transformation as

$$\mathcal{H}_{m,n}(k) = \sum_{j=0}^{N_s-1} h_{m,n}(j)e^{-i2\frac{\pi}{N_s}kj} \tag{3.29}$$

$$= \sum_{j=0}^{v-1} h_{m,n}(j)e^{-i2\frac{\pi}{N_s}kj} \qquad k = 0, 1, \ldots, N_s-1. \tag{3.30}$$

as $h_{m,n}(j) = 0$ for $j = v, \ldots, N_s-1$. The received training signal at the n^{th} receive antenna can be expressed as

$$\mathcal{Y}_n(k) = \sum_{m=1}^{M} \mathcal{H}_{m,n}(k)\mathcal{S}(k) + \mathcal{N}_n(k) \qquad k = 0, 1, \ldots, N_s-1, \tag{3.31}$$

where $\mathcal{N}_n(k)$ denotes the k^{th} sample of the Fourier transformed AWGN at the n^{th} receiver. As the transmitters use non-overlapping frequency tones for training, the FD received signal (3.31) corresponds to those frequency tones. The FD received signal at the receiver array can now be represented by

$$\boldsymbol{\mathcal{Y}}(k) = (\mathcal{S}(k)\bar{\mathbf{I}}_N)\boldsymbol{\mathcal{H}}_m(k) + \boldsymbol{\mathcal{N}}(k), \tag{3.32}$$

where $\boldsymbol{\mathcal{H}}_m(k) = [\mathcal{H}_{m,1}(k), \mathcal{H}_{m,2}(k), ..., \mathcal{H}_{m,N}(k)]^T$. FD channel estimation of $\boldsymbol{\mathcal{H}}_m(k)$ first estimates the frequency components corresponding to the m^{th} transmitted training vector. Then, an iterative process involving the use of complex interpolation filters calculates all other frequency components [1, 25, 27]. The initial estimate is obtained using the maximum likelihood metric formed from (3.32) [12] and written as

$$||\boldsymbol{\mathcal{Y}}(k) - (\mathcal{S}(k)\bar{\mathbf{I}}_N)\boldsymbol{\mathcal{H}}_m(k)||^2 \qquad k = 0, 1, \ldots, N_s - 1 \tag{3.33}$$

Minimization of (3.33) then yields the vector estimate $\hat{\boldsymbol{\mathcal{H}}}_m(k)$ at the k^{th} frequency tone given by

$$\hat{\boldsymbol{\mathcal{H}}}_m(k) = ((\mathcal{S}(k)\mathcal{S}^*(k))^{-1}\mathcal{S}^*(k)\bar{\mathbf{I}}_N)\boldsymbol{\mathcal{Y}}(k) \qquad k = 0, 1, \ldots, N_s - 1 \tag{3.34}$$

By substituting (3.32) in (3.34), we can readily write the least-squares based channel frequency response estimate as

$$\hat{\boldsymbol{\mathcal{H}}}_m(k) = \boldsymbol{\mathcal{H}}_m(k) + ((\mathcal{S}(k)\mathcal{S}^*(k))^{-1}\mathcal{S}^*(k)\bar{\mathbf{I}}_N)\boldsymbol{\mathcal{N}}(k). \tag{3.35}$$

Since (3.35) has the same form as (3.14) we may write the FD channel estimation MSE as

$$MSE_{FD} = \sigma_n^2 N \sum_{k=0}^{N_s-1} ((\mathcal{S}(k)\mathcal{S}^*(k))^{-1}) \tag{3.36}$$

$$\geq \sigma_n^2 N N_s. \tag{3.37}$$

On comparing the lower bounds in (3.37) and (3.25), it is straight forward to write

$$MSE_{FD} = \frac{N_s}{v} MSE_{TD}. \tag{3.38}$$

When $v = N_s$, both approaches yield the same MSE. In this thesis we then investigate the channel estimation problem for FD receivers, in which N_s (FFT size or block size) is chosen to be at least 10 to 15 times[5] the size of v [23]. Then channel estimation based on a TD approach has lower complexity than the FD based approaches.

[5]Complexity savings achieved for FD systems become significant when larger FFT size is used. The maximum FFT size is dictated by the channel coherence time which is very high compared to the channel delay spread under consideration for fixed broadband wireless channels.

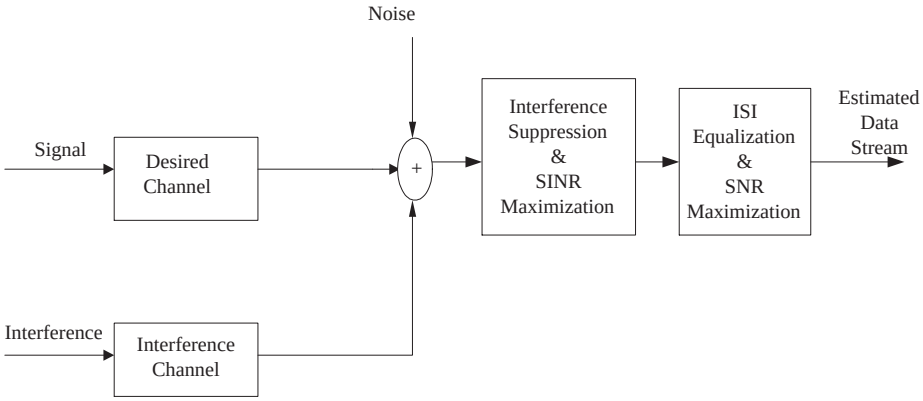

Figure 3.3: Composite system model.

The above FD approach requires the use of frequency interpolation that implements a number of FFT/IFFT operations for reducing the MSE of the channel estimates [27, 56]. This can lead to a large processing delay. Moreover a windowing filter is required to extract the significant taps in the TD [27]. As a result, the MSE of [27] is affected by the windowing deficiencies. Finally, the transmission frame of the FD technique consisting of the FD pilots and received signal is not a pure SC waveform. Hence, the PAPR of this waveform is higher than that of the frame without the FD pilots. Therefore, from (3.38), it is noted that the use of TD based channel estimation leads to both lower complexity and MSE compared to the FD based approaches.

3.1.3 Composite Channel Estimation

As mentioned earlier, for $N_s >> v$, TD channel estimation usually has lower complexity and MSE than FD estimation. However, for larger antenna configurations and delay spreads (M, N and v) complexity is still high. In order to reduce the processing time further, MIMO channel estimation can be carried out in M parallel branches [21, 53] by using the composite system model illustrated in Fig. 3.3. In [53] and [21] the MIMO system is modelled as M parallel single input multiple output (SIMO) branches. The m^{th} SIMO branch is modeled as the superposition of

the desired data stream component from the m^{th} transmitter and CCI from the other $M-1$ transmitters to the receiver array. Hence, estimation of M parallel SIMO channels amounts to estimating the whole MIMO channel [21, 53]. The channel estimation approach in [53] explicitly estimates the CCI whereas [21] resorts to a joint estimation approach. These approaches to channel estimation based on the composite channel model and are discussed in the following. The received signal using the composite system model as in [21, 53] can be expressed as follows

$$\overline{\mathbf{y}} = \overline{\mathbf{h}}_m \overline{\mathbf{s}}_m + \sum_{i \neq m} \overline{\mathbf{h}}_i \overline{\mathbf{s}}_i + \overline{\mathbf{n}} \tag{3.39}$$

$$= \overline{\mathbf{h}}_m \overline{\mathbf{s}}_m + \bar{\mathbf{i}}, M = 1, \ldots, M \tag{3.40}$$

where $\overline{\mathbf{h}}_m$ and $\overline{\mathbf{s}}_m$ are defined as in (3.4) and (3.2) respectively and $\bar{\mathbf{i}}$ represents the interference plus noise matrix. The covariance matrix of the interference plus noise is given by

$$\overline{\psi}_i = E[\bar{\mathbf{i}}\, \bar{\mathbf{i}}^H] \tag{3.41}$$

Receiver processing based on the composite system model of [53] requires estimation of $\overline{\psi}_i$ using known training sequences. However, it is difficult to accurately estimate $\overline{\psi}_i$ at low signal to interference plus noise ratios (SINRs) [53]. As a result, the ψ_i estimated using short training sequences are usually not reliable when the CCI is very strong. Hence, it is useful to consider approaches which avoid direct estimation of $\overline{\psi}_i$.

An approach that does not require explicit estimation of $\overline{\psi}_i$ is given in [21]. This approach involves the joint estimation of the CCI and ISI vector parameters. The CCI vector provides the coefficients of a filter structure to minimize CCI effects and the ISI vector provides an effective overall channel response for the m^{th} receiver branch and which is explicitly used in ISI equalization. For this approach, firstly, a joint estimation problem involving CCI and ISI vector parameters is set up for each SIMO channel. Then, using quadratic optimization principles, the optimal vector parameters for the CCI and the overall effective channel response are estimated.

The set of estimated CCI vector parameters suppress the CCI and maximize the desired signal power with respect to the interference plus noise. After CCI suppression and diversity combining the output is a desired data stream with residual CCI. As part of the joint estimation process, an effective channel response vector is defined which includes the delay due to the channel and CCI mitigation. The objective function is formulated as a function of these two vector parameters. The optimal vector parameters globally maximize the SINR.

The joint estimation approach based on the composite channel model is fairly robust to changes in the interference levels unlike the approach given in [53]. Moreover, the training signals employed are random training sequences generated independently and are not required to be orthonal. Since estimation is performed per transmitter, the complex MIMO channel estimation problem is simplified to estimation of a set of parallel SIMO channels without employing orthogonal training sequences as in [1, 25, 27].

We will adopt the above TD composite channel estimation approach to develop a FD receiver in chapter 4. This results in a hybrid (time and frequency) domain receiver architecture. Before discussing our proposed system in the following chapters we examine state of the art transceiver techniques used with MIMO SC systems using FD receiver processing. But we first summarize some background on SISO equalization.

3.2 SISO Equalization

MLSE receivers are known to be optimal in detecting data transmitted over SISO frequency selective channels [57]. Unfortunately, the complexity of an MLSE receiver grows exponentially with the ISI span of the channel and becomes exorbitant for practical implementation on channels exhibiting large ISI spans. Complexity savings can be achieved when a linear or a non-linear decision feedback equalizer (DFE) is used instead of MLSE for data detection. Both these architectures have

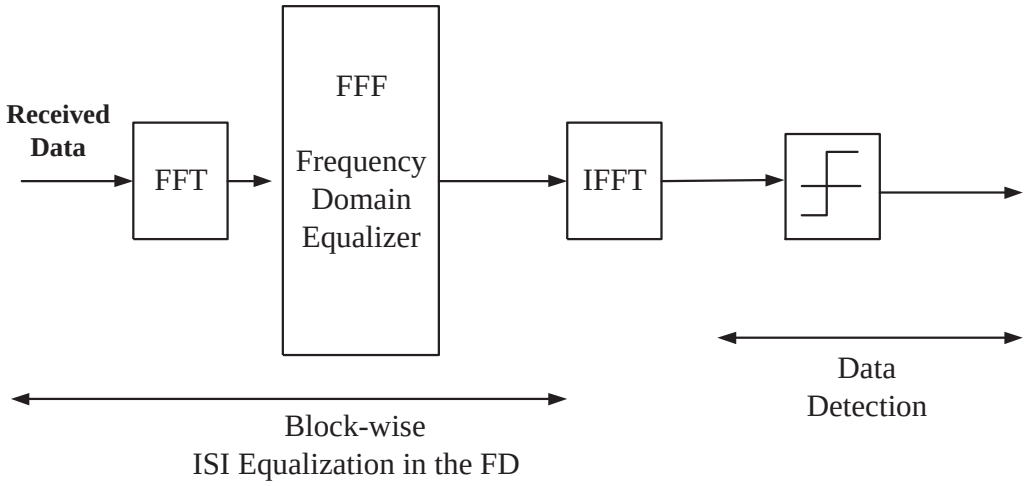

Figure 3.4: Block diagram of a linear FDE.

been studied for SC-FDE systems in both SISO and MIMO frameworks [8, 23]. In the following section, the basic linear FDE architecture in the SISO context is discussed.

3.2.1 Linear Equalization

Due to large delay spreads, the channel often exhibits deep spectral notches. SC transmission through such a channel is severely distorted due to time dispersion. Equalization of the received signal is required to compensate for these channel impairments.

Conventionally, equalization is performed in the TD. This involves a convolution operation to produce an estimate of the transmitted signal. In contrast, FD filtering is implemented as a component-wise multiplication of vectors. Hence, FDE is known to be more efficient when used for compensating large delay spread channels, but does require per-block processing [23]. The equivalence of TD and FD equalization techniques holds provided that the transmission is in frames or blocks.

As mentioned in chapter 2, each received block has essentially undergone cyclic convolution with the channel impulse response. Upon Fourier transformation, the

received FD signal can be represented as a component-wise multiplication of the transmit data with the frequency response of the channel [8, 23].

If the channel frequency response has no zeros and is known to the receiver, it is possible to perfectly remove the effect of the channel using the zero forcing criterion. Since, the FD received block contains the data after element-wise multiplication with the channel frequency response, FDE using the zero-forcing criterion is simply element-wise multiplication with its inverse. The problem with this form of equalization is noise enhancement [6] . For this reason, the minimum mean square error strategies [19] are commonly used, since they equalize the channel while taking into account the effect of channel noise, thereby avoiding noise enhancement..

3.2.2 Non-Linear Equalization

In comparison to a linear equalizer, a decision feedback equalizer (DFE) can cancel inter symbol interference due to previous symbols thus leading to lower noise enhancement on channels exhibiting deep spectral notches [24, 49]. The DFE takes advantage of previously detected data symbols and cancels their interference contribution due to previous symbols from the incoming symbols. The classical DFE consists of a feed-forward filter (FFF) and a feed-back filter (FBF) both implemented in the TD. The received data symbols are equalized by the FFF on a per-symbol basis and after data detection are passed through the FBF to subtract the ISI contribution from the incoming data symbols. This enables the DFE to achieve better performance than linear equalizers. In the following we review some popular receiver architectures used with SC-FDE systems, including the MMSE based hybrid-DFE [24], noise-predictive DFE [13], and iterative block FD-DFE [58–60].

[6] However, at high SNR, ZF and MMSE structures result in the same receiver performance.

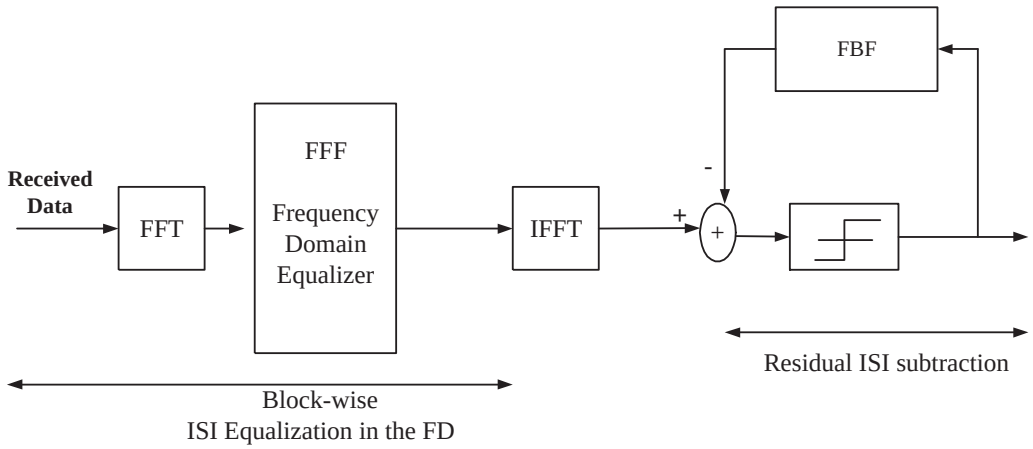

Figure 3.5: Block diagram of a hybrid DFE with FD-FFF and TD-FBF.

3.2.3 Hybrid-DFE

An efficient DFE implementation called the hybrid-DFE, is shown in Fig. 3.5. This structure is suitable for highly dispersive channels due to its implementing the FFF in the FD. This results in lower computational complexity than the TD-FFF [23,49]. The FBF section however, is required to be performed in the TD. This structure is referred to as the hybrid-DFE as it implements a cascade of the FD-FFF and the TD-FBF.

It is known that the performance of a DFE is always better than a linear equalizer for all practical channels as it reproduces the residual post-cursor ISI and cancels it with the help of the FBF [13]. However, an occasional decision error at the detector output results in incorrect estimation of the post-cursor ISI and this can lead to incorrect detection of future data symbols. Despite this error propagation, it can be shown that the error performance of the hybrid-DFE can be guaranteed to be at least as good or in most cases better than that of a linear equalizer [1]. Using a similar approach to the classical DFE, the forward and backward filters of the hybrid-DFE are also jointly optimized.

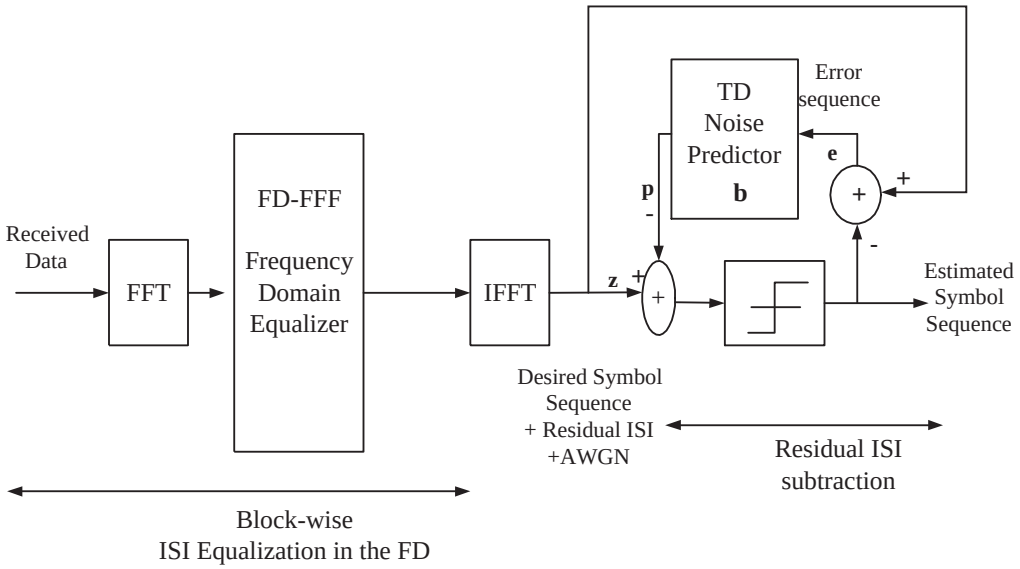

Figure 3.6: Block Diagram of a SISO NP-DFE Architecture.

3.2.4 Noise Predictive DFE

A flexible architecture called the noise-predictive decision feedback equalizer (NP-DFE) was originally investigated by Belfiore and Park for co-axial cable channels in [61]. It provides an alternative to the more traditional FIR structure considered in the previous section. The overall NP-DFE which consists of a cascade of a linear equalizer and a noise predictor is equivalent to DFE receiver processing [61]. It consists of a FFF followed by a NP equivalent of the FBF used in the hybrid-DFE. More recently, [13], a FD implementation of the NP-DFE architecture was proposed. It consists of a FD-FFF (equivalent to a linear FDE) followed by a TD-noise predictor. An NP-DFE architecture suitable for SISO channels is illustrated in Fig. 3.6. An error sequence $\mathbf{e}$ between the equalized vector $\mathbf{z}$ and an estimate of the transmit signal $\hat{\mathbf{x}}$ is given by

$$\mathbf{e} = \mathbf{z} - \mathbf{x}, \tag{3.42}$$

and assuming error free operation, (3.42) may be written as

$$\mathbf{e} = \mathbf{z} - \hat{\mathbf{x}}. \tag{3.43}$$

Given the channel frequency response vector, $\boldsymbol{\mathcal{H}}$, the FD-FFF, $\boldsymbol{\mathcal{F}}$, and TD noise predictor, $\mathbf{b}$, are found by minimizing the MSE given by

$$MSE = Tr(E[\mathbf{e}\mathbf{e}^H]). \tag{3.44}$$

The FD-NP-DFE achieves the same minimum MSE as the hybrid-DFE of [13] (see Sec. 3.2.3). However, unlike the hybrid-DFE the FFF of the NP-DFE in [13] is independent of the length of the noise predictors (the length of $\mathbf{b}$) and hence provides a somewhat more flexible architecture than the hybrid-DFE.

3.2.5 Iterative block FD-DFE

Another class of DFE called the iterative block FD-DFE implements both forward and backward filters in the FD as shown in Fig. 3.7 [60] [59] [58]. Similar to other DFEs it contains a FD-FFF, but now the FBF is also implemented in the FD. The use of FD filtering results in reduced computational complexity for both filter design and signal processing, when compared to the DFEs of [58–60]. In addition, the iterative block FD-DFE operates on blocks of the received signal, thus allowing the use of error correction block codes.

In [60], for the initialization stage, the receiver performs linear FDE to produce linear estimates of the data symbols. An iterative process follows the initialization. The iterative-FD-DFE architecture shown in Fig. 3.7 consists of a FD-FFF, $\boldsymbol{\mathcal{F}}$, and a FD-FBF, $\boldsymbol{\mathcal{B}}$. As can be seen from Fig. 3.7, it requires one extra FFT block to transform the TD data block estimate to the FD. At each iteration, a FD decision error sequence, $\boldsymbol{\mathcal{E}}$, between the current FD equalized signal, $\boldsymbol{\mathcal{Z}}$, and the output of the FD-FBF, $\boldsymbol{\mathcal{P}}$, is formed. At the i^{th} iteration, it computes the difference between $\boldsymbol{\mathcal{Z}}^i$ and $\boldsymbol{\mathcal{P}}^{i-1}$ from the previous iteration using

$$\boldsymbol{\mathcal{E}}^i = \boldsymbol{\mathcal{Z}}^i - \boldsymbol{\mathcal{P}}^{i-1}. \tag{3.45}$$

A correlation matrix of the error sequence denoted by $\overline{\boldsymbol{\rho}}^i$ is computed using this i^{th}

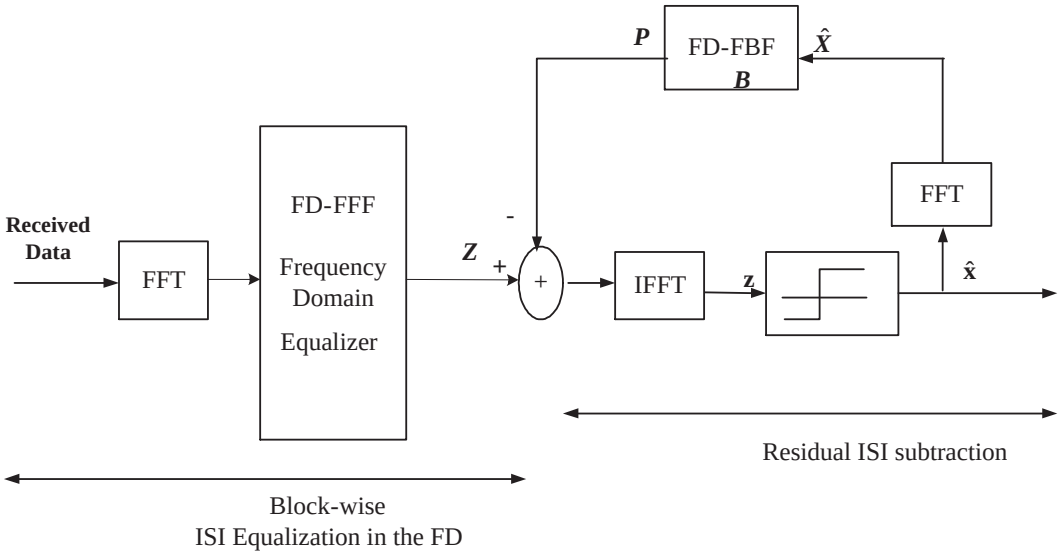

Figure 3.7: Block diagram of a FD-DFE implementing a FD-FFF and a FD-FBF.

error sequence as

$$\overline{\boldsymbol{\rho}}^i = E[\boldsymbol{\mathcal{E}}^i \boldsymbol{\mathcal{E}}^{iH}]. \tag{3.46}$$

Hence the corresponding MSE can be obtained by taking the trace of (3.46) given by

$$MSE = Tr(\overline{\boldsymbol{\rho}}^i). \tag{3.47}$$

Given the channel frequency response vector $\boldsymbol{\mathcal{H}}$ of length N_s, the MMSE optimized FD-FFF, $\boldsymbol{\mathcal{F}}^i$, and the FD-FBF, $\boldsymbol{\mathcal{B}}^i$, at each iteration are found by minimizing (3.47). The k^{th} components of the vectors are given by

$$\mathcal{F}^i(k) = \frac{\mathcal{H}^*(k)}{\sigma_a^2[1-(\rho_k^{i-1})^2]\mathcal{H}(k)\mathcal{H}^*(k)+\sigma_n^2}, \tag{3.48}$$

and

$$\mathcal{B}^i(k) = \rho_k^{i-1}[\mathcal{F}^i(k)\mathcal{H}(k) - \frac{1}{N_s}\sum_{l=0}^{N_s-1}\mathcal{F}^i(l)\mathcal{H}(l)], \tag{3.49}$$

where σ_d^2 and σ_n^2 represent the average power of the transmitted data symbols, and the additive noise power, respectively. And, $\mathcal{H}(k)$ is an element of $\boldsymbol{\mathcal{H}}$. In (3.48) and (3.49) ρ_k^{i-1} is the k^{th} diagonal element of the matrix $\overline{\boldsymbol{\rho}}^{i-1}$ The computation of the correlation at each iteration is computationally intensive and therefore simpler

iterative approaches need to be explored. Moreover, there is a delay of a complete block period due to the FBF operating in the FD.

The iterative FD-DFE architecture of [58] consists of a FD-FFF optimized under the MMSE criterion at the first iteration and shifts linearly from MMSE to reach full matched filtering at the final iteration. The idea is to maximize the SNR by the feedforward filter and cancel the residual interference using the FBF. This iterative scheme is initialized using the estimates obtained from a linear equalizer. It then replaces the linear equalizer by a channel matched filter in the iterative mode.

In [58], given the channel frequency response vector, $\boldsymbol{\mathcal{H}}$, of length N_s, the MMSE optimized FD-FFF and the FD-FBF at the i^{th} iteration are given by

$$\mathcal{F}^i(k) = \alpha^i \frac{\mathcal{H}^*(k)}{\mathcal{H}(k)H^*(k) + \frac{\sigma_n^2}{\sigma_a^2}} + (1-\alpha^i)\mathcal{H}^*(k) \tag{3.50}$$

and

$$\mathcal{B}^i(k) = 1 - \mathcal{F}^i(k)\mathcal{H}(k). \tag{3.51}$$

At the initial processing stage $\alpha^0 = 1$, resulting in a linear MMSE based equalizer in the FD. In succeeding stages α is less than 1 as the parameter α^i decreases with iterations and finally reduces to 0, meaning the FD-FFF becomes a FD matched filter.

An MMSE based iterative FD-DFE architecture that accounts for the decision errors is developed in [58, 59]. A parameter, $\sigma_e^{i\,2}$, which represents the power of the equalized decision errors computed at the i^{th} iteration is defined. This is obtained as

$$\sigma_e^{i\,2} = 2\sigma_a^2 P_e^{i-1}, \tag{3.52}$$

where P_e^{i-1} designates the probability of decision error at the previous iteration. The FD-FFF is derived as a function of this parameter and is given by

$$\mathcal{F}^i(k) = \frac{\mathcal{H}^*(k)}{\mathcal{H}(k)\mathcal{H}^*(k) + \frac{\sigma_n^2}{\sigma_e^{i\,2}}}. \tag{3.53}$$

The FBF is the same as that derived in [58,59] and is given by (3.51). The structure in [58, 59] takes into account the probability of decision errors unlike the design

Architecture	FFF	FBF	Complexity	Latency	Error Propagation
TD-DFE	TDE	TD	High	Low	High
Hybrid-DFE	FDE	TD	Medium	Medium	Medium
NP-DFE	FDE	TD	Low	Medium	Low
Iterative-FD-DFE	FDE	FD	Low	High	Minimum

Table 3.1: Comparison of DFE architectures.

given in [60]. The DFE architectures discussed in the foregoing are summarized in Table 3.2.5. The hybrid-DFE is suitable for broadband channels, as the FFF is implemented in the FD which results in lower computational complexity than the TD-FFF [23,49]. The FFF and the FBF of the hybrid-DFE are jointly optimized (in the MMSE sense). This means that any changes to the FBF affects the FFF design. However, implementing the FDE (which includes an FFT element-wise multiplication and an IFFT operation) on the entire transmission block before feedback filtering in the TD results in higher latency than the TD-DFE [23,49]. The NP-DFE architecture [13] on the other hand has lower complexity and also leads to a more flexible architecture compared to the hybrid-DFE architectures [23,49]. Similar to the hybrid-DFE, the NP-DFE implements the FFF in the FD, however, the latency is slightly lower than the hybrid-DFE as the FFF and the noise predictor coefficients are computed independently of each other.

Broadband wireless channels with large delay spreads require the use of longer FBFs. Hence, computational savings are expected when the FBF section is implemented using any of the iterative block DFEs of [58–60]. Further, the effect of error propagation in the iterative DFE structures is lower than the hybrid-DFE and the NP-DFE structures. Some of the DFE architectures reviewed here have been extended for use in MIMO receivers in conjunction with interference cancellation based approaches. These are discussed in the following section.

3.2.6 MIMO Equalizers

The optimum receiver for channels impaired by CCI and ISI is a multichannel maximum likelihood sequence estimator (MLSE) [57] implemented using a vector Viterbi algorithm. However, its implementation complexity is prohibitively high especially in the presence of CCI. If a reduced state MLSE [53] is used for the system defined in (3.39), a spatial whitening filter is required prior to the Viterbi equalizer for optimal performance. The spatial whitening filter is computed using the inverse of the covariance matrix of the overall interference,

$$\overline{\psi}_i = E[\bar{\mathbf{i}}\bar{\mathbf{i}}^H]. \tag{3.54}$$

It is difficult to estimate this $\overline{\psi}_i$ accurately given short training sequences. Hence, from the standpoint of both complexity and accuracy, reduced complexity receiver structures that are based on practical channel estimation algorithms need to be further explored.

For MIMO systems, a less complex sub-optimal receiver known as the Vertical-Bell Laboratories-Layered-Space-Time (V-BLAST) receiver architecture is widely used. In V-BLAST, the transmitter sends independent data streams from different antennas and the receiver implements multi-stage equalization followed by either successive interference cancellation (SIC) or parallel interference cancellation (PIC) for detection [1, 13, 18, 62].

In the case of SIC, there is a nulling or cancelling process which selects (by ordering according to received signal strength) a subset of the transmitted signals following either of the two criteria, namely zero-forcing or minimum mean squared error (MMSE). The canceling process subtracts the contribution of the estimated data streams from the received signals before they are passed on to the next stage of detection and equalization. These nulling and canceling processes continue successively until all transmitted data streams are equalized and detected. The initial ordering in SIC schemes has a huge impact on the overall performance of the receiver [1]. Moreover, good CSI is required for proper ordering and equalization of

the sub-streams.

In contrast, a PIC scheme does not involve ordering of sub-streams [63]. Nulling and cancelling are implemented in parallel and so the overall processing time is reduced compared to the SIC schemes. The PIC schemes are also implemented as multi-stage detectors. One of the key factors limiting the performance of PIC is caused by imperfect interference cancellation [63]. The sub-streams with low received SNR adversely affect the detection of others. As a result, all the sub-streams with higher SNR tend to suffer from error propagation and have little performance improvement in a multi-stage implementation [18]. Nevertheless, PIC based equalization receivers yield a reasonable complexity-performance trade-off compared to MLSE type receivers. The original V-BLAST receivers implement TD receiver processing for frequency-flat channels. This is still appropriate to compensate the distortions resulting from low delay spread channels. However, MIMO broadband communications are required to cope with large delay spreads due to multipath and hence, FDE is more appropriate [1, 13, 18, 22, 63, 64].

3.2.7 MIMO-FDE

Equalization schemes in the FD based on SIC or PIC are referred to as layered space frequency (LSF) equalization techniques. In [1], a LSF scheme is shown to outperform the TD V-BLAST receivers [65]. In an M-transmit and N-receive antenna system, the LSF receiver performs multi-stage equalization and interference cancelation. The equalization is either multi-input-single-output (MISO) structure producing a single output or a MIMO equalization structure producing multiple outputs. In an LSF receiver, a hybrid-DFE is typically used for equalizing the frequency selective channel [1, 63]. The MIMO-DFE typically consists of a bank of space-time or space-frequency FFFs producing M outputs (each corresponding to a transmitter). This is followed by M feedback filters each consisting of L_b taps. The MIMO receiver shown in Fig. 3.8 implements a hybrid-DFE in conjunction

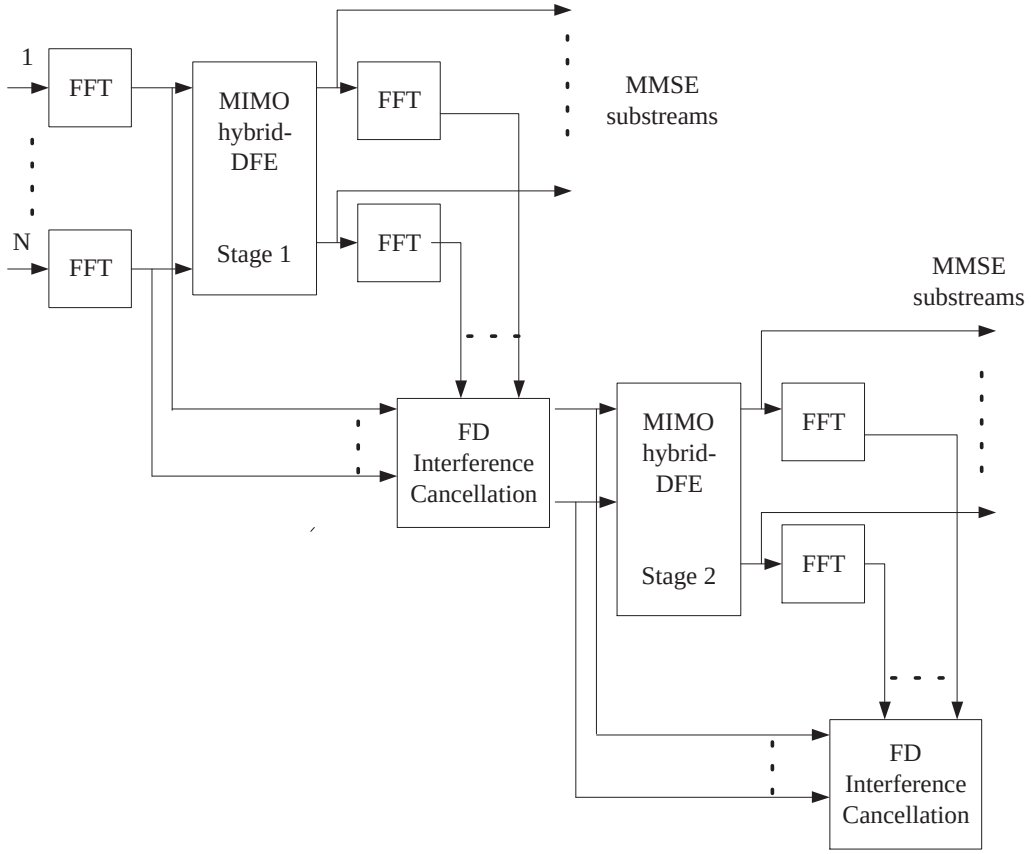

Figure 3.8: Block diagram of hybrid-DFE with SIC

with SIC processing. The hybrid-DFE at the initial stage performs equalization and ISI cancellation producing initial TD estimates of one or more data streams. Following this, the FFT transforms the estimated signal to the FD and interference cancellation is performed in the FD prior to the next stage of equalization and demodulation. It was found in [1, 63] that performance improves with the number of detection stages. However, any improvement is marginal after the first few stages. Due to multi-stage detection, the hybrid-DFE in conjunction with SIC processing at each stage is susceptible to error propagation when using imperfect or estimated CSI. The receiver proposed in [13], is shown in Fig. 3.9. It uses a NP-DFE in place of a hybrid-DFE in conjunction with SIC processing. In section 3.2.3 and 3.2.4 we compared the hybrid-DFE and NP-DFE. From Table 3.2.5, these architectures were shown to have comparable error performance and complexity.

3.3 Conclusions

In this chapter, we have examined several existing channel estimation and equalization approaches for MIMO-SC-FDE systems. It is seen that for practical system parameters as used in SC-FDE, estimating the MIMO channel frequency response in the TD is preferable to doing so in the FD. The system advantages with channel estimation based on a composite channel model are also discussed. The existing FD MIMO receivers employ one of the above mentioned DFE architectures in conjunction with either SIC or PIC processing. Implementing the SIC based DFE using estimated MIMO CSI results in error propagation. In the next chapters we propose a parallel receiver architecture for MIMO SC-FDE based on the estimated CSI. A linear equalizer is considered in chapter 4 and a DFE in chapter 5.

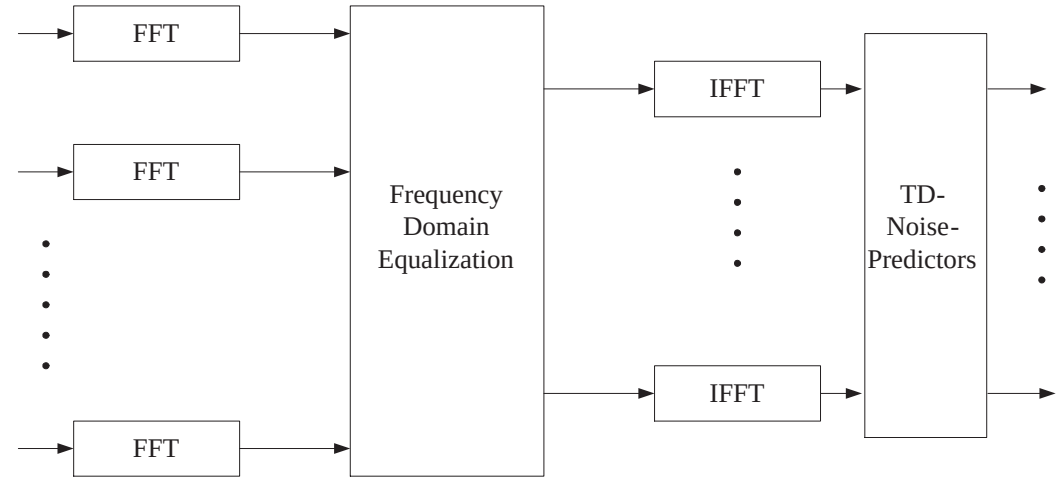

(a)

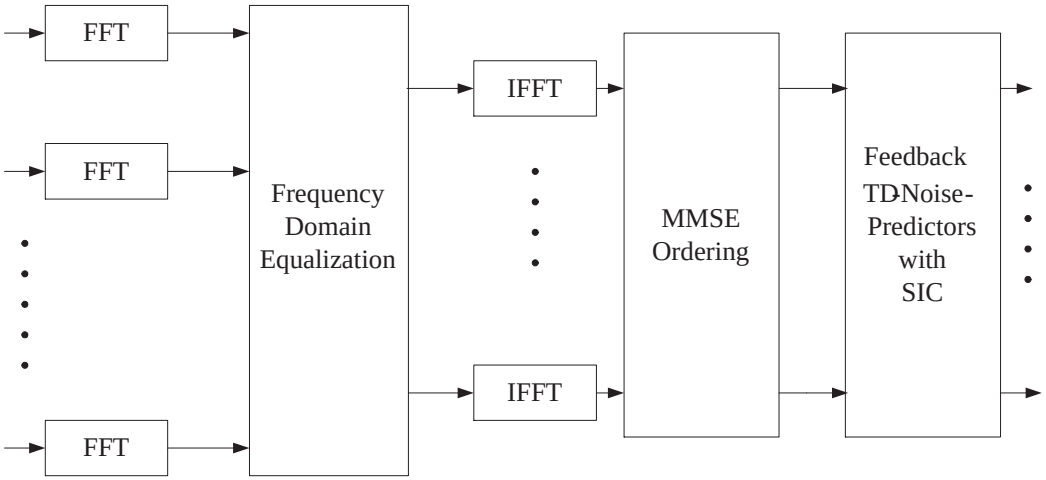

(b)

Figure 3.9: (a) Block diagram of MIMO NP-DFE (b) MIMO NP-DFE with SIC

Chapter 4

Space-Frequency-Equalization

A receiver architecture is developed in this chapter that uses TD estimated channel parameters to perform equalization in the FD for a multiple antenna system. The receiver, referred to as the space-frequency-equalizer (SFE), yields equal diversity gains for all data streams. A QR-decomposition based iterative joint estimation algorithm (QR-JEA) is developed to jointly estimate the channel parameters and CCI mitigation filter in the time domain. These are Fourier transformed and passed to the SFE for FD CCI mitigation and ISI compensation. The SFE has a parallel architecture and hence has lower processing time than SIC based MIMO equalizers. Due to the parallel processing, all data streams achieve equal diversity gains. The receiver exhibits excellent error performance even on highly dispersive wireless channels.

4.1 Introduction

Broadband wireless systems can be used for a variety of high data rate applications. Many of the channels being considered for such systems exhibit large delay spreads. In order to compensate for this, a TD multi-variable equalizer can be employed. However, the signal processing complexity to derive the equalizer coefficients and process multiple signals increases exponentially with channel delay spread. OFDM

has been shown to be effective in this application due to its modest receiver complexity [8, 23, 48, 50, 51]. Compared to OFDM, SC-FDE as discussed in chapter 2 is a practical alternative solution [23, 51] to compensate these channels. The overall complexity and performance of an SC-FDE system is comparable to that of an OFDM system [48, 51]. Moreover, an SC-FDE systems has the advantages of lower peak to average transmitted power ratio and lower sensitivity to frequency offsets than OFDM.

Multipath effects, as discussed in chapter 2, increase with data rate leading to large ISI spans at high data rates. The achievable capacity of systems depends on their ability to accommodate multiple signal transmissions in the same frequency band [66], which results in co-channel interference (CCI) at the receiver. The effects of CCI and ISI are both more pronounced at high data rates. The optimum receiver for channels impaired by CCI and ISI is a multichannel maximum likelihood sequence estimator [57] implemented using a vector Viterbi algorithm. However, its complexity is prohibitively high, especially in the presence of CCI, and hence reduced complexity structures are required.

Spatial multiplexing (SM) and space-time coding have been studied for multiple-input multiple-output (MIMO) SC-FDE systems [1, 14, 50, 64]. We focus here on the implementation of FD receivers based on estimated CSI for uncoded SM-SC systems. The Bell Laboratories Vertical Layered Space-Time (V-BLAST) architecture employing either a FD linear or a non-linear equalizer combined with FD CCI mitigation has been examined in [1, 13, 22, 64]. Successive interference cancellation (SIC) has been used for CCI mitigation and detection of the multiple data streams in [1, 13, 22]. The receiver in [1], called the layered space frequency (LSF) equalizer receiver, can employ a linear FDE for the detection of each layer (data stream). Note that [1] also presents a DFE solution, but we focus on linear structures in this chapter. As illustrated in [1], the multiple stages of SIC schemes tend to accentuate the effect of error propagation when only imperfect CSI is available. The SIC scheme of [22] considers only perfect CSI to implement optimal detection ordering

followed by perfect CCI cancellation at each stage. A channel matched filter followed by a minimum mean squared error (MMSE) FDE detects the data streams in a successive fashion. However, in practice, imperfectly estimated CSI impacts detection ordering and degrades performance due to error propagation. Moreover, SIC processing for large numbers of antennas leads to very high complexity and increased latency [1, 22].

MIMO channel estimation can be performed in the TD. Fourier transformation then yields the channel frequency response matrix. Alternatively, direct FD channel estimation can be used to compute the channel frequency response matrix. In [25, 27], FD channel estimation algorithms for MIMO SC-FDE systems were proposed. In [25], an iterative channel estimation algorithm for low delay spread channels was investigated. Special training sequences are constructed which exhibit constant envelop property in the TD while exhibiting orthonality with other training sequences as in [27] and [25]. The use of such sequences for channel estimation minimizes the effect of CCI. However, in the presence of non orthogonal interference, the channel estimation based on the orthogonal assumption results in noisy estimates. Moreover, this orthogonality is difficult to maintain in mobile environments. Further an iterative process involving Fourier transform based interpolation filters is used to compute the channel frequency response matrix. The channel estimation algorithm of [1] is similar to that of [25, 27] and requires transmission of FD orthogonal training sequences. However, the resulting estimated CSI in the presence of non-orthogonal CCI results in inferior receiver performance. As will be seen later, the MIMO channel impulse response matrix can be estimated in the TD using fewer parameters than the direct frequency response estimation approaches of [25, 27]. Furthermore, the complexity of the TD approach can be reduced by considering composite channel responses as in [21, 53] and estimating the CSI for all transmitted signals in parallel.

In this chapter, we consider MIMO SC-FDE with TD channel estimation of broadband channels that are characterized by large delay spreads. We develop a

space-frequency-equalizer (SFE) receiver that performs joint CCI mitigation and ISI equalization in the FD for M parallel data streams, where M is the number of transmit antennas. The channel and receiver parameters are estimated in parallel using an iterative QR-JEA in the TD. An advantage of the iterative estimation algorithm based on QR decomposition (QR-JEA) estimation algorithm developed here is that the CSI is estimated in the TD using non-orthogonal training sequences. The resulting complexity is lower than that of [21] and comparable to the least squares based channel estimation algorithms of [1, 25, 27].

At the receiver, N received signal streams (usually $N \geq M$) are Fourier transformed and fed into M parallel receiver branches, one for each transmitted data stream. An effective overall channel response vector and a set of weight vectors for CCI suppression are computed for each receiver branch using independent training sequences. Estimation is performed by maximizing the ratio of the power in the desired data stream to the interference plus noise power as in [21]. These estimates are Fourier transformed for use in the FD processing as shown in Fig 4.1. The SFE uses a parallel architecture and hence, all data streams achieve equal diversity gain with reduced processing delays compared to systems employing SIC.

Unlike [1, 22, 25] and [27] we exploit the advantages of both time and frequency domain processing to implement the receiver for the SM-SC system. We use TD processing to estimate the channel and FD processing to implement CCI mitigation and equalization and focus on developing a parallel linear FD architecture. The resulting receiver with only two iterations of the QR-JEA outperforms the 4 stage LSF of [1] and [27].

The organization of this chapter is as follows. In section 4.2, system and channel models are described. Section 4.3 describes the QR-JEA and derives the TD channel parameters. Section 4.4 derives the analytical model for the proposed FD integrated SFE. A complexity analysis is given in section 4.5. Simulation results are presented in section 4.6 and conclusions are drawn in section 4.7.

4.2 System Description

We consider a SC system with M transmit and N (usually $N \geq M$) receive antennas communicating over a frequency selective Rayleigh fading MIMO channel with a delay spread of up to tens of data symbols. A MIMO frame is formed by multiplexing data into M independent sequences each of N_s symbols, which are simultaneously transmitted from M antennas. The usual approach in FD systems to avoid inter-frame interference due to multipath propagation is to use a cyclic prefix/postfix (CP) of length at least equal to the maximum expected channel delay spread [23] of v symbol periods. Here, we use a periodic pseudo random training sequence of length $p \geq v$ symbols as shown in Fig. 4.2. The transmitted frame from the m^{th} ($m = 1, ..., M$) transmit antenna may then be written in the form

$$\mathbf{d}_m = \Big[s_m(-p-L-v), \ldots, s_m(-1), d_m(0), \ldots, d_m(N_s-p-L-v-1) \Big], \tag{4.1}$$

where the first $L+v$ symbols $s_m(-p-L-v), \ldots, s_m(-p-1)$ are used to clear the channel memory and the symbols $s_m(-p), \ldots, s_m(-1)$ are used for channel estimation. The data symbols are denoted as $d_m(0), \ldots, d_m(N_s-p-L-v-1)$

We assume the $M \cdot N$ sub-channels can each be modeled as a tapped delay line filter with v taps, which are independent identically distributed complex Gaussian random variables with zero mean and unit variance. Assuming that the channel response remains constant (quasi-static fading) over a frame and varies independently between frames, the sub-channel impulse response vector between the m^{th} transmitter and the n^{th} receiver is denoted

$$\mathbf{h}_{m,n} = \Big[h_{m,n}(0) \quad h_{m,n}(1) \quad \ldots \quad h_{m,n}(v-1) \Big]. \tag{4.2}$$

A convolution matrix $\overline{\mathbf{h}}_{m,n}$ of dimension $(L+1) \times (L+v+1)$ is then defined for

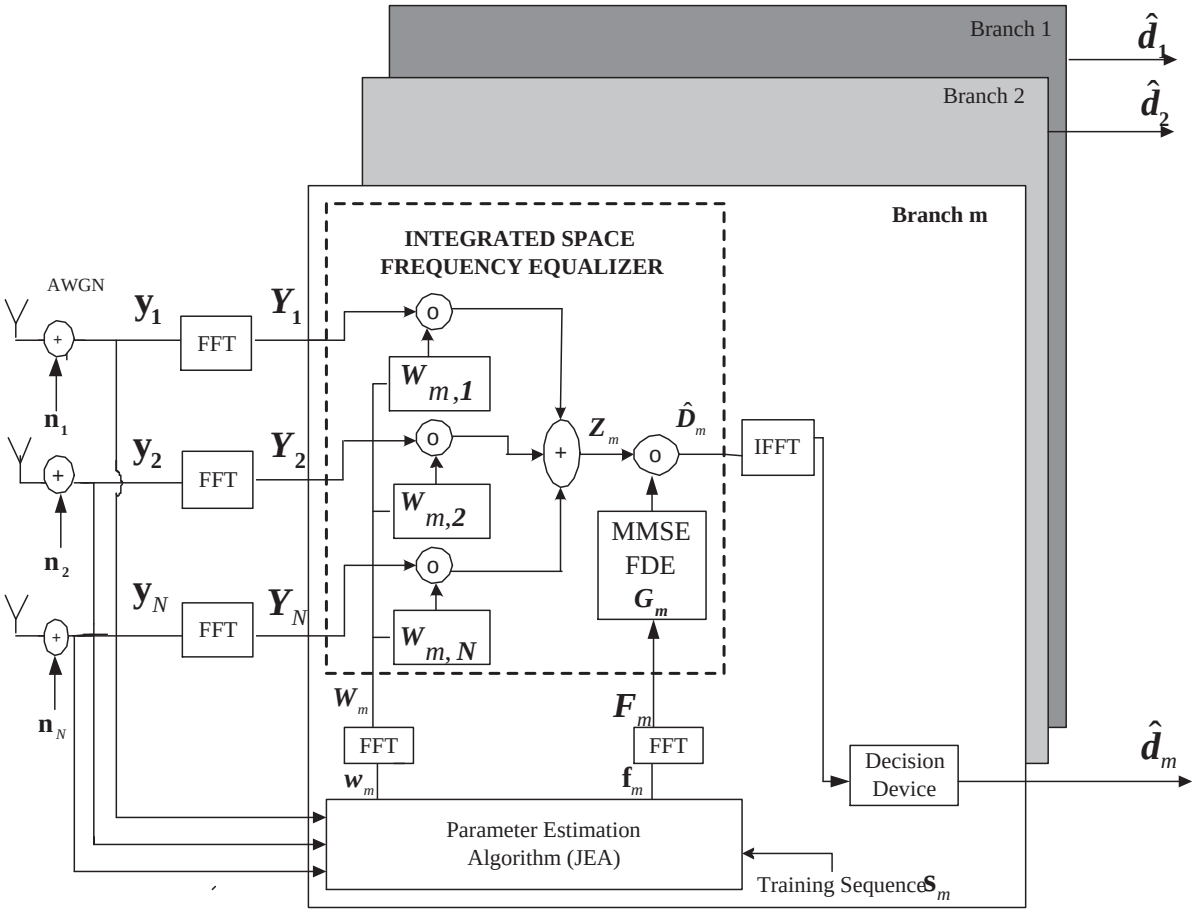

Figure 4.1: The proposed integrated SFE receiver, showing the detailed structure for the m^{th} branch, $m = 1, ..., M$.

each subchannel as

$$\overline{\mathbf{h}}_{m,n} = \begin{bmatrix} h_{m,n}(0) & \dots & h_{m,n}(v-1) & \dots & 0 & 0 \\ 0 & h_{m,n}(0) & \dots & \dots & 0 & \vdots \\ \vdots & \ddots & \ddots & \ddots & \vdots & \vdots \\ 0 & \dots & h_{m,n}(0) & \dots & h_{m,n}(v-1) & 0 \end{bmatrix}, \qquad (4.3)$$

where L is the TD length of the pre-processor which will be specifically defined in section 4.3. If we consider the m^{th} transmitted signal as the desired signal stream and the signals from the other $M-1$ transmitters as interference, then, after discarding the p training symbols, we may write the noisy received signal matrix over

any frame period at the $n^{th}(n = 1, ..., N)$ receive antenna as

$$\overline{\mathbf{y}}_n = \overline{\mathbf{h}}_{m,n}\overline{\mathbf{d}}_m + \sum_{i\neq m, i=1}^{M} \overline{\mathbf{h}}_{i,n}\overline{\mathbf{d}}_i + \overline{\mathbf{n}}_n, \tag{4.4}$$

where

$$\overline{\mathbf{y}}_n = \begin{bmatrix} y_n(0) & y_n(1) & \dots & y_n(N_s-1) \\ y_n(-1) & y_n(0) & \ddots & \vdots \\ \vdots & \ddots & \ddots & \vdots \\ y_n(-L) & y_n(-L+1) & \dots & y_n(N_s-L-1). \end{bmatrix}, \tag{4.5}$$

$$\overline{\mathbf{d}}_m = \begin{bmatrix} d_m(0) & d_m(1) & \dots & s_m(-1) \\ s_m(-1) & d_m(0) & \ddots & s_m(-2) \\ \vdots & \ddots & \ddots & \vdots \\ s_m(-L-v) & \dots & \dots & s_m(-L-v-1) \end{bmatrix}. \tag{4.6}$$

Note that $\overline{\mathbf{d}}_m$ is an $(L + v + 1) \times N_s$ matrix and $d_m(j)$ are independent identically distributed complex random variables with $E[d_m(j)d_m^*(j)] = \rho_d^2$. And, $\overline{\mathbf{n}}_n$ is a $(L + 1) \times (N_s)$ matrix of additive white Gaussian noise (AWGN) samples with $E[n_n(j)n_n^*(j)] = \rho_n^2$. In (4.4), the first term is the desired signal and the second is the CCI due to the other $M - 1$ transmitters.

The receiver is structured into M parallel branches, one corresponding to each transmitted signal as illustrated in Fig. 4.1.Each branch has N inputs, $\overline{\mathbf{y}}_n$, $n = 1, \dots, N$ and produces an output estimated data $\hat{d}_m(j)$, $m = 1, ..., M$. For the SM-SC systems considered here, the CCI and ISI could be compensated by means of a space-time equalizer (STE) (performing temporal equalization as in [67]). However, for highly dispersive channels, SFE has lower complexity than STE due to the compact channel frequency responses that allow for efficient FD processing. Thus, the Fourier transformed received signals from the $N \geq M$ receive antennas[1] are fed to the M receiver branches and the receiver detects all data streams in parallel. Each branch performs CCI suppression, diversity combining and ISI equalization in the FD.

[1]Note, $N < M$ can be used, but this results in performance loss (see section 4.6).

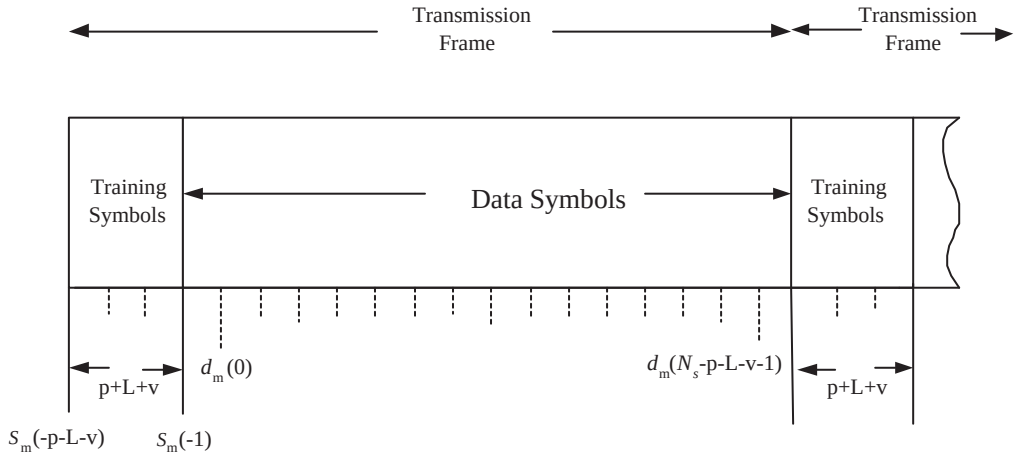

Figure 4.2: Transmission frame of N_s symbol periods including $p \geq L + v$ training symbols.

The SFE coefficients are estimated in the TD so as to maximize the ratio of the power in the desired data stream to the interference plus noise (SINR) as in [21]. In section 4.3, we state the objective function for MIMO parameter estimation and obtain the optimal estimate using an iterative QR-JEA. The m^{th} training sequence and corresponding N received signals are used to estimate both the m^{th} effective channel response vector, $\mathbf{f}_m$, and a set of N interference suppression weight vectors, $\mathbf{w}_m = [\mathbf{w}_{m,1}, ..., \mathbf{w}_{m,N}]$ in the TD. These estimated vectors are zero-padded to form N_s-point vectors and Fourier transformed to perform CCI mitigation and equalization in the FD. Since the processing is identical for all M receiver branches, we will focus throughout only on the m^{th} ($m = 1, ..., M$) receiver branch.

4.3 MIMO Parameter Estimation

In MIMO systems, channel estimation is a complex problem due to the large number of parameters to be estimated. Estimating all $N \cdot M$ multipath sub-channel responses simultaneously is theoretically the optimum approach. For multi-antenna configurations operating on channels with large delay spreads, this task can become

prohibitively complex. Therefore, we resort to a sub-optimum approach that estimates a single composite channel response for each receiver branch based on the overall channel matrix. The required number of parameters to be estimated is then significantly reduced with (as will be seen) little loss in performance.

Channel estimation can be performed either in the TD or the FD. FD estimation directly yields the channel frequency response required for FDE. A direct approach is to Fourier transform the received signals and then to perform least squares channel estimation as in [12]. We note that each of the multipath channel coefficients is determined by a single amplitude and phase in the TD. However, in the FD, it is embedded in N_s amplitudes and phases. These N_s amplitudes and phases are inter-related, but correctly building this relationship into a FD estimator amounts to operating in the TD [9]. The number of estimation parameters given an ISI span of v symbols, is $M \cdot N \cdot N_s$ in the FD and $M \cdot N \cdot v$ in the TD. In most FD receivers, $N_s >> v$ is typically used and this further complicates FD channel estimation. Note also that FD estimation as in [28], [27] and [25] involves numerous FFT/IFFT operations to minimize the mean squared error (MSE). Furthermore, the frequency responses of the M training signals are required to be orthogonal [27].

While usually less complex than FD estimation, the complexity and processing time required for TD least squares channel estimation algorithms is still high. Therefore, we now develop a method to reduce the signal processing time required to estimate the response vectors of (4.2). At the $n^{th}(n = 1, \ldots, N)$ receive antenna, the signal can be represented as a superposition of the desired data stream component and interference from the other $M - 1$ transmitters as in (4.4). The desired signal at the m^{th} receiver branch corresponds to the signal from the m^{th} transmitter, which is received at all N antennas. The interference is the superposition of the other $M - 1$ co-channel signals at each receive antenna.

The desired and interference channel parameters are obtained by processing the composite received signal, $\overline{\mathbf{y}}_n^s$, during the training period ($\overline{\mathbf{y}}_n^s$ is the first p columns

of (4.5)), where

$$\overline{\mathbf{y}}_n^s = \overline{\mathbf{h}}_{m,n}\overline{\mathbf{s}}_m + \sum_{i\neq m, i=1}^{M} \overline{\mathbf{h}}_{i,n}\overline{\mathbf{s}}_i + \overline{\mathbf{n}}_n, \qquad n = 1, \ldots, N \tag{4.7}$$

and the $(L + v + 1) \times (p)$ training matrix $\overline{\mathbf{s}}_m$ is defined as

$$\overline{\mathbf{s}}_m = \begin{bmatrix} s_m(-p) & s_m(-p+1) & \ldots & s_m(-1) \\ s_m(-p-1) & s_m(-p) & \ddots & s_m(-2) \\ \vdots & \ddots & \ddots & \vdots \\ s_m(-p-L-v) & \ldots & \ldots & s_m(-L-v-1) \end{bmatrix}. \tag{4.8}$$

The last two terms in (4.7) are the CCI and noise, respectively. They can be combined into a single disturbance term denoted $\overline{\mathbf{e}}_{m,n}$, so that (4.7) becomes

$$\overline{\mathbf{y}}_n^s = \overline{\mathbf{h}}_{m,n}\overline{\mathbf{s}}_m + \overline{\mathbf{e}}_{m,n}, \qquad n = 1, \ldots, N. \tag{4.9}$$

On stacking the N received matrices of (4.9) we obtain the composite vector

$$\overline{\mathbf{y}}^s = \begin{bmatrix} \overline{\mathbf{y}}_1^s \\ \overline{\mathbf{y}}_2^s \\ \vdots \\ \overline{\mathbf{y}}_N^s \end{bmatrix}. \tag{4.10}$$

We next define the length L pre-processor weight vectors at each receive antenna as

$$\mathbf{w}_{m,n} = \begin{bmatrix} w_{m,n}(0) & w_{m,n}(1) & \ldots & w_{m,n}(L) \end{bmatrix}, \tag{4.11}$$

where $m = 1, ..., M, n = 1, ..., N$.. The actual choice of L will be discussed in section 4.6. The TD weight vectors of (4.11) function to suppress the CCI. The combined pre-processor weight vector is the concatenation of these N vectors and is given by

$$\mathbf{w}_m = \begin{bmatrix} \mathbf{w}_{m,1} & \mathbf{w}_{m,2} & \ldots & \mathbf{w}_{m,N} \end{bmatrix}, \qquad m = 1, ..., M. \tag{4.12}$$

The pre-processor output corresponding to each transmitted signal may then be written as

$$\begin{aligned} \mathbf{z}_m^s &= \mathbf{w}_m \overline{\mathbf{y}}^s \\ &= \sum_{n=1}^{N} \left(\mathbf{w}_{m,n} \overline{\mathbf{h}}_{m,n} \overline{\mathbf{s}}_m + \mathbf{w}_{m,n} \overline{\mathbf{e}}_{m,n}, \right) \qquad m = 1, ..., M. \end{aligned} \tag{4.13}$$

This allows us to write the overall channel impulse response vector between the m^{th} transmitter and the corresponding output of the pre-processor as

$$\mathbf{f}_m = \sum_{n=1}^{N} \mathbf{w}_{m,n} \overline{\mathbf{h}}_{m,n}, \qquad m = 1, ..., M, \tag{4.14}$$

and the remaining residual interference as

$$\mathbf{i}_m = \sum_{n=1}^{N} \mathbf{w}_{m,n} \overline{\mathbf{e}}_{m,n}, \qquad m = 1, ..., M. \tag{4.15}$$

We may then re-write (4.13) in the compact form

$$\mathbf{z}_m^s = \mathbf{w}_m \overline{\mathbf{y}}^s = \mathbf{f}_m \overline{\mathbf{s}}_m + \mathbf{i}_m, \qquad m = 1, ..., M, \tag{4.16}$$

where $\mathbf{f}_m \overline{\mathbf{s}}_m$ is the desired signal component.

Following [21], we may write the pre-processor output SINR as

$$J_m(\mathbf{w}_m, \mathbf{f}_m) = \frac{\| \mathbf{f}_m \overline{\mathbf{s}}_m \|^2}{\| \mathbf{w}_m \overline{\mathbf{y}}^s - \mathbf{f}_m \overline{\mathbf{s}}_m \|^2}, \tag{4.17}$$

Estimation of $\mathbf{w}_m$ and $\mathbf{f}_m$ is achieved by maximizing (4.17) through the use of eigenvalue decomposition techniques [68]. In [21], this problem is solved using a non-iterative eigenvalue decomposition. Here we use a QR decomposition [69] based iterative technique.

Maximizing J_m is equivalent to minimizing its denominator with respect to $\mathbf{w}_m$ with a constant energy constraint on $\mathbf{f}_m$. Using the separation of variables theorem [21], we find the optimal value of $\mathbf{w}_m$ with a constraint on the energy[2] of $\mathbf{f}_m$. To do

[2]The constraint $||\mathbf{f}_m||^2 = 1$ is used to avoid any degenerate solution resulting from the maximization process.

this, we take the partial derivatives of the denominator of (4.17) with respect to the j^{th} element of the vector $\mathbf{w}_m$ and equate the result to zero to obtain the equations

$$\frac{\partial}{\partial(\mathbf{w}_m)_j}\|\mathbf{w}_m\overline{\mathbf{y}}^s - \mathbf{f}_m\overline{\mathbf{s}}_m\|^2 = 0, \qquad j = 1, 2, \ldots, N(L+1). \tag{4.18}$$

The partial derivative with respect to the j^{th} element of $\mathbf{w}_m$ $\quad (j = 1, \ldots, N(L+1))$ may be written as

$$\begin{aligned}\frac{\partial}{\partial(\mathbf{w}_m)_j}\|\mathbf{w}_m\overline{\mathbf{y}}^s - \mathbf{f}_m\overline{\mathbf{s}}_m\|^2 &= \frac{\partial}{\partial(\mathbf{w}_m)_j}\Big(\mathbf{w}_m\overline{\mathbf{y}}^s\overline{\mathbf{y}}^{sH}{\mathbf{w}_m}^H - \mathbf{f}_m\overline{\mathbf{s}}_m\overline{\mathbf{y}}^{sH}{\mathbf{w}_m}^H \\ &\quad -\mathbf{w}_m\overline{\mathbf{y}}^s{\overline{\mathbf{s}}_m}^H{\mathbf{f}_m}^H + \mathbf{f}_m\overline{\mathbf{s}}_m{\overline{\mathbf{s}}_m}^H{\mathbf{f}_m}^H\Big)\end{aligned} \tag{4.19}$$

By setting (4.19) to zero for $j = 1, \ldots, N(L+1)$ and using an identity [70] for the partial derivative of quadratic functions results in

$$(\overline{\mathbf{y}}^s\overline{\mathbf{y}}^{sH}{\mathbf{w}_m}^H)^H + \mathbf{w}_m\overline{\mathbf{y}}^s\overline{\mathbf{y}}^{sH} - \mathbf{f}_m\overline{\mathbf{s}}_m\overline{\mathbf{y}}^{sH} - \left(\overline{\mathbf{y}}^s{\overline{\mathbf{s}}_m}^H{\mathbf{f}_m}^H\right)^H = \mathbf{0} \tag{4.20}$$

Finally, the general relationship is written as

$$\mathbf{w}_m\overline{\mathbf{y}}^s\overline{\mathbf{y}}^{sH} = \mathbf{f}_m\overline{\mathbf{s}}_m\overline{\mathbf{y}}^{sH} \tag{4.21}$$

$$\mathbf{w}_m = \mathbf{f}_m(\overline{\mathbf{s}}_m\overline{\mathbf{y}}^{sH})(\overline{\mathbf{y}}^s\overline{\mathbf{y}}^{sH})^{-1} \tag{4.22}$$

By inspection, the solution to (4.20) can be written as

$$\max_{(\mathbf{f}_m)} J_m(f(\mathbf{f}_m), \mathbf{f}_m) = \max_{(\mathbf{f}_m)} \frac{\| \mathbf{f}_m\overline{\mathbf{s}}_m \|^2}{\| \mathbf{f}_m(\overline{\mathbf{s}}_m\overline{\mathbf{y}}^{sH})(\overline{\mathbf{y}}^s\overline{\mathbf{y}}^{sH})^{-1}\overline{\mathbf{y}}^s - \mathbf{f}_m\overline{\mathbf{s}}_m \|^2} \tag{4.23}$$

$$= \max_{(\mathbf{f}_m)} \frac{\mathbf{f}_m\overline{\mathbf{s}}_m\overline{\mathbf{s}}_m^H\mathbf{f}_m^H}{\mathbf{f}_m\overline{\mathbf{s}}_m\left(\mathbf{I} - \overline{\mathbf{y}}^{sH}(\overline{\mathbf{y}}^s\overline{\mathbf{y}}^{sH})^{-1}\overline{\mathbf{y}}^s\right)\overline{\mathbf{s}}_m^H{\mathbf{f}_m}^H} \tag{4.24}$$

The optimal (maximum SINR sense) estimate of $\mathbf{f}_m$ is then the eigenvector corresponding to the maximum eigenvalue of $\left(\overline{\mathbf{s}}_m\overline{\mathbf{s}}_m^H\right)$ $[\overline{\mathbf{s}}_m\left(\mathbf{I} - \overline{\mathbf{y}}^{sH}(\overline{\mathbf{y}}^s\overline{\mathbf{y}}^{sH})^{-1}\overline{\mathbf{y}}^s\right)\overline{\mathbf{s}}_m^H]^{-1}$ using the result in [21]. The desired pre-processor response $\mathbf{w}_m$ is then found by substituting the this eigenvector scaled by a constant that is found from the training matrix into (4.22).

This eigenvector is chosen as the effective channel response vector, $\mathbf{f}_m$, as it maximizes the output SINR of the m^{th} receiver branch [21]. Ideally, this is done by computing all eigenvalues and eigenvectors and then choosing the maximum eigenvector. Since only the maximum eigenvector is of interest, we can employ an iterative approach that computes only the vector solution for $\mathbf{f}_m$ that maximizes the SINR. This approach uses QR decomposition followed by a simple iterative process to refine the solution vector. This is a simpler approach than that of [30] as it does not involve full matrix inversions and eigenvalue decomposition.

The iterative process is based on a generalized eigenvalue problem where an eigenvector matrix $\overline{\mathbf{X}}$ corresponding to the eigenvalues of the diagonal matrix $\overline{\lambda}$ is obtained by solving the eigenvalue problem defined by

$$\overline{\mathbf{A}\mathbf{X}} = \overline{\lambda \mathbf{B}\mathbf{X}}. \tag{4.25}$$

In our application we have $\overline{\mathbf{A}} = \left[\overline{\mathbf{s}}_m \left(\mathrm{I} - \overline{\mathbf{y}}^{sH}(\overline{\mathbf{y}}^s\overline{\mathbf{y}}^{sH})^{-1}\overline{\mathbf{y}}^s\right)\overline{\mathbf{s}}_m^H\right]$ and $\overline{\mathbf{B}} = \left(\overline{\mathbf{s}}_m\overline{\mathbf{s}}_m^H\right)$. An iterative least squares problem is initiated by replacing the right-hand side of (4.25) with the matrix $\overline{\mathbf{B}}_0$, where $\overline{\mathbf{B}}_0$ is the matrix obtained by multiplying $\left(\overline{\mathbf{s}}_m\overline{\mathbf{s}}_m^H\right)$ with a normalized random matrix[3] . The initial eigenvector estimates of $\overline{\mathbf{X}}$ are obtained by solving

$$\overline{\mathbf{A}\mathbf{X}}_1 = \overline{\mathbf{B}}_0, \tag{4.26}$$

Since the eigenvector of interest is that which corresponds to the maximum eigenvalue [21], we choose the column vector $\mathbf{b}_0$ of $\overline{\mathbf{B}}_0$ with maximum energy and reduce (4.26) to the form

$$\overline{\mathbf{A}}\mathbf{x}_1 = \mathbf{b}_0. \tag{4.27}$$

Since $\overline{\mathbf{A}}$ is square and non-singular, QR decomposition using Householder reflectors [68, 69] produces a unitary $\overline{\mathbf{Q}}$ and an upper triangular matrix $\overline{\mathbf{R}}$ such that

$$\overline{\mathbf{A}} = \overline{\mathbf{Q}\mathbf{R}}. \tag{4.28}$$

[3]The random matrix is only used for initializing the iterative process.

An initial least squares solution is then computed by multiplying both sides of (4.27) by $\overline{\mathbf{A}}^H$ to give

$$\overline{\mathbf{A}}^H\overline{\mathbf{A}}\mathbf{x}_1 = \overline{\mathbf{A}}^H\mathbf{b}_0, \tag{4.29}$$

Substituting (4.28) in (4.29) results in

$$\left(\overline{\mathbf{QR}}\right)^H\left(\overline{\mathbf{QR}}\right)\mathbf{x}_1 = \left(\overline{\mathbf{QR}}\right)^H\mathbf{b}_0, \tag{4.30}$$

from which we obtain

$$\mathbf{x}_1 = \overline{\mathbf{R}}^{-1}\overline{\mathbf{R}}^{H^{-1}}\overline{\mathbf{A}}^H\mathbf{b}_0. \tag{4.31}$$

Note, the first iteration involves computation of $\overline{\mathbf{R}}^{-1}$, however, as it is an upper traingular matrix inverse it is computationally less expensive than computing the inverse of $\overline{\mathbf{A}}$. An iterative process follows (4.31) and improves the solution for $\mathbf{x}$. The process constructs a series of estimates $\mathbf{x}_i$, where $i = 1, 2, ..., I$ corresponds to the iteration number. Given $\mathbf{x}_i$ at the i^{th} iteration, the residual $\mathbf{r}_i = \mathbf{b}_{i-1} - \overline{\mathbf{A}}\mathbf{x}_i$ is computed. An error vector $\triangle\mathbf{x}_i$ is found by solving the system of (4.31) with $\mathbf{r}_i$ replacing $\mathbf{b}_i$, so that

$$\triangle\mathbf{x}_i = (\overline{\mathbf{R}}^H\overline{\mathbf{R}})^{-1}\overline{\mathbf{A}}^H\overline{\mathbf{r}}_i, \qquad i = 1, 2, ..I. \tag{4.32}$$

This computation involves inversion of upper triangular matrices. The new estimate of $\mathbf{x}_i$ is then found as

$$\mathbf{x}_{i+1} = (\mathbf{x}_i + \triangle\mathbf{x}_i), \qquad i = 1, ...I. \tag{4.33}$$

and is scaled by the factor

$$\mathbf{c}_i = ||\mathbf{x}_{i+1}|| \qquad i = 1, ...I \tag{4.34}$$

to result in an eigenvector with unit-energy. The process continues by updating the right-hand side of (4.27) according to

$$\mathbf{b}_i = \lambda_{i+1}\overline{\mathbf{B}}\mathbf{x}_{i+1}, \tag{4.35}$$

where λ_{i+1} is calculated by substituting the vector $\mathbf{x}_{i+1}$ for $\mathbf{f}_m$ in (4.24) as

$$\lambda_{i+1} = \frac{\mathbf{x}_{i+1}\overline{\mathbf{s}}_m\overline{\mathbf{s}}_m^H\mathbf{x}_{i+1}^H}{\mathbf{x}_{i+1}\overline{\mathbf{s}}_m\left(\mathbf{I} - \overline{\mathbf{y}}^{sH}(\overline{\mathbf{y}}^s\overline{\mathbf{y}}^{sH})^{-1}\overline{\mathbf{y}}^s\right)\overline{\mathbf{s}}_m^H\mathbf{x}_{i+1}^H}. \tag{4.36}$$

We have found that $I = 2$ or 3 iterations is sufficient and yields significant performance improvement. The process results in the vector $\mathbf{x}_I$ which approximately maximizes the SINR. This is scaled by the constant $Tr(\overline{\mathbf{s}}_m\overline{\mathbf{s}}_m^H)$ to result in the estimated channel response vector,

$$\mathbf{f}_m = Tr(\overline{\mathbf{s}}_m\overline{\mathbf{s}}_m^H)\mathbf{x}_I. \tag{4.37}$$

Finally, the TD pre-processor weight vectors $\mathbf{w}_m$ are calculated using (4.22). The vectors $\mathbf{w}_m$ and $\mathbf{f}_m$ are zero-padded to length N_s vectors and Fourier transformed for use in FD processing of the received signals.

4.4 MMSE Space Frequency Equalizer

The SFE consists of M parallel branches, each corresponding to a transmitted signal. The vector estimates, $\mathbf{f}_m$ and $\mathbf{w}_m$, are Fourier transformed and all actual signal processing is carried out in the FD. The length N_s desired frequency domain vectors are found as the FFT of the zero-padded vectors $\mathbf{w}_{m,n}$ for $n = 1, ..., N$ and $\mathbf{f}_m$ for the m^{th} branch and are defined by the components

$$\mathcal{W}_{m,n}\left(\frac{2\pi}{N_s}k\right) = \sum_{j=0}^{L}\mathrm{w}_{m,n}(j)e^{-j2\frac{\pi}{N_s}kj}, \tag{4.38}$$

$$\mathcal{F}_m\left(\frac{2\pi}{N_s}k\right) = \sum_{j=0}^{v+L}\mathrm{f}_m(j)e^{-j2\frac{\pi}{N_s}kj}, \quad k = 1, 2, ..., N_s. \tag{4.39}$$

The resulting $1 \times N_s$ FD vectors can be written as

$$\boldsymbol{\mathcal{W}}_{m,n} = [\mathcal{W}_{m,n}(1), \mathcal{W}_{m,n}(2), \ldots, \mathcal{W}_{m,n}(N_s)], \tag{4.40}$$

$$\boldsymbol{\mathcal{F}}_m = [\mathcal{F}_m(1), \mathcal{F}_m(2), \ldots, \mathcal{F}_m(N_s)], \tag{4.41}$$

for $m = 1, \ldots, M$ and $n = 1, \ldots, N$. Each receiver branch uses N of the vectors $\boldsymbol{\mathcal{W}}_{m,n}$ in a preprocessing filter to mitigate the effects of CCI. ISI in each of the M receiver branches is then compensated by an MMSE based FDE implemented using the estimated effective channel frequency response vector defined by $\boldsymbol{\mathcal{F}}_m$.

The Fourier transformed received signal corresponding to each frame at the n^{th} receive antenna is given by the length N_s vector

$$\begin{aligned} \boldsymbol{\mathcal{Y}}_n &= \boldsymbol{\mathcal{H}}_{m,n} \circ \boldsymbol{\mathcal{D}}_m + \sum_{i \neq m} \boldsymbol{\mathcal{H}}_{i,n} \circ \boldsymbol{\mathcal{D}}_i + \boldsymbol{\mathcal{N}}_n & (4.42) \\ &= \boldsymbol{\mathcal{H}}_{m,n} \circ \boldsymbol{\mathcal{D}}_m + \boldsymbol{\mathcal{E}}_{m,n}, \qquad m = 1, 2, ..., M, \quad n = 1, 2, ..., N & (4.43) \end{aligned}$$

where $\circ$ represents component-wise multiplication of vectors. The FD vectors $\boldsymbol{\mathcal{H}}_{m,n}$ and $\boldsymbol{\mathcal{D}}_m$ are obtained on Fourier transformation of (4.2) and (4.1), respectively. The Fourier transformed AWGN samples are denoted by the vector $\boldsymbol{\mathcal{N}}_n$. and $\boldsymbol{\mathcal{E}}_{m,n}$ equals the last two terms of (4.42) representing the overall interference and noise components of $\boldsymbol{\mathcal{Y}}_n$. Note that circular convolution of vectors in the TD is equivalent to their Hadamard product in the FD [46]. The FD vector, $\boldsymbol{\mathcal{D}}_m$, corresponds to the N_s symbols of the transmitted signal from the m^{th} transmitter.

The pre-processor performs CCI suppression on $\boldsymbol{\mathcal{Y}}_n$ using the vectors $\boldsymbol{\mathcal{W}}_{m,n}$ to produce the output in each receiver branch. Hence,

$$\begin{aligned} \boldsymbol{\mathcal{Z}}_m &= \sum_{n=1}^{N} \boldsymbol{\mathcal{W}}_{m,n} \circ [\boldsymbol{\mathcal{H}}_{m,n} \circ \boldsymbol{\mathcal{D}}_m + \boldsymbol{\mathcal{E}}_{m,n}] & (4.44) \\ &= \boldsymbol{\mathcal{D}}_m \circ \boldsymbol{\mathcal{F}}_m + \boldsymbol{\mathcal{I}}_m \qquad m = 1, \ldots, M & (4.45) \end{aligned}$$

where the effective overall channel frequency response vector is given by

$$\boldsymbol{\mathcal{F}}_m = \sum_{n=1}^{N} \boldsymbol{\mathcal{W}}_{m,n} \circ \boldsymbol{\mathcal{H}}_{m,n}, \qquad m = 1, \ldots, M \quad (4.46)$$

$$(4.47)$$

and the residual interference vector seen by the m^{th} transmitted signal is given by

$$\boldsymbol{\mathcal{I}}_m = \sum_{n=1}^{N} \boldsymbol{\mathcal{W}}_{m,n} \circ \boldsymbol{\mathcal{E}}_{m,n}. \quad (4.48)$$

A FD MMSE estimate of the signal vector $\boldsymbol{\mathcal{D}}_m$ that is linear in $\boldsymbol{\mathcal{Z}}_m$ can then be computed as

$$\hat{\boldsymbol{\mathcal{D}}}_m = \boldsymbol{\mathcal{G}}_m \circ \boldsymbol{\mathcal{Z}}_m, \qquad m = 1, \ldots, M, \tag{4.49}$$

where $\boldsymbol{\mathcal{G}}_m$ is the MMSE FDE for the m^{th} data stream. It minimizes the MSE between $\hat{\boldsymbol{\mathcal{D}}}_m$ and $\boldsymbol{\mathcal{D}}_m$, which is given by

$$\begin{aligned} MSE &= E[||\hat{\boldsymbol{\mathcal{D}}}_m - \boldsymbol{\mathcal{D}}_m||^2] && (4.50)\\ &= E\Big[||\boldsymbol{\mathcal{G}}_m \circ [\boldsymbol{\mathcal{D}}_m \circ \boldsymbol{\mathcal{F}}_m + \boldsymbol{\mathcal{I}}_m] - \boldsymbol{\mathcal{D}}_m||^2] && (4.51) \end{aligned}$$

Using the triangle inequality we have

$$\begin{aligned} MSE \leq\ & E[||\boldsymbol{\mathcal{D}}_m \circ (\boldsymbol{\mathcal{G}}_m \circ \boldsymbol{\mathcal{F}}_m - \mathbf{1})||^2 && (4.52)\\ & +2||\boldsymbol{\mathcal{D}}_m \circ (\boldsymbol{\mathcal{G}}_m \circ \boldsymbol{\mathcal{F}}_m - \mathbf{1})||||\boldsymbol{\mathcal{G}}_m \circ \boldsymbol{\mathcal{I}}_m|| \\ & +||\boldsymbol{\mathcal{G}}_m \circ \boldsymbol{\mathcal{I}}_m||^2], && (4.53) \end{aligned}$$

and finally obtain

$$MSE \leq \rho_d^2(||\boldsymbol{\mathcal{G}}_m \circ \boldsymbol{\mathcal{F}}_m - \mathbf{1}||^2) + \rho_n^2||\boldsymbol{\mathcal{G}}_m||^2. \tag{4.54}$$

The derivation of (4.54) assumes that the data samples are statistically independent, have zero mean and variance equal to ρ_d^2 and that the residual interference, $\boldsymbol{\mathcal{I}}_m$, contains negligible CCI, so it may be regarded as white noise with variance equal to ρ_n^2. Taking the partial derivative of (4.54) with respect to the j^{th} element of the equalizer vector, $\boldsymbol{\mathcal{G}}_m$ for $j = 0, 1, \ldots, N_s - 1$, and setting the resulting system of equations to zero we obtain the MMSE FDE vector for the m^{th} receiver branch as

$$\boldsymbol{\mathcal{G}}_m = \boldsymbol{\mathcal{F}}_m^* \circ \left(\boldsymbol{\mathcal{F}}_m \circ \boldsymbol{\mathcal{F}}_m^* + \frac{\rho_n^2}{\rho_d^2}\mathbf{1} \right)^{-1}, \tag{4.55}$$

where $\mathbf{1} = [1, 1, ..., 1]$ is a vector of ones and the inverse here implies the component-wise or element by element inverse.

4.5 Computational Complexity

The computational complexity of the integrated SFE, measured in terms of the required number of complex multiplication operations is discussed in this section. The integrated SFE is implemented based on the iterative QR-JEA channel estimation algorithm. In subsection 4.5.1, the complexity of the iterative QR-JEA that includes the complexity of FFT/IFFT operations, matrix inverses and decompositions are discussed. In subsection 4.5.2, the signal processing complexity which includes the FD pre-processing and the FDE are discussed.

4.5.1 Iterative QR-JEA

In section 4.3, we described how the iterative QR-JEA obtains a solution for the effective channel response $\mathbf{f}_m$. The complexity of this solution is primarily due to the initial computation of the vectors $\mathbf{f}_m$ and $\mathbf{w}_m$ which require matrix inversion. As they are related through (4.22), this inversion is performed only once per branch. The number of complex multiplications for the estimation of the $\mathbf{f}_m$ is $\frac{1}{6}(L+v+1)^3 + (N(L+1))^3$ [21, 69] and that of $\mathbf{w}_m$ is $N(L+v+1)(L+1)$. The Fourier transformation of $\mathbf{w}_{m,n}$ vectors and received signal vectors for $n = 1, \ldots, N$ over all M branches requires $NM\frac{N_s}{2}log_2N_s$ and $N\frac{N_s}{2}log_2N_s$, complex multiplications respectively. The Fourier transformation of the vector $\mathbf{f}_m$ over all M branches requires $M\frac{N_s}{2}log_2N_s$. Then, $M\frac{N_s}{2}log_2N_s$ complex multiplications are used in IFFT operation. Hence, the overall complex multiplications used in FFT/IFFT operations over all M branches is given by $(MN+2M+N)\frac{N_s}{2}log_2N_s$. The complexity for QR decomposition of the $N(L+1) \times N(L+1)$ matrix given in (4.28) requires approximately $(N(L+1))^3$ complex multiplications [69]. This, for M branches is given by $M(N(L+1))^3$. The iterative process following the QR decomposition in (4.31) requires inversion of the product of an upper and a lower triangular matrix. This requires $(N(L+1))^2 + 2N(L+1)$ complex multiplications per iteration. Therefore, the overall iterative QR-JEA channel estimation including the FFT/IFFT operations

overall M branches is given by $M(\frac{1}{6}((L+v+1)^3+(N(L+1))^3)+N(L+v+1)(L+1)+I((N(L+1))^2+2N(L+1)))+(MN+2M+N)N_s log2(N_s)+4(N(L+1))^3$. Where, I denotes the number of iterations.

The FD least squares channel estimation in [1] is similar to that of [27] and [25]. The complexity of the FD channel estimation algorithm of [27] is given as $2MNN_s log_2 N_s + MNN_s$ complex multiplications.

As an example, consider $M = N = 4, v = 6, L = 7$ and $N_s = 1024$ and $I = 1$. QR-JEA requires 304250 complex multiplications assuming 1 iteration (with 1088 additional multiplications per iteration), while the channel estimation technique of [27] requires a total of 344064 complex multiplications. The overall channel estimation complexity of QR-JEA is thus comparable to the technique of [27]. However, on a system basis QR-JEA has significantly lower processing delay than [27] due to the use of parallel signal processing.

4.5.2 System Complexity

We next compare the complexities of the integrated SFE and the 4-stage linear LSF of [1] in terms of the required number of complex multiplications. The FD receiver processing in the SFE includes the FD pre-processing of (4.44) and the MMSE-FDE of (4.55). Detection of each of the M data streams requires $NN_s + 2N_s$ complex multiplications. The overall complexity for the detection of M data streams is then $M(NN_s + 2N_s)$. The proposed SFE and the 4-stage LSF of [1] require the same number of FFT and IFFT operations[4] , and hence we compare only the overall complexity of implementing the equalizers. The complexity for a 4-stage linear LSF which outputs 4 data streams per stage is estimated as $8N_s NM(N-1)$ complex multiplications. Note that reducing either the number of stages or the number of outputs per stage in [1] reduces complexity at the cost of performance. For $M = N = 4$ and $N_s = 1024$ the SFE of the present paper uses 24576 complex

[4]Both these techniques overall require N FFTs to Fourier transform the received signals and M IFFTs to transform them back to the TD.

multiplications, while the 4-stage linear LSF uses 393216 complex multiplications. Therefore, the integrated SFE uses only 6.25 percent of the number of complex multiplications of the 4-stage LSF.

4.6 Simulation

We have simulated SM-SC systems using QPSK and 16 QAM modulations. The channels used are the Stanford University Interim (SUI) models (SUI3-SUI6) and a general 11-tap symbol spaced model with an exponentially decaying power delay profile (PDP) [28]. Figures 4.3 and 4.4 illustrate the frequency responses, with

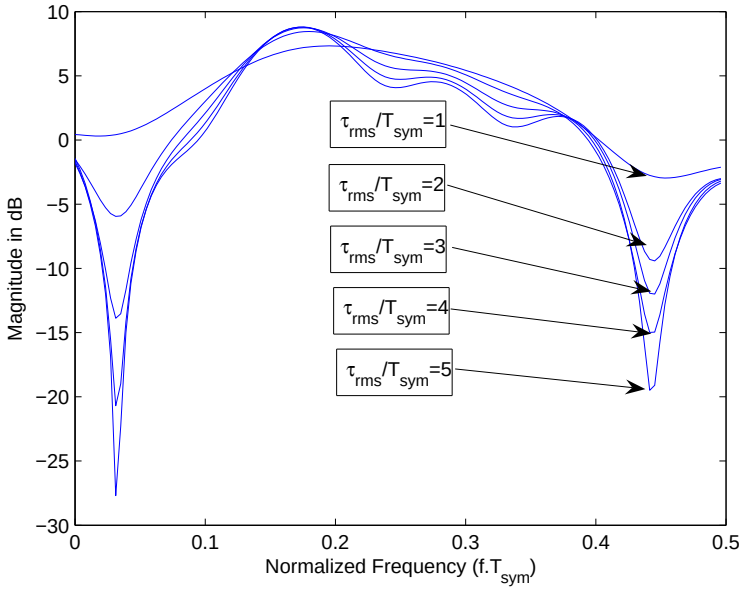

Figure 4.3: Frequency responses of a general exponential 11 tap channel with respect to digital frequency normalized to the signal bandwidth with various normalized RMS delay spreads.

respect to the normalized frequency, $f.T_{sym}$, where f denotes frequency and T_{sym} is the symbol duration. As can be seen, the SUI 5 and 6 channels experience deeper fades. These models exhibit maximum delay spreads of 10μsec and 20μsec with root-mean-squared (RMS) delay spreads of approximately 2.8μsec and 5.2μsec.

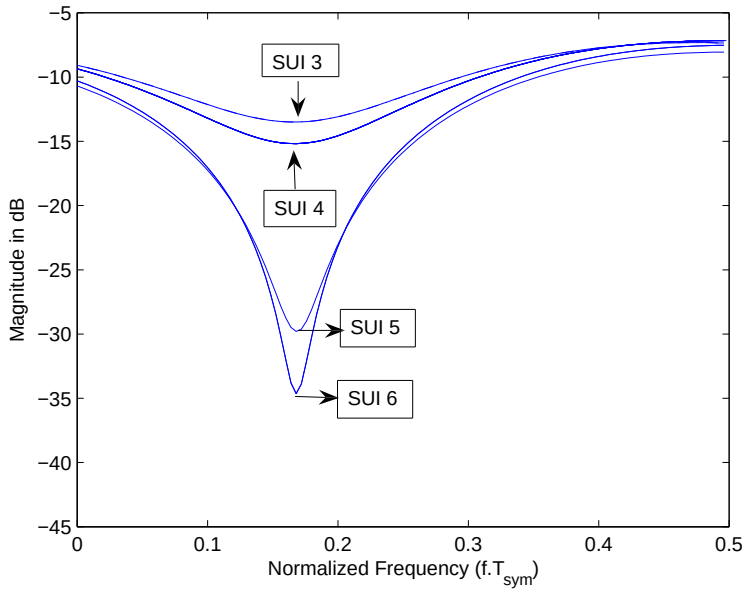

Figure 4.4: Frequency responses of SUI 3-6 channel models.

Assuming a symbol period of 1μsec they result in ISI spans of $v = 10$ and $v = 20$ symbol periods, respectively. The PDP of the sparse SUI channels also exhibits an exponentially decaying delay profile and is characterized by the RMS delay spread defined in chapter 2.

Figures 4.3 and 4.4 demonstrate that larger RMS delay spreads usually lead to deeper fades in the channel frequency responses. We assume that fading is independent across all transceiver pairs and also across all multipath components. The signal to noise ratio (SNR), defined as E_b/N_0, is the ratio of the received signal power per bit E_b, to the noise power, N_0, per receive antenna. The bit-error-rate (BER) is obtained by averaging the instantaneous BER of at least 10,000 transmission frames and 100 bit errors.

An important advantage of the proposed SFE receiver over that of [1] is that essentially the same performance is achieved for all M transmitted data streams as shown in Fig. 4.5 for $N = 4$ receive antennas. Therefore, in the remaining simulations we present performance of only a single data stream. The effect of the number of spatial degrees of freedom or the spatial receive diversity effect on SFE

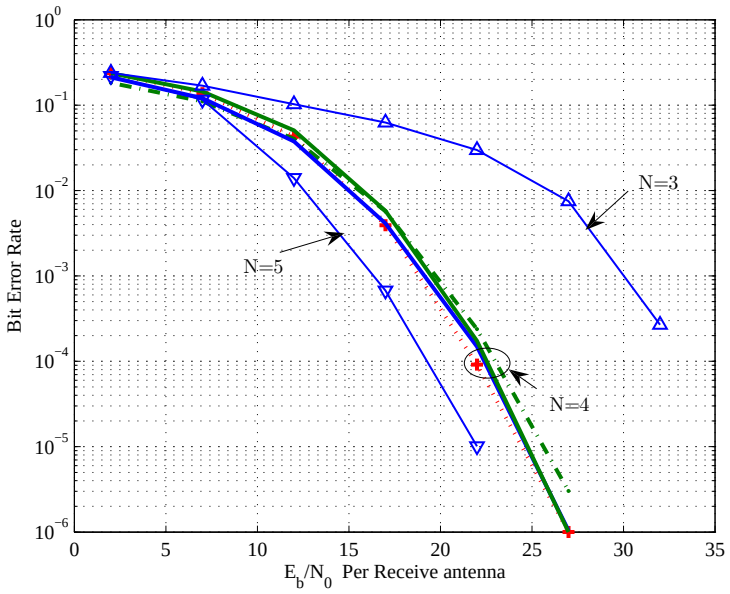

Figure 4.5: Performance of the SFE with $L = 12$ for a system with $M = 4$ and $N = 3, 4, 5$ antennas on an SUI-5 channel with a delay spread of $v = 10$ symbols. The performance of each transmitted data stream is shown for the case of $M = N = 4$ transmit and receive antennas using QR-JEA with $I = 0$ for parameter estimation.

performance can also be observed in Fig. 4.5. At a BER of 10^{-3} the system using $N = 3$ receivers performs 8 to 9dB worse than the one with an equal number of transmitters and receivers ($M = N = 4$). However, no error floor was observed for the range of SNR's considered. An additional receiver, $N = 5$, improves the performance by 3.5dB at a BER of 10^{-5} due to the increased number of spatial degrees of freedom and the improved receive diversity.

We now consider the effect of the length, L, of the pre-processor $\mathbf{w}_{m,n}$ on system error performance. Fig. 4.6 and Fig. 4.7 illustrate results for the integrated-SFE using QR-JEA with $I = 0$ and $I = 2$ iterations, respectively. Clearly, using $L \geq (v + 1)$ significantly reduces the error floor. An issue in practical systems is determining the length of the pre-processor filter required for a given ISI span. The larger the ISI span the larger the required pre-processor length L and the larger the system complexity. Fig. 4.6 considers the SUI-6 channel model with a maximum

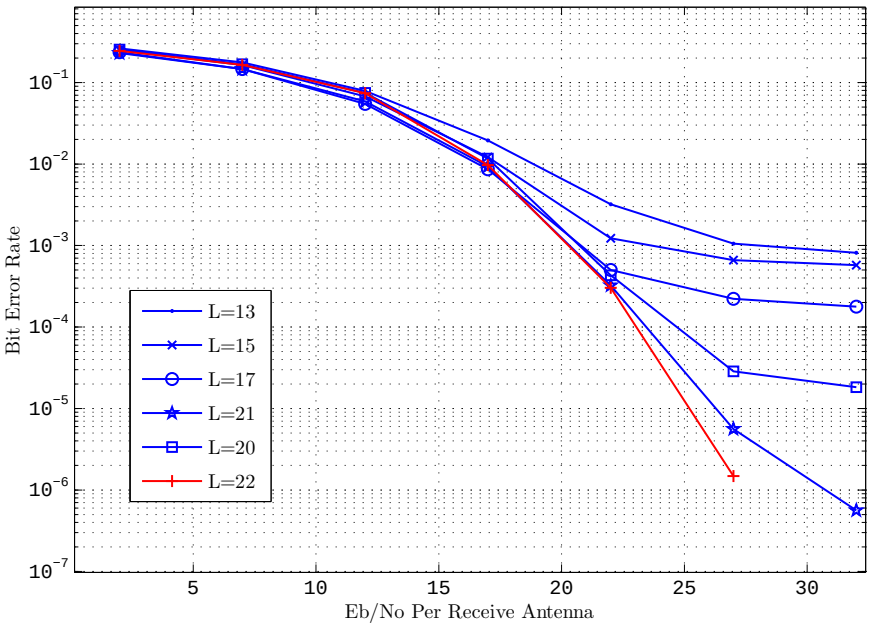

Figure 4.6: Effect of pre-processor time domain filter length L on performance on an SUI-6 channel with $v = 20$ symbols of delay spread and an $M = N = 4$ antenna configuration. QR-JEA with $I = 0$ is employed for parameter estimation, but yields similar performance to that obtained using iterative estimation.

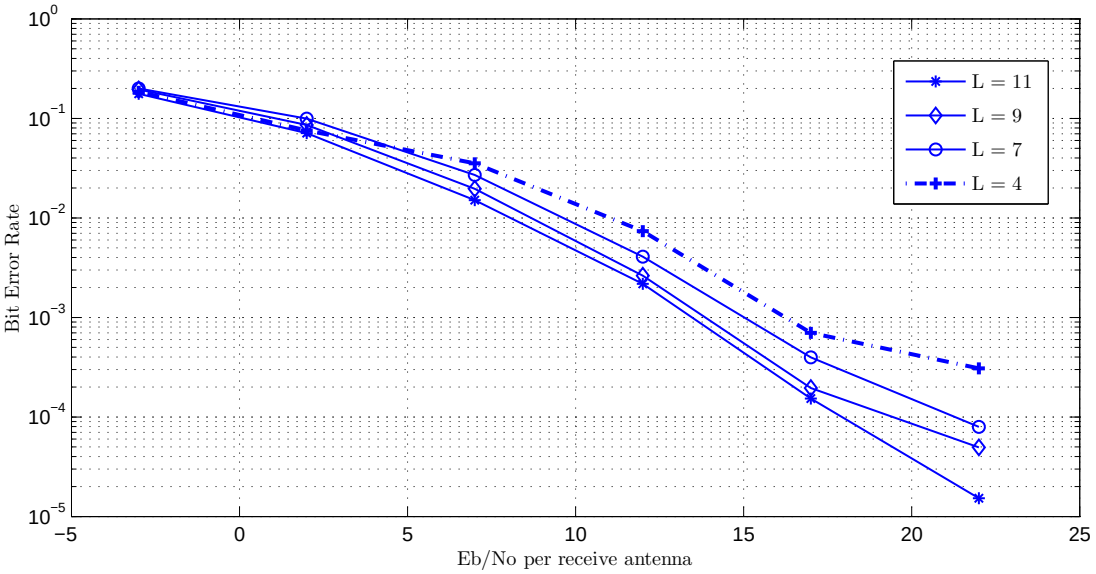

Figure 4.7: Performance of the SFE with iterative QR-JEA and $I = 2$ iterations for various TD pre-processor length, L, on an SUI-5 channel with $v = 10$ symbols and $M = N = 4$ transmit and receive antennas.

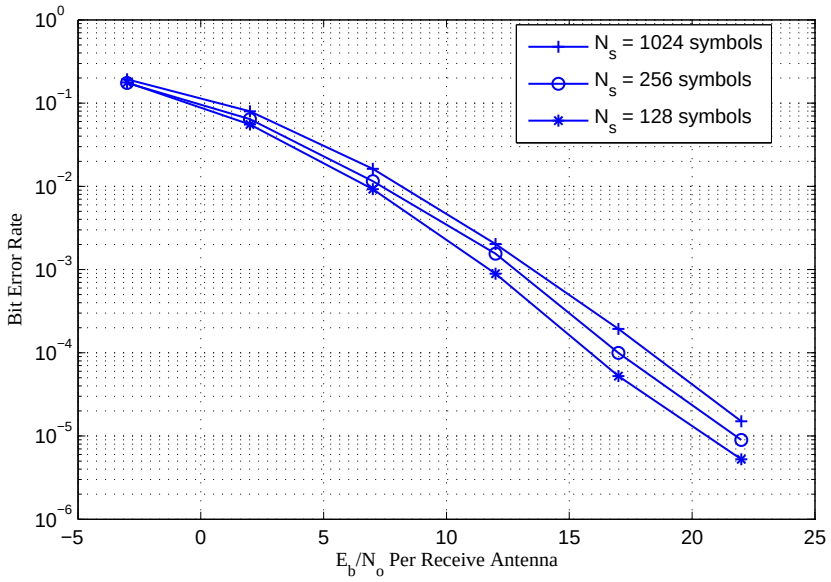

Figure 4.8: Performance of the SFE with iterative QR-JEA ($I = 2$ iterations) for frame lengths of $N_s = 128, 256$, and 1024 symbols on a $v = 10$ SUI-5 channel with a pre-processor TD length of $L = 11$.

ISI span of $v = 20$ symbol periods. In contrast, Fig. 4.7 considers the SUI-5 channel model with a maximum ISI span of $v = 10$ symbol periods. These results show that the SFE using $L \geq v + 1$ results in good performance to at least a BER of 10^{-5} for various values of v (and I).

In Fig. 4.8, the frame size is varied from $N_s = 128$ to 1024 symbols and there is a performance variation of about 2.5dB at a BER of 10^{-4}. Transmission of shorter frames decreases throughput efficiency due to the CP requirement but yields slightly better performance due to more frequent training.

In Fig. 4.9, we compare the performance of the 4-stage LSF of [1] with that of the SFE using the proposed QR-JEA. A general 6-tap multipath channel ($v = 6$) with exponential PDP and $\tau_{rms} = 1.25$ is considered. The SFE using QR-JEA with $I = 0$ and $L \geq v + 3$ is only 1.2dB poorer than the 4-stage LSF of [1] at a BER of 10^{-3}. The QR-JEA based SFE with $I > 0$ significantly outperforms the 4-stage LSF for BER values above 10^{-3} and provides similar performance at a BER of approximately 10^{-5}. In addition, using the effective channel vector $\mathbf{f}_m$

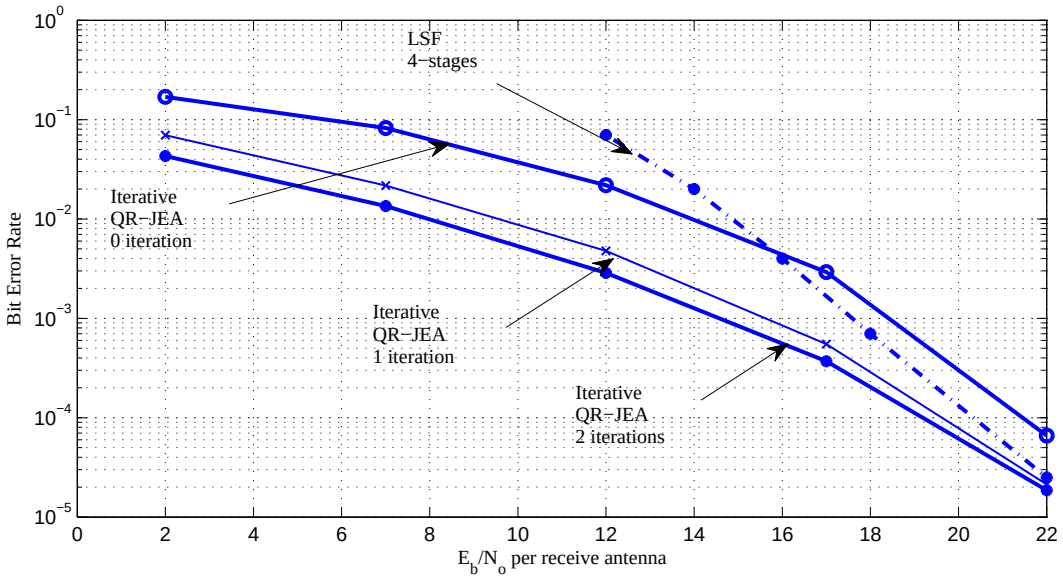

Figure 4.9: Comparative performance of the SFE based on QR-JEA and the 4-stage LSF of [1] on a $v = 6$ channel for $M = N = 4$. For QR-JEA (0, 1 and 2 iterations), $L = 9$ is used for parameter estimation.

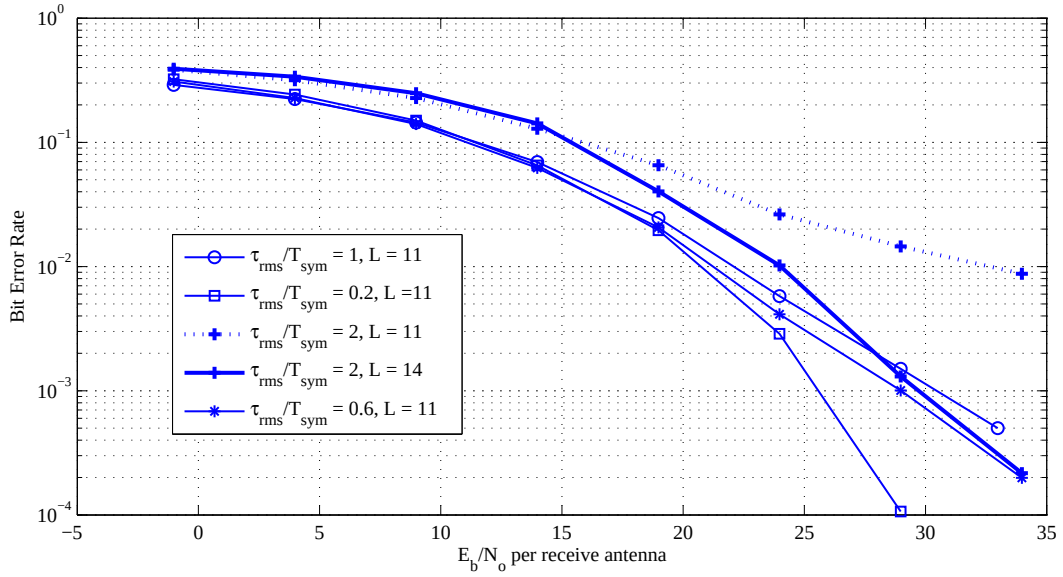

Figure 4.10: Performance of the iterative QR-JEA ($I = 2$ iterations) based SFE using 16 QAM on a general $v = 11$ multipath channel (maximum ISI span of 11 symbols) with a frame length of $N_s = 256$ symbols and employing a pre-processor of TD length $L = 11$ and $L = 14$.

computed using the QR decomposition with one and two iterations outperforms the non-iterative JEA ($I = 0$) based SFE by 3dB and 4.2dB respectively at a BER of 10^{-3}. However, we note that at sufficiently high SNR $(> 23)dB$ it appears that the iterative QR-JEA and 4-stage LSF converge in error rate.

In Fig. 4.10, 16-QAM modulation as in [28] is used and the performance of the SFE with iterative QR-JEA ($I = 2$ iterations) is illustrated. The 11-tap channel model with a maximum ISI span of $v = 11$ symbols is considered for various RMS delay spreads normalized to the symbol period. Fig. 4.10 illustrates that a pre-processor length of $L = 14$ is required on such dense multipath channels with normalized RMS delay spread of $\tau_{rms}/T_{sym} = 2$ in order to achieve good performance. In [28] a SM system with least squares channel estimation is proposed. Our $L = 14$ result in Fig.4.10 achieves a performance gain of 2dB at a BER of 10^{-2} compared to the results given in [28].

4.7 Conclusions

We have developed a linear FD receiver structure for broadband SC systems which jointly performs CCI mitigation and ISI equalization. An iterative QR-JEA approach to channel estimation is developed. It performs parameter estimation in the TD. This requires lower processing time than several known FD orthogonal training sequence based channel estimation algorithms. It is seen that the iterative QR-JEA algorithm can significantly improve performance at moderate SNR, using a few simple iterations. Simulation results show that the proposed receiver achieves excellent performance for channels with large RMS delay spreads. Due to the parallel structure of the SFE, the processing time is lower than that of the successive interference cancellation based LSF approaches of [1, 13, 22, 25]. In addition, equal diversity is achieved by all receiver branches. Finally, it is seen that to achieve good system performance at low BER values the length of the TD CCI mitigation or pre-processor filters must exceed the maximum channel delay spread.

Chapter 5

Space-Frequency Decision Feedback Equalizer

5.1 Introduction

In chapter 4, we developed a linear FD receiver architecture called the integrated SFE that utilizes an iterative QR-JEA approach to channel estimation. We now develop a non-linear space frequency decision feedback equalizer (SF-DFE). It uses the FD pre-processor developed in chapter 4 in conjunction with the hybrid-DFE receiver architecture [23, 49] discussed in chapter 3 (section 3.2.3).

Most existing MIMO DFE based receivers are derived based on complete knowledge of the MIMO channel matrix, and its parameters are derived assuming this perfect CSI in [1, 13, 23, 49]. The effect of imperfect CSI on the performance of the multi-stage LSF-DFE (equivalent to a hybrid DFE with SIC) was examined in [1]. It was concluded there that multi-stage LSF-DFE receivers are more susceptible to imperfect CSI which worsens the effect of error propagation. In [13], two noise predictive (NP)-DFE structures, are studied for MIMO systems, where it was shown that the NP-DFE of [13] and hybrid DFE similar to that of [1] achieve the same MMSE.

The SF-DFE receiver developed here has a parallel-branch receiver architecture, and is not affected by signal processing imperfections in other branches. Hence, the

SF-DFE is not effected by error propagation as in [1]. Further, it is implemented using QR-JEA channel estimation algorithm developed in chapter 4. Due to the parallel processing nature of the receiver, the SF-DFE requires lower processing time than SIC based DFE receivers [1, 13]. Using simulations we show that, as expected, the SF-DFE outperforms its linear counterpart presented in chapter 4 and SIC based DFE receivers.

The rest of this chapter is organized as follows. In section 5.2 we give an overview of the proposed SF-DFE system architecture. In section 5.3, the SF-DFE system model is developed. The derivation of the FD-FFF and the TD-FBF coefficients using MMSE optimization is presented in section 5.3.1. A complexity analysis comparing the SF-DFE with existing MIMO DFE architectures is provided in section 5.4. In section 5.5, performance evaluation by means of simulations is given. Finally, conclusions are drawn in section 5.6

5.2 Proposed Space-Frequency-DFE Structure

We now develop an analytical model for the non-linear FD receiver that utilizes and extends the linear architecture presented in chapter 4. The overall SF-DFE receiver architecture is shown in Fig. 5.1. The N received signal streams are Fourier transformed and fed into the SF-DFE. As with the linear SFE of chapter 4, the SF-DFE consist of M parallel receiver branches each corresponding to a transmitted signal. The front-end implements CCI suppression and ISI equalization in the FD and the back-end implements post-cursor ISI cancelation and detection in the TD.

The CSI for each of the M receiver branches is estimated in parallel using the iterative QR-JEA developed in chapter 4. For the m^{th} branch, the CSI is then provided in the form of an effective overall channel response vector, $\mathbf{f}_m$, and a set of N pre-processor weight vectors, $\mathbf{w}_{m,n}$. The set of weights are concatenated to form the overall vector $\mathbf{w}_m$ (see Sec. 4.3 for details). From Sec. 4.3 (4.22) we know,

$$\mathbf{w}_m = \mathbf{f}_m(\bar{\mathbf{s}}_m\overline{\mathbf{y}}^{sH})(\overline{\mathbf{y}}^{s}\overline{\mathbf{y}}^{sH})^{-1}, \tag{5.1}$$

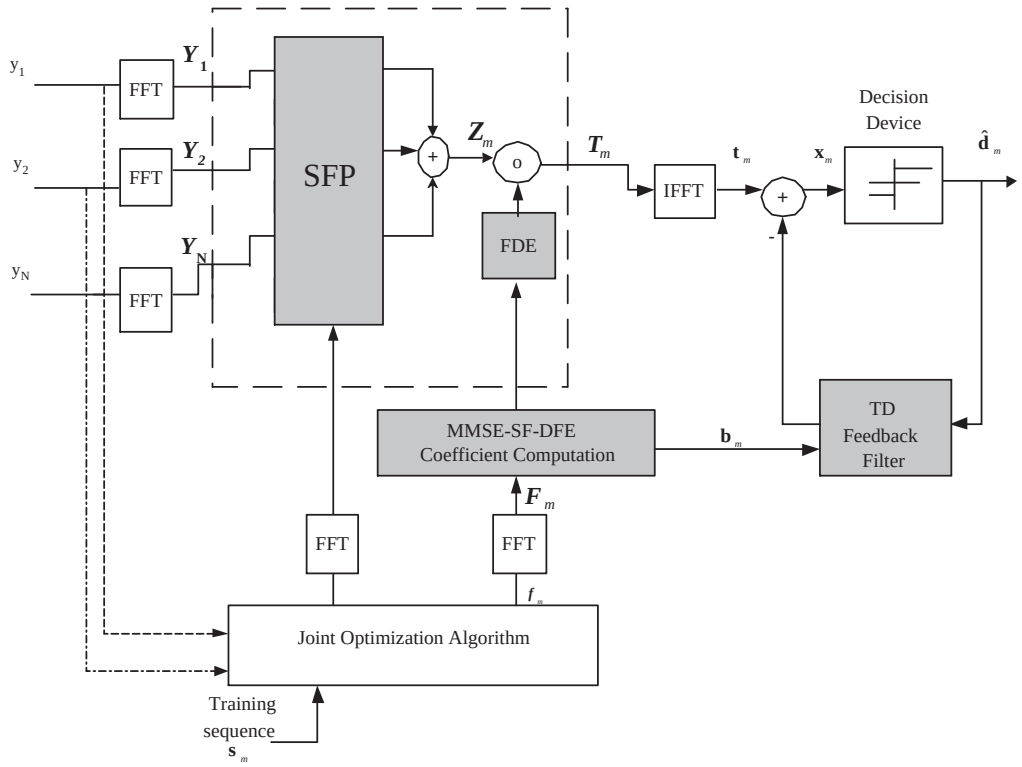

Figure 5.1: Block diagram of the m^{th} $(m = 1, \ldots, M)$ branch of a multi-input space-frequency decision feedback equalizer.

where $\bar{\mathbf{s}}_m$ is the $(L + v + 1) \times p$ training matrix defined in chapter 4, and $\overline{\mathbf{y}}^s$ is the received matrix corresponding to the transmission of $\bar{\mathbf{s}}_m$. The TD vectors $\mathbf{w}_{m,n}$ and $\mathbf{f}_m$ have zeros appended at one end of the vector to form length N_s vectors. Fourier transformation of these results in the frequency domain preprocessor weight vector $\boldsymbol{\mathcal{W}}_{m,n}$ vectors and the effective channel frequency response vector $\boldsymbol{\mathcal{F}}_m$.

The vector $\boldsymbol{\mathcal{W}}_{m,n}$ processes the n^{th} received signal in the FD to suppress CCI. All N preprocessor path outputs within each receiver branch are then combined to form the front-end processor branch output $\boldsymbol{\mathcal{Z}}_m$, $m = 1, \ldots, M$ as shown in Fig. 5.1. The hybrid-DFE described in section 3.2.3 is used here for equalization and data detection. The effective channel frequency response vector $\boldsymbol{\mathcal{F}}_m$ is used in computing the coefficients of the frequency domain- feed forward filter (FD-FFF) and the time domain-feedback filter (TD-FBF) of the SF-DFE.

The hybrid-DFE is optimized in terms of MMSE and is implemented individually within each of the M parallel branches of the SF-DFE. A slight increase in signal processing complexity occurs due to the additional feedback processing. This non-linear extension of the SFE yields performance improvement over the linear architecture developed in chapter 4.

5.3 System Model

The m^{th} branch of the SF-DFE receiver used with an M-transmit and N-receive antenna system is shown in Fig. 5.1. Here the transmission frame, $\mathbf{d}_m$, of length N_s, defined in chapter 4 is considered. A frequency selective channel as described in chapters 2 and 4, with a maximum ISI span of v symbol periods is considered. The SF-DFE has M parallel branches which detect all M signals in parallel based on estimated CSI. Each of the m branches consist of a SFP of effective TD length L, a FD-FFF (similar to the MMSE-FDE of chapter 4) followed by a TD-FBF. Assuming that CSI is provided by the iterative QR-JEA, the SF-DFE is derived as follows:

We start the analysis by writing the N_s dimensional TD received signals at the receiver array as

$$\overline{\mathbf{y}}_n = \overline{\mathbf{h}}_{m,n}\overline{\mathbf{d}}_m + \overline{\mathbf{e}}_{m,n}, \qquad n = 1, \ldots, N, \tag{5.2}$$

where $\overline{\mathbf{h}}_{m,n}$ represents a convolution matrix of dimension $(L+1) \times (L+v+1)$ and $\mathbf{e}_{m,n}$ corresponds to the overall distortion (noise and CCI). After an N_s-point FFT, the received FD signal is written as

$$\boldsymbol{\mathcal{Y}}_n = \boldsymbol{\mathcal{H}}_{m,n} \circ \boldsymbol{\mathcal{D}}_m + \boldsymbol{\mathcal{E}}_{m,n}, \quad m = 1, 2, \ldots, M, \;\; n = 1, 2, \ldots, N, \tag{5.3}$$

where $\boldsymbol{\mathcal{H}}_{m,n}$ is the channel frequency response and $\boldsymbol{\mathcal{E}}_{m,n}$ is the FD distortion term given by

$$\boldsymbol{\mathcal{E}}_{m,n} = \sum_{i \neq m} \boldsymbol{\mathcal{H}}_{i,n} \circ \boldsymbol{\mathcal{D}}_i + \boldsymbol{\mathcal{N}}_{m,n}, \qquad m = 1, \ldots, M, \;\; n = 1, \ldots, N. \tag{5.4}$$

The SF-DFE uses the FD-preprocessor of chapter 4 for CCI mitigation. Therefore, CCI mitigation on $\boldsymbol{\mathcal{Y}}_n$ at the n^{th} receiver is implemented using the vectors $\boldsymbol{\mathcal{W}}_{m,n}$ to produce the output,

$$\begin{aligned} \boldsymbol{\mathcal{Z}}_m &= \sum_{n=1}^{N} \boldsymbol{\mathcal{W}}_{m,n} \circ \boldsymbol{\mathcal{Y}}_n & (5.5) \\ &= \boldsymbol{\mathcal{D}}_m \circ \boldsymbol{\mathcal{F}}_m + \boldsymbol{\mathcal{I}}_m, \qquad m = 1, \ldots, M. & (5.6) \end{aligned}$$

where

$$\boldsymbol{\mathcal{F}}_m = \sum_{n=1}^{N} \boldsymbol{\mathcal{W}}_{m,n} \circ \boldsymbol{\mathcal{H}}_{m,n}, \qquad m = 1, \ldots, M. \tag{5.7}$$

is the effective channel frequency response vector and the residual interference vector is given by

$$\boldsymbol{\mathcal{I}}_m = \sum_{n=1}^{N} \boldsymbol{\mathcal{W}}_{m,n} \circ \boldsymbol{\mathcal{E}}_{m,n}. \tag{5.8}$$

In the following sections, the effective channel response vector, $\boldsymbol{\mathcal{F}}_m$, is used to derive the MMSE based non-linear equalizer employing a hybrid DFE structure as described in chapter 3. As with linear SFE, the SF-DFE consists of M parallel branches each corresponding to a transmitted signal. Since processing is similar in all M branches, in the following, we derive the FD-FFF and TD-FBF coefficients of the hybrid DFE for the m^{th} receiver branch based on the effective channel response vector, $\boldsymbol{\mathcal{F}}_m$.

5.3.1 MMSE based DFE

Following the pre-processor, the signal corresponding to the m^{th} transmitter, $\boldsymbol{\mathcal{Z}}_m$, is passed into an MMSE based DFE for equalization and detection. In this section we derive the DFE filter coefficients using the estimated effective channel parameters derived in chapter 4. Using the DFE coefficients, we compute the MSE of the SF-DFE and show that it is less than the MSE of the linear SFE in chapter 4.

The SF-DFE consists of a block-wise FD-FFF (or an FDE) followed by a symbol-wise FBF operating in the TD. The FD-FFF equalizes ISI over a block of symbols,

while the TD-FBF section operates on a per-symbol basis to cancel the interference contribution due to previously detected data symbols. The FBF has an FIR structure of length L_b, which is the number of previous symbols considered in detecting the current symbol.

The FD-FFF vector of the DFE is represented by $\boldsymbol{\mathcal{G}}_m$. It performs ISI equalization in the FD on $\boldsymbol{\mathcal{Z}}_m$, and its output may be written as

$$\boldsymbol{\mathcal{T}}_m = \boldsymbol{\mathcal{G}}_m \circ \boldsymbol{\mathcal{Z}}_m. \tag{5.9}$$

The vector $\boldsymbol{\mathcal{T}}_m$ is inverse Fourier transformed to yield the length N_s TD vector

$$\mathbf{t}_m = \sum_{k=0}^{N_s-1} \mathcal{T}_m(k) e^{i\frac{2\pi}{N_s}kj}, \qquad j = 0, 1, \ldots, N_s - 1. \tag{5.10}$$

where $\mathcal{T}_m(k)$ is the k^{th} element of $\boldsymbol{\mathcal{T}}_m$. We can represent (5.10) in matrix form by defining the FFT matrix $\overline{\mathbf{Q}}_{N_s}$ as

$$\overline{\mathbf{Q}}_{N_s} = \begin{pmatrix} 1 & 1 & 1 & 1 & 1 & \ldots & 1 \\ 1 & w & w^2 & w^3 & \ldots & & w^{N_s-1} \\ 1 & w^2 & w^4 & w^6 & \ldots & & w^{2N_s-1} \\ 1 & w^3 & w^6 & w^9 & \ldots & & \vdots \\ \vdots & \vdots & \vdots & & \vdots & & \\ 1 & w^{N_s-1} & w^{2N_s-1} & w^{3N_s-1} & \ldots & & w^{(N_s-1)(N_s-1)} \end{pmatrix}, \tag{5.11}$$

where $w^n = e^{-i\frac{2\pi n}{N_s}}$ is the primitive n^{th} root of unity [71] and $n = kj$, where k, j $(k, j = 0, \ldots, N_s - 1)$ are the row and column indices. Consequently, the IFFT matrix is defined by its Hermitian $\overline{\mathbf{Q}}_{N_s}^H$. Using (5.11) we may then write (5.10) as

$$\begin{aligned} \mathbf{t}_m &= \overline{\mathbf{Q}}_{N_s}{}^H \boldsymbol{\mathcal{T}}_m, \\ &= \overline{\mathbf{Q}}_{N_s}{}^H (\boldsymbol{\mathcal{G}}_m \circ \boldsymbol{\mathcal{Z}}_m). \end{aligned} \tag{5.12}$$

This forms the TD input to the FBF section of the DFE.

The TD-FBF is defined as a FIR structure, $\mathbf{b}_m$, of length $L_b < L + v$ given by

$$\mathbf{b}_m = [\ 1 \quad b_m(1) \quad \ldots \quad b_m(L_b)\ ]. \tag{5.13}$$

We form a length N_s vector from (5.13) by zero-padding and define the $N_s \times N_s$ FBF matrix as

$$\overline{\mathbf{b}}_m = \begin{pmatrix} 1 & 0 & \dots & \dots & \dots & \dots & \vdots & 0 \\ b_m(1) & 1 & \dots & \dots & \dots & \dots & \vdots & 0 \\ b_m(2) & b_m(1) & 1 & \ddots & \ddots & \dots & & 0 \\ \vdots & b_m(2) & \ddots & \ddots & \ddots & \ddots & & \\ b_m(L_b) & \vdots & \ddots & \ddots & & \ddots & & \\ 0 & b_m(L_b) & & b_m(1) & 1 & & & \\ \vdots & 0 & & & & & & \\ 0 & 0 & \dots & b_m(L_b) & \dots & & b_m(1) & 1 \end{pmatrix}. \tag{5.14}$$

Contributions from the FD-FFF and TD-FBF are combined and fed into to the decision device in Fig. 5.1. Its input can be written as

$$\mathbf{x}_m = \mathbf{t}_m - (\overline{\mathbf{b}}_m - \bar{\mathbf{I}})\hat{\mathbf{d}}_m, \tag{5.15}$$

The TD error vector may then be written as

$$\boldsymbol{\delta}_{TD} \;=\; \mathbf{x}_m - \mathbf{d}_m. \tag{5.16}$$

The presence of the hard decision device makes the optimization problem non-linear [72]. To proceed, we linearize[1] the problem by assuming that the decision device delivers error-free data estimates. Note that in practice erroneous decisions may occur and get fed back into the equalizer through the TD-FBF. When a longer TD-FBF is used, the effect of these erroneous decisions is greater and may degrade the performance especially at low SNR [13]. Still, it can be shown that non-linear equalizers such as DFE's always tend to outperform linear equalizers [1]. Substituting $\hat{\mathbf{d}}_m = \mathbf{d}_m$ and (5.15) in (5.16) we have

$$\begin{aligned} \boldsymbol{\delta}_{TD} &= \mathbf{t}_m - (\overline{\mathbf{b}}_m - \bar{\mathbf{I}})\mathbf{d}_m - \mathbf{d}_m \\ &= \mathbf{t}_m - \overline{\mathbf{b}}_m \mathbf{d}_m. \end{aligned} \tag{5.17}$$

[1] In all cases of interest, the symbol error rate is less than or equal to 0.5, and this assumption leads to optimal results.

Using the FFT matrix of (5.11) we can then write the error vector in the FD as

$$\begin{aligned} \boldsymbol{\delta}_{FD} &= \overline{\mathbf{Q}}_{N_s}\boldsymbol{\delta}_{TD} \\ &= \overline{\mathbf{Q}}_{N_s}\big(\mathbf{t}_m - \overline{\mathbf{b}}_m\mathbf{d}_m\big). \end{aligned} \tag{5.18}$$

Since $\overline{\mathbf{Q}}_{N_s}$ represents the FFT we can rewrite (5.18) as

$$\boldsymbol{\delta}_{FD} = \boldsymbol{\mathcal{T}}_m - \sum_{j=0}^{N_s-1}(\overline{\mathbf{b}}_m\mathbf{d}_m)e^{-i\frac{2\pi}{N_s}kj}, \tag{5.19}$$

where the output vector $\boldsymbol{\mathcal{T}}_m$ of the FD-FFF is given by (5.9) and $\overline{\mathbf{b}}_m\mathbf{d}_m$ represents the convolution between the vectors $\mathbf{b}_m$ and $\mathbf{d}_m$. The Fourier transform of this is equivalent to component-wise multiplication in the FD according to the convolution theorem [46] and is expressed as

$$\sum_{j=0}^{N_s-1}(\overline{\mathbf{b}}_m\mathbf{d}_m)e^{-i2\frac{\pi}{N_s}kj} = \boldsymbol{\mathcal{B}}_m \circ \boldsymbol{\mathcal{D}}_m \quad k = 0, \ldots, N_s - 1. \tag{5.20}$$

Substituting (5.9) and (5.20) in (5.19) we obtain the error vector in the FD as

$$\boldsymbol{\delta}_{FD} = \boldsymbol{\mathcal{G}}_m \circ \boldsymbol{\mathcal{Z}}_m - \boldsymbol{\mathcal{B}}_m \circ \boldsymbol{\mathcal{D}}_m. \tag{5.21}$$

This allows us to write the FD-MSE of the SF-DFE as

$$\begin{aligned} MSE_{SF-DFE} &= Tr\left(E[\boldsymbol{\delta}_{FD}^H\boldsymbol{\delta}_{FD}]\right) \\ &= Tr\left(E[\parallel \boldsymbol{\mathcal{G}}_m \circ \boldsymbol{\mathcal{Z}}_m - \boldsymbol{\mathcal{B}}_m \circ \boldsymbol{\mathcal{D}}_m \parallel^2]\right). \end{aligned} \tag{5.22}$$

The MMSE solutions for the vectors $\boldsymbol{\mathcal{G}}_m$ and $\boldsymbol{\mathcal{B}}_m$ can now be obtained by minimizing (5.22). This is done by applying the orthogonality principle, which states that the output sequence of a linear filter optimized in the MMSE sense is orthogonal to the error sequence [73]. Therefore, we may write

$$\frac{1}{N_s}E[\boldsymbol{\mathcal{Z}}_m^H\boldsymbol{\delta}_{FD}] = \frac{1}{N_s}E[\boldsymbol{\mathcal{Z}}_m^H(\boldsymbol{\mathcal{G}}_m \circ \boldsymbol{\mathcal{Z}}_m - \boldsymbol{\mathcal{B}}_m \circ \boldsymbol{\mathcal{D}}_m)] = 0. \tag{5.23}$$

Rewriting (5.23) yields

$$E[\boldsymbol{\mathcal{Z}}_m{}^H(\boldsymbol{\mathcal{G}}_m \circ \boldsymbol{\mathcal{Z}}_m) - \boldsymbol{\mathcal{Z}}_m{}^H\boldsymbol{\mathcal{B}}_m \circ \boldsymbol{\mathcal{D}}_m] = 0$$

or

$$\overline{\boldsymbol{\mathcal{G}}}_m E[\boldsymbol{\mathcal{Z}}_m^H \boldsymbol{\mathcal{Z}}_m] = \overline{\boldsymbol{\mathcal{B}}}_m E[\boldsymbol{\mathcal{Z}}_m^H \boldsymbol{\mathcal{D}}_m], \tag{5.24}$$

where the matrices, $\overline{\boldsymbol{\mathcal{G}}}_m$ and $\overline{\boldsymbol{\mathcal{B}}}_m$ are obtained by the diagonalization of the vectors, $\boldsymbol{\mathcal{G}}_m$ and $\boldsymbol{\mathcal{B}}_m$, respectively. Similarly diagonal matrices, $\overline{\boldsymbol{\mathcal{Z}}}_m$, $\overline{\boldsymbol{\mathcal{F}}}_m$ and $\overline{\boldsymbol{\mathcal{D}}}_m$ are obtained by diagonalizing the FD vectors $\boldsymbol{\mathcal{Z}}_m$, $\boldsymbol{\mathcal{F}}_m$ and $\boldsymbol{\mathcal{D}}_m$. This diagonalization of allows us to write the element wise multiplication of two vectors as multiplication of diagonal matrices. Also, it is not difficult to show that

$$E[\boldsymbol{\mathcal{Z}}_m^H \boldsymbol{\mathcal{Z}}_m] = E[\overline{\boldsymbol{\mathcal{Z}}}_m^H \overline{\boldsymbol{\mathcal{Z}}}_m], \tag{5.25}$$

$$E[\boldsymbol{\mathcal{Z}}_m^H \boldsymbol{\mathcal{D}}_m] = E[\overline{\boldsymbol{\mathcal{Z}}}_m^H \overline{\boldsymbol{\mathcal{D}}}_m], \tag{5.26}$$

The variance of the transmitted data symbols is defined as $\rho_d^2 = E[d_m d_m^*] = E[\mathcal{D}_m \mathcal{D}_m{}^*]$ and the interference plus noise variance as $\rho_i^2 = E[i_m i_m^*] = E[\mathcal{I}_m \mathcal{I}_m{}^*]$, so that.

$$\begin{aligned} E[\overline{\boldsymbol{\mathcal{Z}}}_m^H \overline{\boldsymbol{\mathcal{Z}}}_m] &= E[(\overline{\boldsymbol{\mathcal{D}}}_m \overline{\boldsymbol{\mathcal{F}}}_m + \overline{\boldsymbol{\mathcal{I}}}_m)^H (\overline{\boldsymbol{\mathcal{D}}}_m \overline{\boldsymbol{\mathcal{F}}}_m + \overline{\boldsymbol{\mathcal{I}}}_m)], \\ &= {\rho_d}^2 \overline{\boldsymbol{\mathcal{F}}}_m \overline{\boldsymbol{\mathcal{F}}}_m{}^H + {\rho_i}^2 \overline{\mathbf{I}} \quad m = 1, \ldots, M. \end{aligned} \tag{5.27}$$

Therefore,

$$E[\boldsymbol{\mathcal{Z}}_m^H \boldsymbol{\mathcal{Z}}_m] = {\rho_d}^2 \overline{\boldsymbol{\mathcal{F}}}_m^H \overline{\boldsymbol{\mathcal{F}}}_m + {\rho_i}^2 \overline{\mathbf{I}}. \tag{5.28}$$

Since $E[\mathcal{D}_m \mathcal{I}_m{}^*] = 0$

$$E[\boldsymbol{\mathcal{Z}}_m^H \boldsymbol{\mathcal{D}}_m] = E[(\overline{\boldsymbol{\mathcal{D}}}_m \overline{\boldsymbol{\mathcal{F}}}_m + \overline{\boldsymbol{\mathcal{I}}}_m)^H \overline{\boldsymbol{\mathcal{D}}}_m] = \rho_d^2 \overline{\boldsymbol{\mathcal{F}}}_m^H. \tag{5.29}$$

Substituting (5.28) and (5.29) in (5.24) we obtain

$$\overline{\boldsymbol{\mathcal{G}}}_m ({\rho_d}^2 \overline{\boldsymbol{\mathcal{F}}}_m^H \overline{\boldsymbol{\mathcal{F}}}_m + {\rho_i}^2 \overline{\mathbf{I}}) = \overline{\boldsymbol{\mathcal{B}}}_m \rho_d^2 \overline{\boldsymbol{\mathcal{F}}}_m^H. \tag{5.30}$$

Finally, we obtain the FD-FFF matrix as

$$\overline{\boldsymbol{\mathcal{G}}}_m = \overline{\boldsymbol{\mathcal{B}}}_m \overline{\boldsymbol{\mathcal{F}}}_m^* \left(\overline{\boldsymbol{\mathcal{F}}}_m \overline{\boldsymbol{\mathcal{F}}}_m^* + \frac{\rho_i^2}{\rho_d^2} \overline{\mathbf{I}} \right)^{-1}, \tag{5.31}$$

with corresponding vector

$$\begin{aligned}\boldsymbol{\mathcal{G}}_m &= \boldsymbol{\mathcal{B}}_m \circ \boldsymbol{\mathcal{F}}_m^* \circ \left(\boldsymbol{\mathcal{F}}_m \circ \boldsymbol{\mathcal{F}}_m^* + \frac{\rho_i^2}{\rho_d^2}\mathbf{1}\right)^{-1} \\ &= \boldsymbol{\mathcal{B}}_m \circ \boldsymbol{\mathcal{F}}_m^* \circ \left(\boldsymbol{\mathcal{F}}_m \circ \boldsymbol{\mathcal{F}}_m^* + \frac{\rho_i^2}{\rho_d^2}\mathbf{1}\right)^{.-1}. \end{aligned} \tag{5.32}$$

The FD-FFF is a function of the estimated effective channel response vector, $\boldsymbol{\mathcal{F}}_m$ and the Fourier transform of the TD-FBF, $\mathbf{b}_m$, which is yet to be derived. Using (5.32), we can compute $\mathbf{b}_m$ by minimizing the TD-MSE of the SF-DFE. The TD-MSE can be written using the error vector defined in (5.17) as

$$\begin{aligned} MSE_{SF-DFE} &= \frac{1}{N_s}E[\boldsymbol{\delta}_{TD}^H\boldsymbol{\delta}_{TD}] \qquad (5.33)\\ &= \frac{1}{N_s}E[\left(\mathbf{t}_m - \overline{\mathbf{b}}_m\mathbf{d}_m\right)^H\left(\mathbf{t}_m - \overline{\mathbf{b}}_m\mathbf{d}_m\right)] \\ &= \frac{1}{N_s}E[\mathbf{t}_m^H\mathbf{t}_m] + E[\mathbf{d}_m^H\overline{\mathbf{b}}_m^H\overline{\mathbf{b}}_m\mathbf{d}_m] - E[\mathbf{d}_m^H\overline{\mathbf{b}}_m^H\mathbf{t}_m] \\ &\quad -E[\mathbf{t}_m^H\overline{\mathbf{b}}_m\mathbf{d}_m]. \qquad (5.34)\end{aligned}$$

After computing (5.34), the MSE of the SF-DFE reduces to [24, 49]

$$MSE_{SF-DFE} = \frac{\rho_i^2}{N_s}\left(\overline{\mathbf{b}}_m^H\overline{\mathbf{Q}}_{N_s}{}^H\overline{\boldsymbol{\Phi}}_m\overline{\mathbf{Q}}_{N_s}\overline{\mathbf{b}}_m\right), \tag{5.35}$$

where we have the diagonal matrix $\overline{\boldsymbol{\Phi}}_m = (\overline{\boldsymbol{\mathcal{F}}}_m\overline{\boldsymbol{\mathcal{F}}}_m^H + \frac{\rho_i^2}{\rho_d^2}\overline{\mathbf{I}})^{-1}$. The derivation of (5.35) from (5.34) is included in Appendix A. We denote the element in the s^{th} row and j^{th} column of $N_s \times N_s$ matrix $\overline{\mathbf{b}}_m$ as $b_m^{s,j}$ where $s, j = 0, \ldots, N_s - 1$. Similarly we denote the element in the s^{th} row and t^{th} column of $\overline{\mathbf{b}}_m^H$ with $b_m^{*t,s}$ where, $s, t = 0, \ldots, N_s - 1$. Now (5.35) can be written as

$$MSE_{SF-DFE} = \frac{\rho_i^2}{N_s}\sum_{s=0}^{N_s-1}\sum_{l=0}^{N_s-1}\Phi_m(l,l)\left[\sum_{j=0}^{N_s-1} b_m^{s,j}e^{i\frac{2\pi jl}{N_s}}\sum_{t=0}^{N_s-1} b_m^{*s,t}\right]e^{-i\frac{2\pi tl}{N_s}}, \tag{5.36}$$

where $\Phi_m(l,l) = \left(\mathcal{F}_m(l)\mathcal{F}_m^*(l) + \frac{\rho_i^2}{\rho_d^2}\right)^{-1}$ represents the l^{th} diagonal element of the matrix $\overline{\boldsymbol{\Phi}}_m$. Now, the gradient method [24, 63] as given in [73] can be used to find the optimal feedback matrix $\overline{\mathbf{b}}_m$ that minimizes the MSE given in (5.36). The s^{th} row of the optimal $\overline{\mathbf{b}}_m$ obtained using the gradient method [24] is Fourier

transformed to obtain the FD-FBF $\boldsymbol{\mathcal{B}}_m$. The $N_s \times 1$ vector $\boldsymbol{\mathcal{B}}_m$ is substituted into (5.32) to compute the FD-FFF $\boldsymbol{\mathcal{G}}_m$.

In order to obtain the optimal FBF coefficients that minimize the MSE of the SF-DFE in (5.36), we form the matrix $\overline{\mathbf{A}}_{SF-DFE}$ with the $(t,j)^{th}$ element defined by

$$\sum_{l=0}^{N_s-1} \Phi_m(l,l) e^{-i\frac{2\pi(t-j)l}{N_s}}, \qquad j=[1,\ldots,L_b], t=[1,\ldots,L_b] \tag{5.37}$$

and a vector $\mathbf{a}_{SF-DFE}$ with its j^{th} element given by

$$\sum_{l=0}^{N_s-1} \Phi_m(l,l) e^{i\frac{2\pi jl}{N_s}}, \qquad j=[1,\ldots,L_b]. \tag{5.38}$$

Using the gradient method [73], it is found similarly to [24, 49], that the s^{th} row of $\overline{\mathbf{b}}_m$ denoted by $\mathbf{b}_m^s = [b_m^{s,0}, b_m^{s,1}, \ldots, b_m^{s,s-1}, 1, 0, \ldots, 0]$, optimal in the MMSE sense, is obtained by solving the linear system of equations with L_b unknowns,

$$\overline{\mathbf{A}}_{SF-DFE}\mathbf{b}_m^s = \mathbf{a}_{SF-DFE}. \tag{5.39}$$

Techniques such as the Levinson-Durbin algorithm [24] can be used to obtain this optimal solution for $\mathbf{b}_m^s$. This can be computed using the QR decomposition of $\overline{\mathbf{A}}_{SF-DFE}$.

On examining $\overline{\mathbf{A}}_{SF-DFE}$ we notice that it is square and non-singular and hence QR decomposition using Householder reflectors [69], [68] produces a unitary matrix $\overline{\mathbf{Q}}$ with $\overline{\mathbf{Q}}^H\overline{\mathbf{Q}} = \bar{\mathbf{I}}$, and, an upper triangular matrix $\overline{\mathbf{R}}$ such that

$$\overline{\mathbf{A}}_{SF-DFE} = \overline{\mathbf{QR}}. \tag{5.40}$$

Generally, solving the linear system of equations in (5.39) involves computation of the inverse of the matrix which is computationally expensive. Computation of the matrix inverse can be avoided by exploiting the properties of QR decomposition as follows: The optimal $\mathbf{b}_m^s$ in the MMSE sense is computed by multiplying both sides

of (5.39) with $\overline{\mathbf{A}}^H_{SF-DFE}$. Then substituting (5.40) we have

$$\left(\overline{\mathbf{QR}}\right)^H \left(\overline{\mathbf{QR}}\right) \mathbf{b}^s_m = \overline{\mathbf{A}}^H_{SF-DFE}\mathbf{a}_{SF-DFE} \tag{5.41}$$

$$\overline{\mathbf{R}}^H \left(\overline{\mathbf{Q}}^H \overline{\mathbf{Q}}\right) \overline{\mathbf{R}}\mathbf{b}^s_m = \overline{\mathbf{A}}^H_{SF-DFE}\mathbf{a}_{SF-DFE} \tag{5.42}$$

$$\tag{5.43}$$

The TD-FBF coefficients are now computed as

$$\mathbf{b}^s_m = (\overline{\mathbf{R}}^H\overline{\mathbf{R}})^{-1}\overline{\mathbf{A}}^H_{SF-DFE}\mathbf{a}_{SF-DFE}. \tag{5.44}$$

After computing the MMSE optimized solution for $\mathbf{b}^s_m$ we substitute its Fourier transform into (5.32) to calculate the FD-FFF. The Fourier transform of $\mathbf{b}^s_m$ is given by

$$\boldsymbol{\mathcal{B}}_m = [\mathcal{B}_m(0), \mathcal{B}_m(1), \ldots, \mathcal{B}_m(N_s - 1)], \tag{5.45}$$

where

$$\mathcal{B}_m(k) = \sum_{j=1}^{L_B} b^{s,j}_m e^{-i\frac{2\pi jk}{N_s}} \qquad k = [0, \ldots, N_s - 1]. \tag{5.46}$$

It can be observed that when the number of taps in the TD-FBF is set to zero that is $L_b = 0$, then the SF-DFE reduces to that of the linear SFE of (4.55). The MSE of the linear-SFE $MSE_{linear-SFE}$ can be obtained by substituting $s, j, t = 0$ in (5.36) giving

$$MSE_{linear-SFE} = \frac{\rho^2_i}{N_s} \sum_{l=0}^{N_s-1} \Phi_m(l,l) \left[b^{0,0}_m e^{i\frac{2\pi 0l}{N_s}} b^{*0,0}_m\right] e^{-i\frac{2\pi 0l}{N_s}} \tag{5.47}$$

$$= \frac{\rho^2_i}{N_s} \sum_{l=0}^{N_s-1} \Phi_m(l,l). \tag{5.48}$$

Further, it is not difficult to show that the MSE_{SF-DFE} defined in (5.36) is always smaller than (5.48).

5.4 Complexity Analysis

An analytical model of the SF-DFE has been developed in this chapter. In this section, we evaluate its computational complexity in comparison with the MIMO

DFE architectures given in [1, 13, 31]. We quantify complexity in terms of the number of complex multiplications required for the detection of a block of data. The overall receiver complexity is split into two parts

1. Complexity of coefficient calculation that includes the computational complexity of the space-frequency pre-processor, the FD-FFF and the TD-FBF.

2. Complexity of signal processing in the time and the frequency domains.

Channel estimation complexity is not addressed here as it is the same for both the linear and non-linear receivers and can be found in chapter 4. As noted previously, the CSI is provided in the form of the TD vectors $\mathbf{f}_m$ and $\mathbf{w}_m$ by the iterative QR-JEA. These vectors are used in constructing the SF-DFE in the FD.

The TD-FBF coefficients of the SF-DFE are computed by solving the linear system of equations with L_b unknowns in (5.39). Computation of the $L_b \times L_b$ matrix $\overline{\mathbf{A}}_{SF-DFE}$ using (5.37) and the vector $\mathbf{a}_{SF-DFE}$ using (5.38) requires a total of $N_s L_b^2 + N_s L_b$ multiplications. Then, the QR-decomposition of $\overline{\mathbf{A}}_{SF-DFE}$ in (5.40) requires $\frac{2}{3}L_b^3 + \frac{3}{2}L_b^2 + 3L_b$ complex multiplications. The FBF vector $\mathbf{b}_m^s$ is finally obtained by solving (5.44) requiring $\frac{5}{3}L_b^3 + 2L_b^2 - \frac{5}{3}L_b$ complex multiplications. Therefore, the total complexity to compute the FBF is obtained by adding the complexities of (5.37), (5.38), (5.39), (5.40) and (5.44), which is given by $\frac{7}{3}L_b^3 + \frac{7}{2}L_b^2 + \frac{4}{3}L_b + N_s L_b^2 + N_s L_b$. Then, the FD-FFF of the SF-DFE, given by (5.32), is computed using $N_s log_2(N_s) + 3N_s$ complex multiplications.

The signal processing complexity of the SF-DFE is calculated including FD-CCI suppression using (5.5), FD-ISI equalization using (5.9) and TD-FBF processing using (5.44). The overall signal processing complexity of which includes (5.5), (5.9) and (5.44) is given by $(N+1)N_s + N_s^2$.

Consider a numerical example, with $M = N = 4$, $v = 6$, $N_s = 64$ and $L_b = 5$. Then the complexity of coefficient calculation for the m^{th} branch is given by $\frac{7}{3}L_b^3 + \frac{7}{2}L_b^2 + \frac{4}{3}L_b + N_s L_b^2 + N_s L_b + N_s log_2(N_s) + 3N_s = 2882$ and the overall signal processing complexity is given by $(N+1)N_s + N_s^2 = 4416$ complex

multiplications. Therefore, the SF-DFE system complexity per branch is given by $4416 + 2882 = 7298$ complex multiplications. Since, there are $M = 4$ branches the overall complexity amounts to 29192 multiplications.

DFE Architecture	Coefficient computation	Signal processing	Total
SF-DFE	4(4416)	4(2882)	29192
LST-DFE	135988	131172	267160
MIMO hybrid-DFE	24384	6912	31296
MIMO NP-DFE	23040	29488	52528
MIMO-NP-SIC	29928	8064	37992

Table 5.1: Numerical complexity comparison of MIMO DFE architectures.

In [31], the complexity and performance of a layered space-time DFE (LST-DFE) and a MIMO hybrid DFE receivers are given. The overall complexity of the LST-DFE [31], for the numerical example here at each stage requires $(2N + M - 1)\frac{N_s}{2}log_2 N_s + N_s MN + N_s NL_b + \frac{N_s M^3 N^3}{2} + ML_b^3 + N_s N^3 M^3/2 + NL_b^2 = 267160$ complex multiplications. The complexity of the proposed SF-DFE is roughly 11 percent the complexity of the LST-DFE [1, 31].

The MIMO hybrid-DFE of [31] is similar to layered space-frequency DFE (LSF-DFE) of [1]. A single stage of the MIMO hybrid-DFE given in [31] requires a total of $\frac{NN_s}{2}log_2(N_s) + N_s MN + N_s N^2 L_b + N_s MN^3 + M^3 L_b^3 = 31296$ complex multiplications and is comparable to the proposed SF-DFE system complexity.

In [13], a MIMO NP-DFE and a MIMO-NP-SIC (discussed in chapter 3) receivers using FDE were examined. The computation complexity of the FD-FFF and NP coefficient is given as $N_s(M^3 + N^3) + L_b M^3 + (2L_b^2 + 2L_b - 3)M^3 + N_s MN^2 + ((N_s - 1)L_b + 2N_s N)M^2$ which is equal to 29488 complex multiplications. The signal processing complexity of [13] is given by $(M+N)(N_s/2)(log_2(N_s)) + N_s MN + NsL_b M^3$ which is equal to 23040 complex multiplications. The overall complexity of MIMO NP DFE is then given by 52528 complex multiplications. The complexity of SF-DFE is only 55 percent of the MIMO-NP DFE. This is because the SF-DFE processing is based on the effective channel response vector as opposed to the complete MIMO channel matrix as in [13].

The MIMO NP-SIC of [13] has a complexity of $N_s(M^3+N^3)+L_bM^3+(2L_b^2+3L_b-3)M^3+N_sMN^2+((N_s-1)L_b+2N_sN)M^2+L_b\frac{M^3-M^2}{2}$ for coefficient computation. And, $(M+N)\frac{N_s}{2}log_2(N_s)+N_sMN+N_sL_bM^2+N_s\frac{M(M-1)}{2}$ for signal processing. The overall complexity is then given by 37992 complex multiplications for the numerical example. The complexity of the SF-DFE is 76 percent of the complexity of MIMO NP-SIC given in [13]. This comparison does not consider MIMO channel estimation complexity.

In Table 5.1, the computational complexities of DFE architectures [1, 13, 31] compared to the SF-DFE for the numerical example are summarized. From Table 5.1, it can be observed that the MIMO hybrid DFE of [31] and MIMO NP-SIC of [13] have similar system complexities and are only slightly more complex than the proposed SF-DFE. When channel estimation complexities are considered, then, SF-DFE system results in significantly lower complexity than the DFE architectures of [1, 13, 31]. Moreover, multi-stage LSF-DFE receiver of [1], and NP-SIC of [13] have higher latency than the parallel branch SF-DFE receiver.

5.5 Simulations

In simulation, we have considered QPSK modulation for SM-SC systems with$M = 2, 4$ transmit antennas and $N = 4$ receive antennas to examine the performance of the proposed SF-DFE. The symbol period is assumed as 1μsec. The channel models considered here are

1. The SUI-6 channel model with three taps is used to simulate a hilly terrain communication channel with light tree densities. These have τ_{max} =20μsec and $\tau_{rms} = 5.2\mu$sec resulting in a maximum delay spread of 20 symbol periods and an RMS delay spread of 5.2 symbol periods for the assumed 1μsec symbol period. This type of channel exhibits very deep fades as noted in chapter 2 Fig. 2.1.

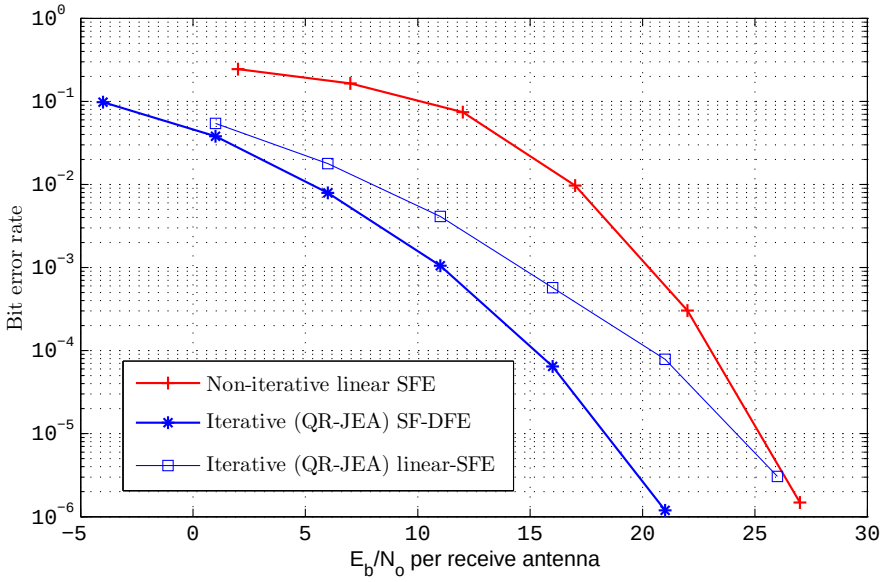

Figure 5.2: Performance comparison of the SF-DFE with the linear SFE using both iterative (QR-JEA) and a non-iterative JEA on an SUI-6 channel with maximum ISI span of 20 data symbols.

2. A general six tap channel with a maximum delay spread of 6 symbol periods and τ_{rms} of 1.25 and 5.2 symbol periods is considered to compare the performance of the SF-DFE with that of [1]. The channel with $\tau_{rms} = 5.25$ symbol periods is challenging as fading is then more significant due to stronger multipath components.

For the above two channel profiles, the different paths corresponding to different multipath components are assumed independent. The channel multipath gains are complex Gaussian random variables with zero mean and the average power in the multipath is normalized to unity. We consider quasi-static fading which is time-invariant over the transmission frame of length N_s symbols.

Since the multipath channel is normalized, the signal to noise ratio (SNR), defined as E_b/N_o, is the ratio of the received signal energy per bit from all transmitters E_b, to the noise power, N_o, per receive antenna. The bit-error-rate (BER) is obtained

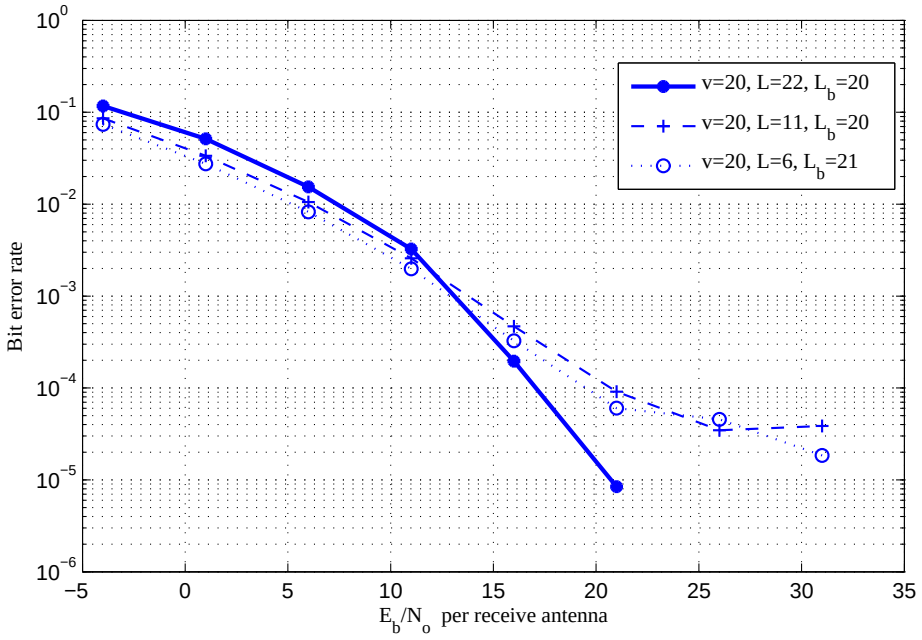

Figure 5.3: Effect of L on the performance of SF-DFE over an SUI-6 channel with a maximum ISI span of $v = 20$.

by averaging the instantaneous BER of at least 10,000 transmission frames and 100 bit errors. Assuming error propagation is limited, the SF-DFE performs significantly better than the linear SFE on heavily dispersive channels.

Fig. 5.2 illustrates the comparative performance of three receivers, namely the linear developed in chapter 4, a linear iterative QR-JEA based SFE and the non-linear iterative QR-JEA based SF-DFE receiver, on the SUI-6 channel. At a BER of 10^{-4}, the SF-DFE outperforms the linear non-iterative JEA based SFE by 8.5dB and gains 5.5dB over the linear iterative QR-JEA based SFE (using 2 iterations). A preprocessor FIR filter length of $L = 22$ is used for all three receivers.

Fig. 5.3 illustrates that, as with the linear-SFE, a space frequency pre-processor with $L \geq v + 2$ results in good performance for the SF-DFE. The FD-FFF then compensates for the ISI present at the output of the pre-processor in the FD. Most of the residual ISI following the FD-FFF is cancelled by the TD-FBF. To refine the structure, the required FBF length is examined in the following.

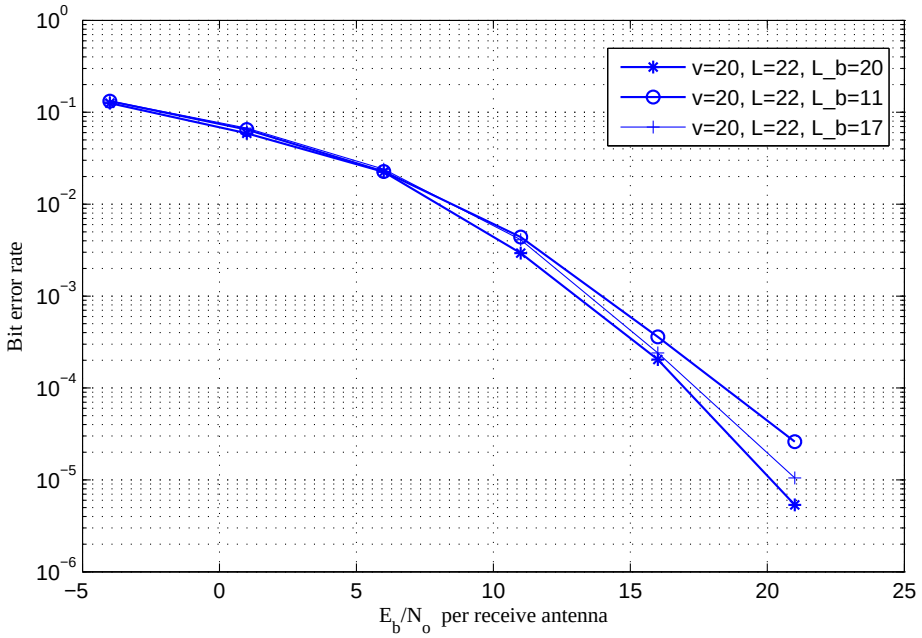

Figure 5.4: Effect of feedback filter length L_b on the overall performance of SUI-6 channel with a maximum ISI span of 20.

The effect of feedback filter length, L_b, on the overall performance of the SF-DFE is illustrated in Fig. 5.4. As can be seen, for an ISI span of $v = 20$ and pre-processor with $L = 22$ we find $L_b = 20$ gives good performance of the SF-DFE. As seen in Fig. 5.4, the degradation for $L_b = 17$ is small ($\approx$ 1dB), but increases as L_b decreases.

In Fig. 5.5 we compare the performance of SF-DFE with linear SFE for an exponentially decaying six tap channel [1]. Using simulations we noticed that the 6 tap channel with a maximum ISI span of $v = 6$ required a pre-processor length of $L = 10$ which is slightly more than that required for the 3 tap SUI channel profiles. However, the FBF length requirement is similar for both channels, that is $L_b = 6$ for the 6 tap channel. Using these filter lengths for $v = 6$, we vary the RMS delay spread[2] τ_{rms} in Fig. 5.5. At a BER of 10^{-4}, a performance improvement of less than 2dB over the linear-SFE is achieved on a channel with $\tau_{rms} = 1.25$ symbol periods

[2]As the RMS delay spread increases, the channel is known to exhibit more frequency selectivity. For such channels, use of a DFE is more effective than a linear receiver.

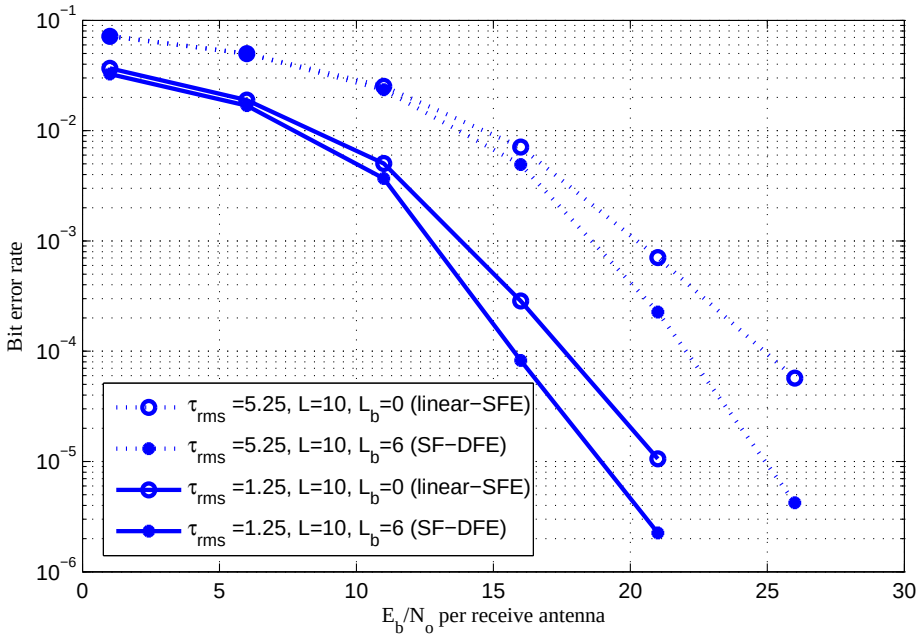

Figure 5.5: Performance comparison of the SF-DFE with the linear-SFE on a 6 tap multipath channel with RMS delay spread of 1.25 and 5.25 with four transmitters and four receivers.

(low RMS delay spread). Whereas on a channel with $\tau_{rms} = 5.25$ symbol periods (high RMS delay spread), the SF-DFE achieves a 3dB performance improvement over the linear-SFE. This suggests that the proposed SF-DFE is more effective for use on channels with higher delay spread.

The result for $\tau_{rms} = 1.25$ on a six tap channel is comparable to that achieved by the MIMO hybrid DFE in [31]. At a SNR of 16 dB, both receivers exhibit a BER of 10^{-4}. Although the system complexities and performance are comparable, due to the parallel receiver architecture and channel estimation, SF-DFE has lower processing time than the MIMO hybrid DFE. The LSF DFE of [1] on a similar channel is 2 dB worse than the SF-DFE performance at a BER of 10^{-4}. In [13], an 8-ray channel model with an RMS delay spread of 2 is considered. There performance is illustrated under the assumption of perfect CSI, however the actual performance using practical channel estimation algorithms can deviate from the ideal performance, and hence no quantitative comparison is made.

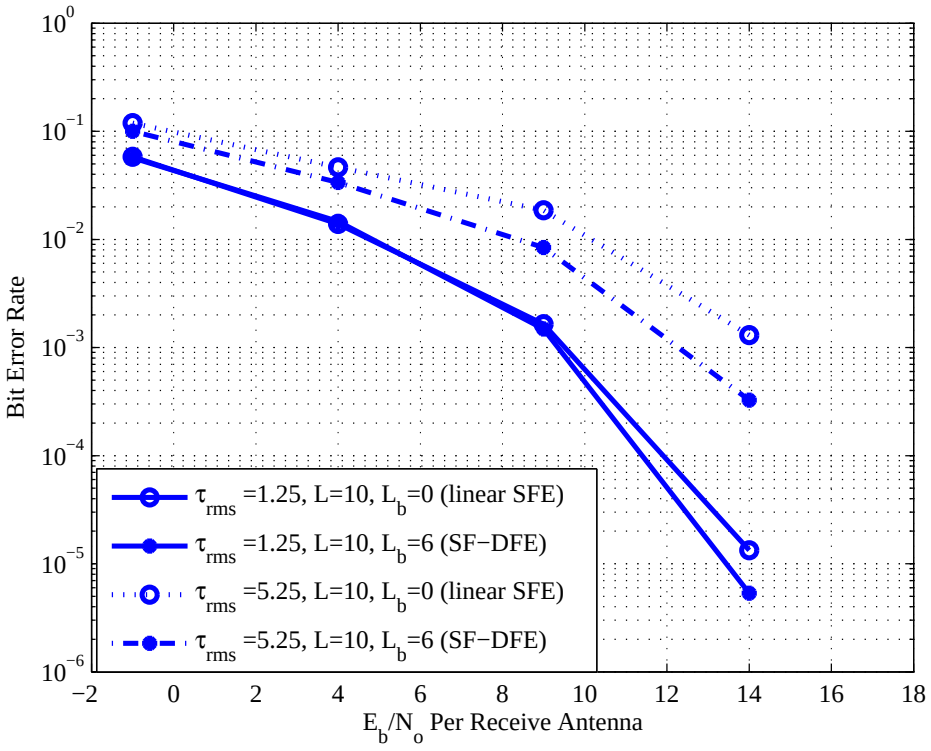

Figure 5.6: Performance comparison of SF-DFE with linear-SFE on a 6 tap multipath channel with RMS delay spread of 1.25 and 5.25 with two transmitters and four receivers.

The effect of delay spread for a system with $M = 2, 4$ transmitters and $N = 4$ receivers is examined in Fig. 5.6. On comparing the dotted curves representing $\tau_{rms} = 5.25$ symbol periods (large RMS delay spread) in Fig. 5.6 and Fig. 5.5, the improvement of SF-DFE over linear receivers is around 2dB. For $\tau_{rms} = 1.25$ symbol periods the improvement achieved due to SF-DFE is less than 1dB. This confirms that the SF-DFE is more effective on channels with high delay spreads (hence highly frequency selective channels).

5.6 Conclusions

Performance by means of simulations for two channel profiles (3 tap and 6 tap) is examined for the proposed SF-DFE using the iterative QR-JEA developed in

chapter 4. The SF-DFE is implemented based on the TD effective channel and receiver vectors provided by the QR-JEA. Hence, the effect of pre-processor length L on overall SF-DFE performance is investigated. We found that as with the linear SFE it typically requires $L \geq v + 2$ for good performance. Moreover, on highly dispersive channels (high RMS delay spread), the SF-DFE is more effective yielding more SNR improvement over the linear SFE. The system complexity of the SF-DFE is also compared to other time and frequency domain MIMO DFE architectures. The proposed SF-DFE uses only 25 percent of the computations of the TD based MIMO DFE and is comparable to other FD based MIMO DFE architectures.

Chapter 6

Conclusions and Suggested Future Work

6.1 Conclusions

In this thesis, the focus has been on developing low complexity FD receiver architectures for broadband wireless systems operating in heavily time dispersive propagation media. The importance of wireless channel characteristics on broadband data communications is discussed in chapter 2. This chapter also points out the advantages of employing FD receiver processing for single carrier modulation on such channels.

The use of multiple antennas at the transmitter and receiver along with spatial multiplexing (SM) can offer a linear increase in transmission rate without additional expenditure of bandwidth and or power for SC systems. SM is only possible in MIMO channels [10]. Traditionally, receiver processing is carried out in the TD. However, TD receive processing techniques involving estimation of the MIMO channel matrix and equalization may not be feasible for heavily dispersive channels. Therefore, FDE for SC systems has been studied.

Chapter 3 looks at the existing channel estimation techniques used in conjunction with SC-FDE for SISO and MIMO systems. It is understood that MIMO channel estimation in the TD results in lower complexity as it involves estimation of

fewer unknowns. A TD composite channel estimation model is introduced that estimates the MIMO channel matrix as a set of parallel channel parameter vectors. This approach is observed to result in lower processing time than previous time or frequency domain approaches.

A space-frequency receiver architecture is developed for SM-SC systems using the TD estimated channel parameters to perform equalization in the FD for channels with very long ISI span. The receiver is referred to as the space-frequency-equalizer (SFE). The SFE is based on a QR-decomposition based iterative joint estimation algorithm (QR-JEA). The QR-JEA uses the composite channel model and estimates the TD MIMO CSI in parallel which is then fed into the SFE. The proposed receiver yields equal diversity gains for all data streams. The integrated SFE employing iterative QR-JEA is shown to have lower processing time and comparable complexity to other frequency domain receivers. The resulting receiver exhibits excellent error performance even on highly dispersive broadband wireless channels as seen in chapter 4.

In chapter 5, the linear SFE developed in chapter 4 is extended to a non-linear receiver architecture described as a space frequency decision feedback equalizer (SF-DFE). The SF-DFE uses the FD pre-processor developed in chapter 4 in conjunction with a hybrid-DFE receiver architecture discussed in chapter 3. We provide derivation of the SF-DFE's FD-FFF and FBF coefficients. The existing MIMO-DFE architectures [1, 13] are derived based on the knowledge of complete MIMO channel matrix. In contrast, the SF-DFE is implemented using the effective channel and receiver parameter vectors given by the iterative QR-JEA. This provides time and complexity savings due to parallel processing. Using simulations, we show that the SF-DFE outperforms the linear SFE presented in chapter 4.

6.2 Future Work

As a natural extension to chapter 5, an MLSE based receiver can be developed. The front-end of the SF-DFE performs CCI mitigation and ISI compensation in the FD. Following this an MLSE detector can be used to further improve the performance.

The SF-DFE has a completely independent parallel branch receiver architecture. In order to cancel residual interference at the output of the FDE some form of PIC can be employed resulting in a multi-stage SF-DFE which further improves the performance. It would be interesting to compare error propagation effects across multiple stages with that of LSF receivers. The first stage in a multi-stage SFE would be the same as SF-DFE, however, for the following stages, the QR-JEA would use the output from the previous stage as the received signal streams and would generate new sets of effective channel parameters.

Throughout this thesis, we have focused only on the receiver processing techniques. Exploiting some form of transmit processing for example, Tomlinson Harashima precoding [13, 15, 16] techniques in conjunction with the non-linear SF-DFE receivers may further improve the performance and is a subject of interest in future.

Bibliography

[1] X. Zhu and R. D. Murch, "Layered space-frequency equalization in a single carrier MIMO system for frequency selective channels," *IEEE Transactions on Wireless Communications*, vol. 3, no. 3, pp. 701–708, May 2004.

[2] H. Sari, "Trends and challenges in broadband wireless access," in *Communications and Vehicular Technology, 2000. SCVT-200. Symposium on*, Leuven, Belgium 2000, pp. 210–214.

[3] H. Bolcskel, A. Paulraj, K. Hari, R. Nabar, and W. Lu, "Fixed broadband wireless access: state of the art, challenges, and future directions," *Communications Magazine, IEEE*, vol. 39, no. 1, pp. 100–108, Jan 2001.

[4] J. G. Andrews, A. Ghosh, and R. Muhamed, *Fundamentals of WiMAX: Understanding Broadband Wireless Networking (Prentice Hall Communications Engineering and Emerging Technologies Series)*. Upper Saddle River, NJ, USA: Prentice Hall PTR, 2007.

[5] W. C. Wong, I.-K. Fu, D. Chen, M. Hart, and P. Wang, "Comparison of multipath channel models for ieee 802.16j relay task group," in *IEEE 802.16j-06/044r1*, July 2006.

[6] "Mobile broadband wireless access (MBWA)," in *IEEE 802.20 http://ieee802.org/20*.

[7] E. Dahlman, S. Parkvall, J. Skold, and P. Beming, *3G Evolution*. Great Britain: Academic Press, Jul 2007.

[8] H. Sari, G. Karam, and I. Jeanclaude, "Transmission techniques for digital terrestrial TV broadcasting," *IEEE Communications Magazine*, vol. 33, pp. 100–109, Feb. 1995.

[9] P. Alexander, D. Haley, and A. Grant, "Outdoor mobile broadband access with 802.11," *IEEE Communications Magazine*, vol. 45, no. 11, pp. 108–114, Nov. 2007.

[10] E. Biglieri, R. Calderbank, A. Constantinides, A. Goldsmith, A. Paulraj, and V. H. Poor, *MIMO Wireless Communications*. Cambridge, UK: University Press, 2007.

[11] J. H. Sung, "Transmitter strategies for closed-loop mimo-ofdm," Ph.D. dissertation, Georgia Institute of Technology, Georgia, July 2004.

[12] E. G. Larsson and P. Stoica, *Space-time Block Coding for Wireless communications*. Cambridge, UK: University Press, 2003.

[13] Y. Zhu and K. B. Lataief, "Single-carrier frequency domain equalization with noise prediction for MIMO systems," *IEEE Transactions on Communications*, vol. 55, no. 5, pp. 1063–1076, May 2007.

[14] P. Du, G. Bi, and Q. Li, "Single carrier frequency domain equalization for high data rate transmission systems over frequency selective fading channels," in *Proc. IEEE 6th CAS Symp. Emerging Technologies: Mobile and Wireless Comm.*, May 2004, pp. 361–364.

[15] R. Fischer, C. Windpassinger, A. Lampe, and J. Huber, "Tomlinson-Harashima precoding in space-time transmission for low-rate backward channel," Feb 2002, pp. 7–1 – 7–6.

[16] R. Fischer, J. Huber, and C. Windpassinger, "Signal processing in decision-feedback equalization of intersymbol-interference and multiple-input/multiple-output channels: a unified view," *Signal Proc.*, vol. 83, no. 8, pp. 1633–1642, 2003.

[17] K. Takeda, H. Tomeba, and F. Adachi, "Joint Tomlinson-Harashima precoding and frequency-domain equalization for broadband single-carrier transmission," *IEICE Trans Commun*, vol. E91-B, no. 1, pp. 258–266, 2008.

[18] R. J. W. Wang and J. Geng, "Improved partial parallel multistage detection for v-blast systems," *IEEE Elect. Lett.*, vol. 43, no. 1, Jan. 2007.

[19] A. Goldsmith, *Wireless Communications*. New York, NY, USA: Cambridge University Press, 2005.

[20] V. Tarokh, N. Seshadri, and A. Calderbank, "Space-time codes for high data rate wireless communication: performance criterion and code construction," *Information Theory, IEEE Transactions on*, vol. 44, no. 2, pp. 744–765, Mar 1998.

[21] J. W. Liang and A. J. Paulraj, "Two-stage CCI / ISI reduction with space-time processing in TDMA cellular networks," in *Proc. 30th Asilomer Conf. Signals, Sytems and Computers*, Oct. 1996, pp. 607–611.

[22] R. Steffen, B. Tufik, and H. Mario, "Successive interference cancellation for SC FDE MIMO systems," in *Proc. PIMRC*, vol. 2, Oct 2006, pp. 1142–1146.

[23] D. Falconer, S. Ariyavisitakul, A. Benyamin-Seeyar, and B. Eldson, "Frequency domain equalization for single-carrier broadband wireless systems," *IEEE Communications Magazine*, pp. 58–66, Apr. 2002.

[24] F. Pancaldi and G. M. Vitetta, "Block channel equalization in the frequency domain," *IEEE Transactions on Communications*, vol. 53, no. 3, pp. 463–471, Mar. 2005.

[25] R. Dinis, R. Kalbasi, D. Falconer, and A. Banihashemi, "Channel estimation for MIMO systems employing single-carrier modulations with iterative frequency-domain equalization," in *Proc. VTC*, Sept. 2004, pp. 4942– 4946.

[26] F. Siddiqui, F. D. Lemoine, and D. Falconer, "On interference in uplink SDMA SC-FDE system," in *Proc. IEEE Fifth Annual Conference on Communications Networks and Services Research.*, Canada, May 2007, pp. 231–238.

[27] J. Siew, J. Coon, R. J. Piechocki, A. Dowler, A. Nix, M. Beach, S. Armour, and J. M. Geehan, "A channel estimation algorithm for MIMO-SCFDE," *IEEE Communications Letters*, vol. 8, no. 9, pp. 555–557, Sept. 2004.

[28] J. Siew, J. Coon, R. Piechocki, A. Nix, M. Beach, S. Armour, and J. M. Geehan, "A bandwidth efficient channel estimation algorithm for MIMO-SCFDE," in *Proc. VTC*, Oct. 2003, pp. 1142–1146.

[29] C.-T. Lam, D. D. Falconer, F. Danilo-Lemoine, and R. Dinis, "Channel estimation for SC-FDE systems using frequency domain multiplexed pilots," in *Proc. VTC*, vol. 33, Sep 2006, pp. 1–5.

[30] G. Kongara, D. Taylor, and P. Martin, "Space-frequency equalization for broadband single carrier MIMO systems," in *Proc. VTC*, Calgary, Sept. 2008, pp. 58–66.

[31] R. Kalbasi, D. Falconer, A. Banihashemi, and R. Dinis, "A comparison of frequency-domain block MIMO transmission systems," *Vehicular Technology, IEEE Transactions on*, vol. 58, no. 1, pp. 165–175, Jan. 2009.

[32] W. H. Tranter, K. S. Shanmugan, T. S. Rappaport, and K. L. Kosbar, *Principles of Communication Systems Simulation with Wireless Applications*. Upper Saddle River, NJ, USA: Prentice Hall Press, 2004.

[33] W. C. J. Jakes, *Microwave Mobile Communications*. John Wiley and Sons, New York :, 1974.

[34] J. W. Liang, *PhD Thesis: Interference Reduction and Equalization with Space-Time processing in TDMA Cellular Networks*. Stanford University: University Press, 1998.

[35] D. C. Cox, R. R. Murray, and A. W. Norris, "800 MHz attenuation measured in and around suburban houses," *Bell Labs Tech. J.*, vol. 63, no. 6, pp. 921–954, July 1984.

[36] V. Erceg and K. V. S. Hari, "Channel models for fixed wireless applications," in *http://ieee802.org/16*.

[37] V. Erceg, L. J. Greenstein, S. Y. Tjandra, S. R. Parkoff, A. Gupta, B. Kulic, A. A. Julius, and R. Bianchi, "An empirically based path loss model for wireless channels in suburban environments," *Selected Areas in Communications, IEEE Journal on*, vol. 17, no. 7, pp. 1205–1211, 1999.

[38] B. Sklar, "Rayleigh fading channels in mobile digital communication systems Part I: characterization," *Communications Magazine, IEEE*, vol. 35, no. 7, pp. 90–100, 1997.

[39] ——, "Rayleigh fading channels in mobile. digital communication systems. Part II: mitigation," *Communications Magazine, IEEE*, vol. 35, no. 7, pp. 90–100, 1997.

[40] M. V. Clark, "Adaptive frequency-domain equalization and diversity combining for broadband wireless communications," *IEEE Journal on Selected Areas in Communications*, vol. 16, no. 8, pp. 1385–1395, Oct. 1998.

[41] Y. Zhang and H.-H. Chen, *Mobile WiMAX: Toward Broadband Wireless Metropolitan Area Networks*, illustrated, Ed. Florida: CRC Press, 2007.

[42] R. V. Nobelen and D. P. Taylor, "Multiple symbol differentially detected multilevel codes for the rayleigh fading channel," *IEEE Transactions on Communications*, vol. 45, no. 5, pp. 1529–1537, Dec. 1997.

[43] H. Sari, G. Karam, and I. Jeanclaude, "Channel equalization and carrier synchronization in OFDM systems," in *Tirrenia Int. Workshop on Digital Communications.*, Sep 1993.

[44] T. Walzman and M. Schwartz, "Automatic equalization using the discrete frequency domain," *IEEE Transactions on Information Theory*, vol. 19, no. 1, pp. 59–68, Jan. 1973.

[45] E. R. F. Jr, *Frequency Domain Adaptive Filtering*, chapter 6 in Adaptive Filters, C. F. N Cowan and P. M. Grant (Editors), Ed. Englewood Cliffs, NJ:: Prentice-Hall.

[46] R. A. Horn, *Matrix Analysis*. Cambridge United Kingdom: Cambridge University Press, 1985.

[47] F. Pancaldi, G. Vitetta, R. Kalbasi, N. Al-Dhahir, M. Uysal, and H. Mheidat, "Single-carrier frequency domain equalization," *IEEE Signal Processing Magazine*, vol. 25, no. 5, pp. 37 – 56, Sept. 2008.

[48] J. Tubbax, B. C'ome, L. V. der Perre, L. Deneire, and M. Engels, "OFDM vs single-carrier with cyclic prefix a system-based comparison," in *Proc. VTC*, 2001, pp. 1115–1119.

[49] N. Benvenuto and S. Tomasin, "On the comparison between OFDM and single carrier modulation with a DFE using a frequency-domain feedforward filter," *IEEE Transactions on Communications*, vol. 50, no. 6, pp. 947–955, June 2002.

[50] J. Coon, J. Siew, M. Beach, A. Nix, S. Armour, and J. McGeehan, "A comparison of MIMO-OFDM and MIMO-SCFDE in WLAN environments," in *Proc. 2003 IEEE Global Telecommunications Conf.*, Dec. 2003, pp. 3296–3301.

[51] A. Czylwik, "Comparison between adaptive OFDM and single carrier modulation with frequency domain equalization," in *Proc. VTC*, 1997, pp. 865–869.

[52] M. Ran, D. Falconer, and A. B. Seeyar, "A mixed OFDM downlink and single carrier uplink for the 2-11 ghz licensed bands," in *IEEE C802.16a-02/83*.

[53] C. Tidestav, M. Sternad, and A. Ahlen, "Reuse within a cell-interference rejection or multiuser detection?" *Communications, IEEE Transactions on*, vol. 47, no. 10, pp. 1511–1522, Oct 1999.

[54] Z. Cheng and D. Dahlhaus, "Time versus frequency domain channel estimation for OFDM systems with antenna arrays," in *6th Proc. IEEE Int'l. Conf. on Signal Processing*, Aug. 2002, pp. 1340–1343.

[55] Y. G. Li, N. Seshadri, and S. Ariyavisitakul, "Channel estimation for ofdm systems with transmitter diversity in mobile wireless channels," *IEEE Transactions on Wireless Communications*, vol. 17, no. 3, pp. 461–471, 1999.

[56] J. Coon, S. Armour, M. Beach, and J. MacGeehan, "Adaptive frequency domain equalization for single carrier MIMO systems," in *Proc. IEEE Int'l. Conf. on Communications*, vol. 4, June 2004, pp. 2487–2491.

[57] W. Van Etten, "Maximum likelihood receiver for multiple channel transmission systems," *IEEE Transactions on Communications*, vol. 24, no. 2, pp. 276–283, Feb. 1976.

[58] F. Sainte-Agathe and H. Sari, "Single-carrier transmission with frequency-domain decision-feedback equalization," in *EUSIPCO*, Antalya, Turkey, Sept. 2005, pp. 607–611.

[59] H. Sari and F. Sainte-Agathe, "New results in iterative frequency-domain decision-feedback equalization," in *EUSIPCO*, 2006.

[60] N. Benvenuto and S. Tomasin, "Block iterative dfe for single carrier modulation," *Electronics Letters*, vol. 38, no. 19, pp. 1144–1145, Sep 2002.

[61] C. Belfiore and J. Park, J.H., "Decision feedback equalization," *Proceedings of the IEEE*, vol. 67, no. 8, pp. 1143–1156, Aug. 1979.

[62] X. Zhu and R. D. Murch, "Novel frequency-domain equalization architectures for a single-carrier wireless MIMO system," in *Proc. VTC*, Sept. 2002, pp. 874–878.

[63] J. Xu, H. Wang, S. Cheng, and M. Chen, "Parallel multistage decision feedback equalizer for single-carrier layered space-time systems in frequency-selective channels," *EURASIP*, no. 1, pp. 1489 – 1497, Jan. 2004.

[64] R. Kalbasi, R. Dinis, and D. Falconer, "Hybrid time-frequency layered space-time receivers for severe time dispersive channels," in *Proc. SPAWCF*, Portugal, Lisbon, July 2004, pp. 218–222.

[65] G. J. Foschini, "Layerd space-time architecture for wireless communications in a fading environment when using multi-element antennas," *Bell Labs Tech. J.*, pp. 41–59, Autumn 1996.

[66] C. L. Miller, D. P. Taylor, and P. T. Gough, "Estimation of co-channel signals with linear complexity," *IEEE Transactions on Communications*, vol. 49, no. 6, pp. 1997–2005, Nov. 2001.

[67] S. L. Ariyavisitakul, J. H. Winters, and I. Lee, "Optimum space-time processors with dispersive interference-unified analysis and required filter span," *IEEE Transactions on Communications*, vol. 47, no. 7, pp. 1073–1083, July 1999.

[68] G. H. Golub and C. F. V. Loan, *Matrix computations (3rd ed.)*. Baltimore MD: Johns Hopkins University Press, 1996.

[69] J. W. Stewart, *Eigen Decompositions*. London United Kingdom: Prentice-Hall, 1989.

[70] K. B. Petersen and M. S. Pedersen, “The matrix cookbook,” in *http://matrixcookbook.com*, Nov. 2008.

[71] K. R. Rao and P. Yip, Eds., *The Transform and Data Compression Handbook (chapter 2)*. Boca Raton, FL, USA: CRC Press, Inc., 2000.

[72] A. H. Sayed, *Fundamentals of Adaptive Filtering*. Hoboken, NJ: John Wiley and Sons.

[73] S. Haykin, *Adaptive Filter Theory (4th Edition)*. Prentice Hall, 2001.

Appendix A

SF-DFE TD MSE analysis:

In this appendix, we show additional detail on the derivation of the TD MSE of the SF-DFE. Recall in (5.33-5.34) we wrote the TD MSE of the SF-DFE as

$$\begin{aligned} MSE_{SF-DFE} &= \frac{1}{N_s}E[\boldsymbol{\delta}_{TD}^H\boldsymbol{\delta}_{TD}] \\ &= \frac{1}{N_s}(E[\left(\mathbf{t}_m - \overline{\mathbf{b}}_m\mathbf{d}_m\right)^H\left(\mathbf{t}_m - \overline{\mathbf{b}}_m\mathbf{d}_m\right)] \\ &= E[\mathbf{t}_m^H\mathbf{t}_m] + E[\mathbf{d}_m^H\overline{\mathbf{b}}_m^H\overline{\mathbf{b}}_m\mathbf{d}_m] - E[\mathbf{d}_m^H\overline{\mathbf{b}}_m^H\mathbf{t}_m] \\ &\quad -E[\mathbf{t}_m^H\overline{\mathbf{b}}_m\mathbf{d}_m]). \end{aligned} \tag{1}$$

Using (5.12), we have

$$E[\mathbf{t}_m^H\mathbf{t}_m] = E[\left(\overline{\boldsymbol{\mathcal{G}}}_m\overline{\boldsymbol{\mathcal{Z}}}_m\right)^H\left(\overline{\boldsymbol{\mathcal{G}}}_m\overline{\boldsymbol{\mathcal{Z}}}_m\right)] \tag{2}$$

We now use (5.28) and (5.32) to write

$$E[\mathbf{t}_m^H\mathbf{t}_m] = E\left[\left(\overline{\boldsymbol{\mathcal{D}}}_m^H\overline{\boldsymbol{\mathcal{B}}}_m^H\overline{\boldsymbol{\mathcal{F}}}_m^H\left(\overline{\boldsymbol{\mathcal{F}}}_m\overline{\boldsymbol{\mathcal{F}}}_m^H + \frac{\rho_i^2}{\rho_d^2}\overline{\boldsymbol{\mathcal{I}}}\right)^{-1}\overline{\boldsymbol{\mathcal{F}}}_m\overline{\boldsymbol{\mathcal{B}}}_m\overline{\boldsymbol{\mathcal{D}}}_m\right)\right] \tag{3}$$

We let $\overline{\boldsymbol{\mathcal{F}}}_m^H\left(\overline{\boldsymbol{\mathcal{F}}}_m\overline{\boldsymbol{\mathcal{F}}}_m^H + \frac{\rho_i^2}{\rho_d^2}\overline{\mathbf{I}}\right)^{-1}\overline{\boldsymbol{\mathcal{F}}}_m = \overline{\boldsymbol{\mathcal{A}}}_m$ and re-write (3) as

$$\begin{aligned} E[\mathbf{t}_m^H\mathbf{t}_m] &= E\left[\left(\overline{\boldsymbol{\mathcal{D}}}_m^H\overline{\boldsymbol{\mathcal{B}}}_m^H\overline{\boldsymbol{\mathcal{A}}}_m\overline{\boldsymbol{\mathcal{B}}}_m\overline{\boldsymbol{\mathcal{D}}}_m\right)\right] &(4)\\ &= E[\mathbf{d}_m^H\overline{\mathbf{b}}_m^H\overline{\mathbf{Q}}_{N_s}^H\overline{\boldsymbol{\mathcal{A}}}_m\overline{\mathbf{Q}}_{N_s}\overline{\mathbf{b}}_m\mathbf{d}_m], &(5)\end{aligned}$$

where $\overline{\boldsymbol{\mathcal{B}}}_m\overline{\boldsymbol{\mathcal{D}}}_m = \overline{\mathbf{Q}}_{N_s}\overline{\mathbf{b}}_m\mathbf{d}_m$ and its Hermitian are used in writing the (5). Similarly, it can be shown that

$$E[\mathbf{d}_m^H\overline{\mathbf{b}}_m^H\mathbf{t}_m] = E[\mathbf{d}_m^H\overline{\mathbf{b}}_m^H\overline{\mathbf{Q}}_{N_s}^H\overline{\boldsymbol{\mathcal{A}}}_m\overline{\mathbf{Q}}_{N_s}\overline{\mathbf{b}}_m\mathbf{d}_m]. \tag{6}$$

$$E[\mathbf{t}_m^H \overline{\mathbf{b}}_m \mathbf{d}_m] = E[\mathbf{d}_m^H \overline{\mathbf{b}}_m^H \overline{\mathbf{Q}}_{N_s}^H \overline{\boldsymbol{\mathcal{A}}}_m \overline{\mathbf{Q}}_{N_s} \overline{\mathbf{b}}_m \mathbf{d}_m]. \tag{7}$$

$$\begin{aligned} E[\mathbf{d}_m^H \overline{\mathbf{b}}_m^H \overline{\mathbf{b}}_m \mathbf{d}_m] &= E[\mathbf{d}_m^H \overline{\mathbf{b}}_m^H \overline{\mathbf{I}\mathbf{b}}_m \mathbf{d}_m] && (8) \\ &= E[\mathbf{d}_m^H \overline{\mathbf{b}}_m^H \overline{\mathbf{Q}}_{N_s}^H \overline{\mathbf{Q}}_{N_s} \overline{\mathbf{b}}_m \mathbf{d}_m] && (9) \end{aligned}$$

Substituting (4), (6), (7) and (8) in (1) and re-arranging some terms we can write the MSE of the SF-DFE as

$$MSE_{SF-DFE} = \frac{1}{N_s} E\left[\left(\mathbf{d}_m^H \overline{\mathbf{b}}_m^H \overline{\mathbf{Q}}_{N_s}^H \left(\bar{\mathbf{I}} - \overline{\boldsymbol{\mathcal{A}}}_m\right) \overline{\mathbf{Q}}_{N_s} \overline{\mathbf{b}}_m \mathbf{d}_m\right)\right]. \tag{10}$$

Using the matrix inversion lemma from [12], given matrices A, B, C, D we have,

$$A^{-1} + A^{-1}C(B - DA^{-1}C)^{-1}DA^{-1} = (A - CB^{-1}D)^{-1} \tag{11}$$

We let

$$\begin{aligned} A &= \bar{\mathbf{I}} \\ C &= -\overline{\boldsymbol{\mathcal{F}}}_m^H \\ D &= \overline{\boldsymbol{\mathcal{F}}}_m \\ B &= \frac{\rho_i^2}{\rho_d^2}\bar{\mathbf{I}} \\ -DA^{-1}C &= \overline{\boldsymbol{\mathcal{F}}}_m^H \overline{\boldsymbol{\mathcal{F}}}_m, \end{aligned}$$

where we represented element-wise multiplication of vectors as multiplication of their diagonal matrices that is $(\overline{\boldsymbol{\mathcal{F}}}_m^H \overline{\boldsymbol{\mathcal{F}}}_m) = diag(\boldsymbol{\mathcal{F}}_m^H \circ \boldsymbol{\mathcal{F}}_m)$. As $\overline{\boldsymbol{\mathcal{F}}}_m$ is diagonal, $\overline{\boldsymbol{\mathcal{F}}}_m^H = \overline{\boldsymbol{\mathcal{F}}}_m^*$. Therefore,

$$\begin{aligned} \left(\bar{\mathbf{I}} - \overline{\boldsymbol{\mathcal{A}}}_m\right) &= \frac{\rho_i^2}{\rho_d^2}\left(\overline{\boldsymbol{\mathcal{F}}}_m \overline{\boldsymbol{\mathcal{F}}}_m^* + \frac{\rho_i^2}{\rho_d^2}\bar{\mathbf{I}}\right)^{-1} && (12) \\ &= \frac{\rho_i^2}{\rho_d^2}\overline{\boldsymbol{\Phi}}_m && (13) \end{aligned}$$

where, $\overline{\boldsymbol{\Phi}}_m = \left(\overline{\boldsymbol{\mathcal{F}}}_m \overline{\boldsymbol{\mathcal{F}}}_m^H + \frac{\rho_i^2}{\rho_d^2}\bar{\mathbf{I}}\right)^{-1}$. Substituting (12) in (10) we have the MSE of the SF-DFE as

$$\begin{aligned} MSE_{SF-DFE} &= \frac{\rho_i^2}{\rho_d^2 N_s} E\left[\left(\mathbf{d}_m^H \overline{\mathbf{b}}_m^H \overline{\mathbf{Q}}_{N_s}{}^H \overline{\boldsymbol{\Phi}}_m \overline{\mathbf{Q}}_{N_s} \overline{\mathbf{b}}_m \mathbf{d}_m\right)\right] && (14) \\ &= \frac{\rho_i^2}{N_s}\left(\overline{\mathbf{b}}_m^H \overline{\mathbf{Q}}_{N_s}{}^H \overline{\boldsymbol{\Phi}}_m \overline{\mathbf{Q}}_{N_s} \overline{\mathbf{b}}_m\right), && (15) \end{aligned}$$

where $E[\mathbf{d}_m^H \mathbf{d}_m] = \rho_d^2 \bar{\mathbf{I}}$. This is the same result as (5.35).